Design of a steerable needle for low dose rate brachytherapy of the prostate

by

H.M. Sickler

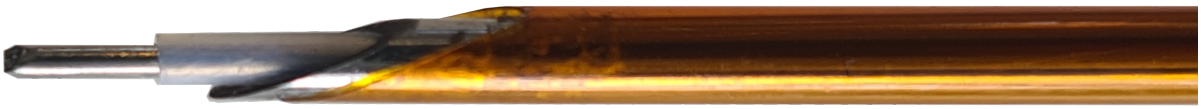

To obtain the degree of

Master of Science
Biomedical Engineering

at the Delft University of Technology,
to be defended publicly on 30 June 2022.

Supervisor: dr. J.J. van den Dobbelsteen
Supervisor: Ir. M. de Vries

Abstract

Prostate cancer is the most frequently diagnosed cancer type among men, and the third deathliest form of cancer. Several treatments are available to treat prostate cancer. Low Dose Rate Brachytherapy (LDR BT) is one of them, which inserts permanent radioactive seeds into the prostate using a needle. The literature review performed prior to this thesis, investigates if LDR BT is an effective method and how the quality of life is affected by the treatment compared to other treatments. Furthermore, the various anatomical variations that could intervene with the procedure are analyzed and how they are currently dealt with. It was found that during this treatment multiple complications can arise; first pubic arch interference could prevent the needle from reaching all parts of the prostate. Second, unwanted needle deflection can cause incorrect dose distribution, and third, delicate tissues like the urethra can obstruct the path of the needle. The introduction of a steerable needle in the field of brachytherapy could have the potential of treating patients with particular anatomical variations, add more maneuverability for the surgeon to steer around certain tissues and adjust unwanted needle deflections. All contributing to an accurate dose distribution and therefore an improved quality of life of the patient.

This thesis aims to design and develop a steerable needle for LDR BT of the prostate along with defining the design parameters of the steering capabilities to predict the bending of the needle. The needle should have a lumen for radioactive seeds to pass through, should use the steering mechanism of the preceding high dose rate wire needle and it should be able to steer 30mm laterally over 150mm insertion in order to reach the entire prostate.

Multiple theories are developed to predict the deflection behaviour of the needle. A theory that can predict the needle tip path, two theories that predict the distal deflection in air, and lastly a theory that predicts the deflection in tissue. One of the theories that predict the distal deflection in air is based on the proximal angle and the other one on the proximal force. To test these theories, a steerable wire needle, made of spring steel, for high dose rate brachytherapy is borrowed. From these experiments it can be concluded that the theory for the prediction of the needle tip path gives results close to the measured values and the prediction of the distal deflection based on proximal force give adequate results with an error of 1.77mm ±1.6mm. This error is in between the acceptable threshold of 2mm-5mm. The other two models presented errors of 15.1mm ±15.2mm and 14.4mm ±14.6mm, which give inaccurate predictions and are therefore not used as basis for the design of the steerable needle. An analysis is performed on the individual parameters within the two models. This provides insight into which variables need to be adjusted to design a steerable needle that complies with the requirements.

Based on the two models and the analysis of the individual parameters, a steerable needle that complies with the requirements, is designed, manufactured and tested. The manufacturing of the needle was limited by the availability of materials, causing the inner lumen to be slightly smaller than initially designed. The first tests are performed in air to compare the results with the previous experiments done with the wire spring steel needle and to verify the prediction models. The needle tip path and distal deflection based on the proximal force predictions both proof to be adequate models with the latter having an error of 2.75mm ±2.99mm. The steerable nitinol needle with a lumen, is also tested in tissue stimulant to provide a proof of principle and verify the theory of deflection in tissue. It is demonstrated that the needle can steer within the tissue stimulant, and insert an object though its lumen into the tissue. The model for the prediction of the deflection in tissue can be proven empirically. In addition, the prediction of the distal deflection based on the proximal force can also be applied for bending in tissue, if a constant is added to account for the bevel tip of the needle.

To provide an additional substantiation for the prediction model, a third needle is tested in air. This needle is borrowed and is intended to be used in high dose rate brachytherapy. This needle, made of tungsten, also proofs that the model can make adequate predictions with an error of 1.76mm ±1.4mm.

One of the requirements of the needle is that the inner lumen must accommodate the passing of a radioactive seed. Due to the unavailability of certain materials this was not accomplished. Therefore, a theoretical design is made with a larger inner lumen. For further research this design can be manufactured and tested.

The steerable needle presented in this thesis provides a proof of principle for a steerable needle with a lumen. It could have the potential of overcoming the anatomical obstacles presented in the literature review and therefore aiding in an accurate dose distribution. Furthermore, it can also provide the surgeon with the capability of adjusting unwanted deflection created by the needle. In addition, by analyzing the variables that influence the steering, a model is made that can predict the deflection based on the proximal force applied.

Acknowledgements

I would like to express my appreciation to Martijn de Vries and John van den Dobbelsteen, who provided me with encouragement and support throughout the duration of this research project. The development of this project is in part thanks to the knowledge, constructive criticism and general advice they have shared with me. Guiding me in the right direction and providing broader alternative perspectives have been very valuable for both my own progress and the progress of the project.

In addition, I would like to thank Mario van der Wel, for his astonishing craftsmanship. Without his help there would not have been a needle to present and test.

A special thanks to my friends: Susan Potters and Nebo Wemekamp. I would like to thank them for their support and time to thoroughly check my work and support me throughout the months of my thesis project.

Last but not least, I wish to thank my family for their love and encouragement through this thesis project and my entire studies.

H.M. Sickler
Delft, June 2022

Abbreviations

Abbreviation	Description
3D	Three dimensional
ADT	Androgen deprivation therapy
BT	Brachytherapy
CES	Cambridge engineering selector
CT	Computer tomography
DAQ	Data acquisition system
EDM	Electrical discharge machine
FEM	Finite element method
G	Gauge
LDR	Low dose rate
MR/MRI	Magnetic resonance imaging
PAI	Pubic arch interference
PETE	Polyethylene terephthalate
PMMA	Polymethylmethacrylate
POM	Polyoxymethylene
SMA	Shape memory alloy

Table 1: Abbreviations used throughout this thesis

Contents

1 Design initiation

1.1. Introduction

This chapter will discuss the conclusions from the literature review, present the design question and goal of this thesis. Furthermore, additional literature will be presented which will form the basis of the design requirements. After which the requirements will be elaborated.

1.2. Conclusions from literature study

Prostate cancer is the most frequently diagnosed cancer type among men, and comes in third place for most deathliest kind of cancer [1]. The prostate is an organ, that is closely associated with its surrounding structures, organs and tissues. During the treatment of the cancer, these surrounding structures need to be taken into account. There are numerous types of treatments that can be used to treat prostate cancer, each with their own patient specific indications or contraindications, method and advantages or disadvantages. Brachytherapy is one of these treatments that can be applied to treat prostate cancer.

Brachytherapy uses a needle to insert a radioactive source into the prostate, there is either low dose rate or high dose rate brachytherapy. Low dose rate brachytherapy inserts permanent radioactive seeds and can be used as either a monotherapy or as a booster with external beam radiation therapy. High dose rate brachytherapy also inserts a radioactive source into the prostate using a needle, but this source will be kept in place temporarily and therefore has a much higher dose. The quality of life after these brachytherapy treatments is comparable with other prostate cancer treatments like external beam radiation or radical prostatectomy. Brachytherapy has the worst score when it comes to urinary irritation/obstruction, but has the best score for urinary incontinence. For bowel and sexual function the scores for quality of life after brachytherapy also seem acceptable. The dose distribution during the treatment has significant influence on the quality of life of the patient. There are some patient specific anatomical variations, like the size of the prostate or pubic arch, which can pose to be interfering with an accurate and successful implantation of the radioactive source, and therefore affect the dose distribution.

Pubic arch interference (PAI) is present in about 25% of the patients treated with brachytherapy [2]. The current solutions for PAI are androgen deprivation therapy (ADT), inserting the needle free-handed in an oblique manner, repositioning the body of the patient or using a curvilinear approach. These solution have a good chance of still correctly treating the patient, but all have their drawbacks. From the literature study it can be concluded that brachytherapy is a viable option for the treatment of prostate cancer and even has a few advantages compared to other typical treatments. Since the amount of patients that can be treated with brachytherapy is limited due to anatomical variation, a solution should be found to included them.

The introduction of a steerable needle in the field of brachytherapy could have the potential of treating patients with particular anatomical variation, thus creating a more inclusive treatment. Furthermore, a steerable needle will also add more maneuverability for the surgeon to steer around the pubic arch and delicate tissue surrounding the prostate. In addition, the accuracy could also be improved since errors made during the procedure can easily be corrected, which will improve the quality of life of the patient.

These corrections also reduce the amount of re-insertions during the treatment, meaning fewer insertion points and therefore possibly less complications and less recovery time for the patient.

A steerable needle for brachytherapy is not only a possibility for cancer treatment in the prostate, but can also be applied in other organs and other treatments. For the design initiation and requirements the focus will be on low dose rate brachytherapy in the prostate, this is chosen to create a delimitation for this thesis. Later on there is still the possibility to look at different organs like the liver, breasts or brains, and see how the needle will react in these tissues.

1.3. Design question

Problem statement: current conventional Low Dose Rate brachytherapy (LDR BT) in the prostate is performed using rigid needles, which lack the flexibility to adjust for unexpected obstacles and unwanted deflection. Anatomical variations like pubic arch interference and urethral occlusion could cause some parts of the prostate to be more difficult or even impossible to reach. This can affect the placement of the seeds, and disturb the dose distribution plan, therefore affecting the quality of the implantation. Furthermore, needle placement faces additional challenges like tissue movement and deformation, tissue inhomogeneity and needle deflection. A steerable needle for LDR brachytherapy could contribute to overcoming these challenges, and thereby improving the treatment for the patient.

The goal of this thesis will be to develop a manual steerable needle for low-dose rate brachytherapy of the prostate based on the current compliant steering concept.

In this thesis the steering mechanism used in the high-dose-rate steerable needle of de Vries [3] will be translated to be applied in a design for a low-dose rate brachytherapy needle. In addition, this thesis will focus on the parameters that determine the operation of the needle, and how they affect the steerability of the needle. By researching the variables that affect the steering of the needle, the deflection could potentially be predicted. The parameters that are going to be investigated are:

- Diameter
- Wall thickness
- Slot width
- Slot length
- Insertion depth
- Flexural rigidity

To determine the requirements for the design of the needle, the focus will be on low-dose-rate brachytherapy in the prostate. However, when the parameters of the needle are all mapped out; there is potential to research the broadening of the applications of a steerable needle.

1.4. Additional literature

Although an extensive literature review was performed, additional literature is still required to formulate the requirements of the steerable needle.

1.4.1. State of the art: low dose rate brachytherapy needles

The classic needles that are used for low dose rate brachytherapy are commercially available, including their properties. These needles are rigid and hollow to allow the radioactive seeds to pass though. For low dose rate brachytherapy these needles range from 15.5G to 18G with a length between 150mm and 250mm [4]. The commercially available seeds that are used are 0.8mm in diameter and 4.5mm/5mm in length as can be seen in figure 1.1, or 0.5mm in diameter and 3.4mm long [5]. When stranded seeds are used, there is an extra nylon layer around the seeds, which extends the diameter to 0.96mm [6].

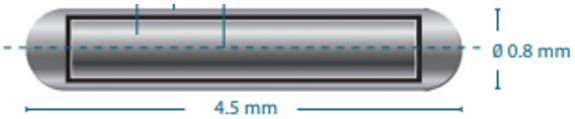

Figure 1.1: Measurements of a radioactive seed that is used in low dose rate brachytherapy [5].

To establish the dimensions of the steerable needle, a 3D simulations was made in the program SolidWorks. The needle needs to be able to allow a radioactive seeds to pass through its hollow structure, or lumen. To make sure that the needle can accommodate both single seeds and stranded seeds the inner lumen was designed to allow a 0.96mm diameter seed to pass through. An inner lumen was created according to the sketch in figure 1.2, with varying inner diameters. This sketch has a curvature in the distal part of the needle like the maximum curvature in the current system intended for high dose rate brachytherapy [3]. The seed was also created in SolidWorks according to the dimensions mentioned above. Both parts were combined in an assembly and mated to each other by introducing a 'path mate'. By dragging the seed through the inner lumen a simplified simulation is created to check the movement of the seed relative to the inner lumen. If the seed does not touch the inner lumen while passing through the maximum curvature, the size of the inner lumen will be large enough for the real radioactive seed to pass through. The inner diameter of the inner lumen was determined at 1.10mm.

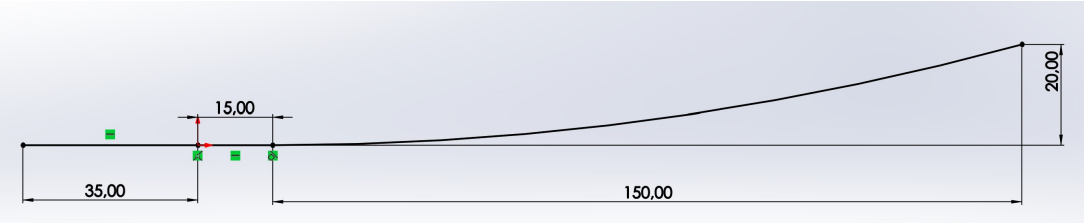

Figure 1.2: Maximum curvature according to the current steerable needle [3]

1.4.2. Proposed steerable needle mechanism

The high dose rate steerable needle that was designed by M. de Vries [3], and the Delft University of Biomechanical Engineering department, serves as a starting point for my design. This existing needle is made up of two components, the outer catheter that is made of polyamide and the inner needle that is made of a spring steel solid wire. The outer catheter can slide over the inner needle. The inner needle is a rod that is divided into four segments, by so called slots, which are still connected and both ends of the needle. These slots are created by using an electrical discharge machine (EDM), and have a width of 0.12mm. These slots form the bases of the compliant mechanism of the needle that creates the steering. A compliant mechanism is completely determined by their geometry and stiffness, since the elastic body deformation achieves the force and motion transmission. They are flexible and do not have any joints since the forces are transmitted through the material. Within the needle this principle works the same; the four segments will be pulled and pushed axially due to the force that the hand of the surgeon applies laterally on the proximal end of the needle. In order for this steerable needle mechanism to work, a minimal of two constraints is needed to withhold the needle from translating and rotating. These constraints are provided by the outer catheter that surrounds the inner needle.

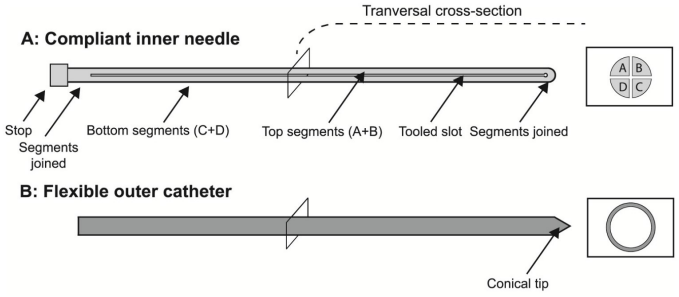

Figure 1.3: The outer catheter and inner needle as designed by M. de Vries [3].

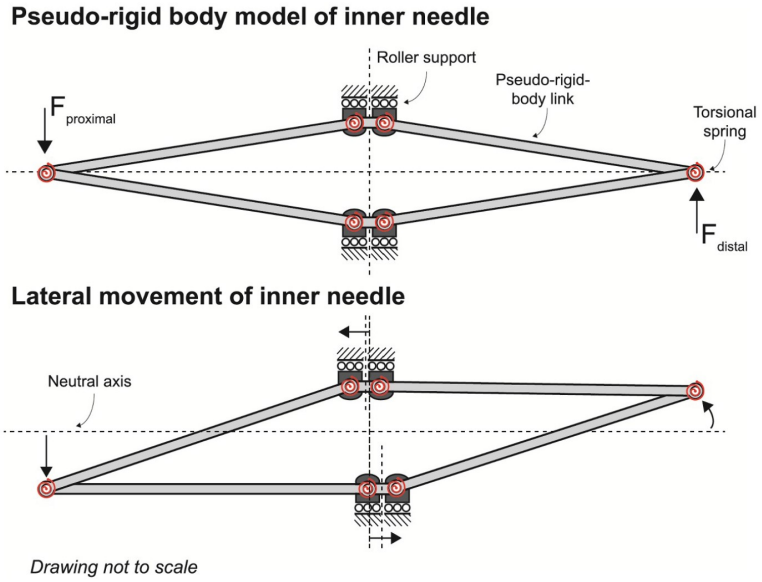

Figure 1.4: Model to explain the mechanics of the steerable needle [3].

In figure 1.4 the outer catheter that constrains the inner needle is presented as a roller support. When a force is applied on the proximal side of the needle, the segments start to move creating a lateral displacement. This causes the distal end to bend to the opposite side of the proximal side.

1.4.3. Forces acting on the needle

The forces that act on the needle affect the way that it will deflect within the tissue, and could possibly decrease the accuracy of the placement of the seeds. Within the human body there are several factors that affect the forces that are applied to the needle like tissue deformation, tissue heterogeneity, nonlinear elastic stiffness and anisotropy. The forces are also affected by the variables of the needle and procedure, like the size of the needle, the stiffness of the needle and the velocity with which the needle is inserted into the body. Podder et al. [7] performed a study that measured the forces of a surgical needle in vivo during prostate brachytherapy in the prostate. They performed these procedures on 20 patients with needle of 17G and 18G, that had a length of 200mm and a diamond tip. According to this study the maximum needle insertion forces are 15.6N and 8.9N for the 17G and 18G needles respectively. These forces are influenced by the insertion velocity, therefore they will be mentioned, the average velocity for the 17G needle was 1.3m/s and for the 18G needle 1.05m/s. These axial forces are the largest for penetration through the skin and the prostate capsule. They also measured the maximum transverse force on the needle which turned out to be 1.6N and 0.71N for the 17G and 18G needle respectively.

Lehmann et al. [8] also performed a study to measure the forces on a 18G brachytherapy needle, they used this experiment to estimate the needle tip deflection. They inserted a needle in a phantom, with an estimated velocity of 10mm/s. The transverse force on the needle inside the tissue was approximately 0.6N at 60mm insertion and 0.7N at 120mm insertion. This seems to be corresponding with the 0.71N that was found by Podder et al. [7].

1.4.4. Reachability of the prostate

Another requirement of the steerable needle for low dose rate brachytherapy in the prostate would be: what is the desired amount of steering of this specific needle? The amount of steering can be derived from the dimension of the prostate, the anatomical obstacles that need to be avoided during insertion and how much compensation is needed for unwanted needle deflection.

1.4.4.1. Prostate dimensions

The dimensions of the patients body and their prostate are crucial for defining the steering ability of the needle. If the patient is quite large, then there is need for a longer needle to be able the reach the entire prostate. The size of the prostate ranges greatly between patients. First of all the age of the patient is a crucial factor, since the prostate grows with age [9]. The steerable needle will be designed to overcome anatomical obstacles, like Pubic Arch Interference (PAI). PAI often occurs in patients with large prostate volumes >50cc, but could also be present in patients with smaller prostates who have a large pubic arch. To determine the minimal length of the needle, a prostate volume of 50cc will be maintained. The needle will hit the prostate capsule at about 92mm of penetration [7]. The required length for the needle can be determined by adding this insertion depth with the prostate size and then adding a specific length of the needle that is still outside of the body for the surgeon to hold onto and steer. According to a study performed by Collins [10] the mean dimensions of the longitudinal, antero-posterior and transverse sides of the prostate are 41.8mm , 48.3mm and 27.8mm respectively. Adding 92mm with approximately 40mm as the prostate size, results in an insertion depth of about 130mm. By leaving some length outside of the body to steer the needle, a total of 200mm is found. Using the dimensions and calculations mentioned above, and verifying them with the previous research of Nobel [11] and de Vries [3]; the required amount of steering of the needle is set at 30mm over 150mm insertion.

1.4.4.2. Pubic arch interference

Pubic arch interference means that the bones of the pubic arch obstructs the path of the needle when it is supposed to be inserted into the prostate via a percutaneous transperineal approach. This commonly occurs when the prostate volume of the patient is larger than $50cm^3$, but can also occur in patients with smaller prostate volumes when they have a narrow pubic arch [12]. This overlap of the bone and the needle path could cause inaccurate seed placement due to the fact that the needle cannot reach all the parts of the prostate, which in turn causes an inaccurate dose distribution into the prostate. Yale University School of Medicine investigated variations in the brachytherapy plan due to significant PAI. Of the 109 patients receiving the treatment of permanent prostate implants, 25% had such a significant case of pubic arch interference [2].

PAI can be characterized by means of three different parameters; the height of PAI, the angle of PAI and the percentage of the prostate that is overlapped by the pubic arch. According to the pacific northwest cancer foundation, major PAI would be described as an overlap of more then one-third of the prostate by the pubic arch [13]. Sejpal et al. [14] states that with PAI >1cm or a blockage of more then 25%, of the diameter of the prostate, a hormonal downsizing is required to reduces the excessive PAI. In a study on PAI, performed by Sejpal et al. [14] they found that 19.3% of the 243 patients had intra-operative PAI. Which meant that the needle had to be repositioned by at least 0.5cm. Out of the 7806 needles that were implanted during the treatment of the 243 patients, 1.4% had to be repositioned due to PAI. The median PAI was 6mm, with a range between 0mm and 10mm.

Bellon [16] performed a pubic arch study on 97 patients. They evaluated pubic arch interference of transperineal prostate brachytherapy using pelvic CT scanning and found that there was a considerable variability in PAI between the patients. The amount of overlap varied from -11mm to 20mm. The prostate volumes that were associated with these results ranged from 15cc to 131cc with a median of 36cc. It should be noted that an overlap of 20mm is very exceptional and that usually the amount of PAI ranges up to 10mm [17]. Zheng et al. [18] assessed the amount of PAI by measuring the angle of PAI and height

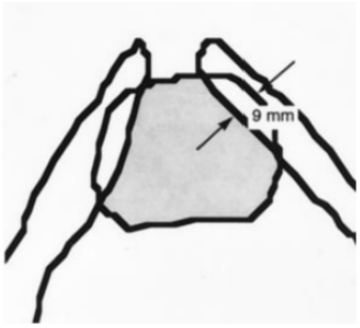

Figure 1.5: Visualisation of pubic arch interference over the prostate [15]

of PAI. The discussion about height will be omitted, since the conclusion of the paper states that: ''The angle is the key factor of PAI, since it is difficult to confirm the highest point of the anterior prostate''. The angle would be the more reliable parameter to predict possible PAI. The mean angle of PAI was 59.35 ±5.57 degrees.

1.4.4.3. Placement accuracy

The endpoint accuracy is an important factor of the steerable needle, since this will determine where the radioactive seeds are planted. As explained above, in the conclusion of the literature review, the dose of the radiation and therefore the positioning of the seeds is crucial for the treatment of the cancer. The threshold at which to prevent a significant change of the radiation dose lies between 2mm and 5mm [19]. The preceding high dose rate brachytherapy needle [3] was tested on endpoint accuracy; over a lateral distance of 15mm, his steerable needle had an endpoint error between 1.59mm - 2.45mm in adipose tissue simulant and 0.91mm - 1.64mm in prostatic tissue simulant.

1.4.5. Materials used in previous steerable needles

There are numerous steerable needles which already exist, each with their own mechanisms of steering and materials that assist their purpose. In this section, these materials will be discussed, and this will function as inspiration for possible materials to be used in the design of this steerable needle. Besides that the material is an important factor for the strength and flexibility of the needle, it is also important to look at the bio-compatibility and MR-compatibility.

The steerable needle of de Vries [3] is made of spring steel wire and the steerable needle designed by Nobel [11] is made of patented steel wire, both in combination with a polyamide catheter. Nobel also suggests potential materials like M42 tool steel, super-elastic nickel titanium wire, cobalt-nickel-aluminum alloys and copper-aluminium-nickel alloys. Podder et al. [20] designed a needle for the so called curvilinear approach, to create a needle that can be used for the placement of seeds during low dose rate brachytherapy of the prostate. They used nitinol for their four wires and for the needle body. Podder [21] also designed another steerable mechanisms using shape memory alloy (SMA) wires. They proposed two different designs, one with flexible joints made of shape memory polymer and one with flexible joints made of nylon, and the wires are made of flexinol. The main body of this needle is a nitinol tube. SMA's are considered because of their lightweight, high force and energy density. The needle that was designed by Berg et al. [22], is actively controlled with tendon actuation. This needle is composed of three components; the stylet, cannula and outer layer. These are made from stainless steel, peek plastic and pet plastic respectively. Lastly, in the review by Dhaliwal et al. [23], on clinical and technological consideration for MRI-guided robotic prostate brachytherapy, several materials are mentioned that can be used for brachytherapy in an MRI. For example, titanium and titanium alloys like nitinol. However titanium is still at risk of heating up too much inside of an MRI due to the radio frequency. The other material mentioned in this paper are plastics like nylon, PETE, POM, teflon, Delrin, Acrylic, Ultem etc. There are also some metals mentioned, which are non-ferromagnetic, like brass, phosphor bronze and aluminum. In addition to plastics and non-ferromagnetic metals, ceramics materials could also provide a solution, but they are very brittle.

1.5. Design requirements

The requirements that are presented below focus on the design for a low dose rate brachytherapy steerable needle that is used in the prostate. Such a steerable needle could also be used for other approaches and applications, however a more specific focus is chosen to narrow down the design requirements.

1.5.1. Requirements

1.5.1.1. Functional requirements

The needle should..

1. **..allow radioactive seeds to pass through in single-file** (not-stranded/stranded)
   The radioactive seeds that have to pass through the needle have a diameter of 0.8mm and a length of 4.5mm-5mm [5]. Stranded seeds are connected by an extra nylon layer, resulting in a diameter of 0.96mm [6]. The needle should allow these radioactive seeds to pass through.

2. **..have a minimal length of 150mm to be inserted inside the patient**
   The prostate is located approximately 90mm within the body [7]. For the needle to reach to end of the prostate an additional minimum of 40mm is needed. To ensure that also larger prostates can be treated, the minimum insertion depth of the needle should be 150mm.

3. **..be able to acquire a lateral deflection of 30mm when the needle is inserted 150mm**
   As explained in section 1.4.4 the needle must be flexible enough to compensate for anatomical variation within the patient, like pubic arch interference and urethral occlusion. Therefore the minimal deflection of the needle is set at 30mm over 150mm.

4. **..allow the radioactive seeds to pass through the curvature of 30mm over 150mm**
   As presented in the previous requirement, the needle should allow a deflection of 30mm over 150mm. This deflection creates a curve within the needle which could prevent the seeds from passing though. Therefore the needle should allow the radioactive seeds to pass through this curvature. In section 1.4.1 the minimum inner lumen for a radioactive seed to pass though the curve was determined to be 1.10mm

5. **..allow omnidirectional needle tip movement**
   The needle tip should be able to be steered in all directions

1.5.1.2. Technical requirements

The needle should..

6. **..have an outer diameter between 14G (2.108mm) and 18G (1.270mm)**
   Rigid low-dose-rate brachytherapy needles are generally 17G or 18G [4], which is equal to an outer diameter of 1.473mm and 1.270mm respectively. This steerable needle designed in this thesis will have a comparable diameter. Due to the fact that this steerable needle requires a stylet inside of the needle, the needle will most likely turn out to be larger. The limit is set just around 2mm, which is equal to 14G (2.108mm). The goal will be to keep the needle as thin as possible, while still being functional, to decrease the tissue damage. Although tissue damage is not only dependent on the diameter of the needle, but also the manner of insertion and the type of needle tip that is used, it is still preferable to keep the diameter small.

7. **..use the compliant active steering mechanism**
   The compliant mechanism for the steering of the needle as explained in section 1.4.2 should be incorporated into this design of the steerable needle.

8. **..not undergo plastic deformation**
   During the design of the needle, it should be taken into account that the forces acting on the needle could cause the needle to deform plastically. This permanent deformation can cause a blockage for the seed passage.

1.5.1.3. Usability/interface requirements

The needle should..

9. **..allow the seed(s) to be inserted in 1 action**
   The design should be such that the radioactive seeds can be inserted with 'one' action. This means that the stylet is not removed to provide a lumen, and that such a lumen must be integrated within the design.

10. **..be operable in the limited workspace between the legs of the patient in lithotomy position**
    The workspace of the surgeon to operate is limited due to the fact that the patient is in an lithotomy position. The space in between the legs is roughly between the $8x8cm^3$ and $12x12cm^3$ [7]. The design of the needle should be compact enough to stay within these boundaries. In addition, the mechanism used to operate the needle should also fit within these boundaries.

11. **..be compatible with ultrasound**
    Currently, brachytherapy procedures in the prostate are assisted with ultrasound, to ensure that the needle is compatible with the current methods, it should be compatible with ultrasound. A material is compatible with ultrasound if the density of this material can be distinguished from the density of the tissue.

12. **..be hand operated, either 1 or 2 hands**
    The surgeon should be able to operate the needle using his/her hands. If it will become 1 hand operated or 2 hands operated will be either concluded in this thesis, or will be a surgeons own preference.

13. **..be manually operable**
    The needle should be operated manually, so no electronics or robots will be involved.

14. **..be compatible with the existing template**
    The steerable needles will be an addition to the brachytherapy treatment, not all the insertions require a steerable needle. Therefore, the rigid needles will still be used, in combination with the template. The steerable needle must therefore also be compatible with this template.

1.5.2. Optimisation

In addition to the requirements for the needle, which represent the hard demands that the needle must comply with, there are also some wishes which can optimize the design and function of the steerable needle. It would be preferable if the needle met these wishes, but it is not obligated to deliver a functioning product. They are mainly actions that could make the needle more versatile.

It would be preferable if the needle..

1. **..requires as little additional equipment as possible**
   To keep the design simplistic, the wish is introduced to not add too many additional equipment's. To guide the needle, the template is needed, and this addition is acceptable because it is already part of the current treatment. But the new design for the steerable needle should not require multiple products to be introduced into the operation room.

2. **..has an needle tip endpoint error as low as possible**
   One of the challenges that this steerable needle should help to overcome, is the accuracy of the seed placement and therefore the dose distribution. To accomplish this the needle must have an endpoint error of less then 2mm. As mentioned in section 1.4.4 the threshold at which a significant change of the radiation dose is still avoided lies between 2mm and 5mm.

3. **..can be used for LDR brachytherapy treatments in other organs in addition to the prostate**
   Apart from using the LDR brachytherapy needle to treat prostate cancer, it might provide an advantage for other cancer treatments as well. Like in the liver or breasts.

In addition to the requirements and wishes described above, there are a few more design demands. These requirements are not important for this thesis, but should however be kept in mind, since they

will be relevant when production starts for this steerable needle. First of all, the needle should be bio-compatible. Meaning that the material that is used to manufacture the needle should not be harm full to the patient. Secondly, the needle will be used within the operation room and within a patient, so for future design the steralizability of the needle should be considered. In addition, the manufacturing process should be easy to mass produce. Finally, it would be preferable to make the needle MRI compatible, so that surgeons can choose if they want to operate using ultrasound or MR.

2

Needle deflection in air theory

The goal of this chapter is to develop an equation that can predict the behaviour of the needle based on its own parameters. When such a formula is created, the design for the steerable needle for low dose rate brachytherapy can be based on these equations. First the needle tip path will be researched for a range of inputs, this creates a curve that can predict the range of the needle. In addition, a theory will be produced that can predict the distal deflection based on the proximal angle of the needle. After which a theory will be discussed which could predict the distal deflection according to the precise proximal force that is applied. All theories will be tested in chapter 3

2.1. Deflection theory 1 - needle tip path

The aim of creating an equation for the prediction of the needle tip path, is to determine what the range will be of a specific needle. This could predict what parts of the body the needle can reach, and therefore for which procedure such a needle can be used.

The theory behind the path of the needle tip is based on a paper by Yamada et al. [24], which describes a loop-shaped flexible mechanism for robotic needle steering. They created a kinematic model based on their FEM-based numerical simulation. The needle used in their paper has two segments instead of four. Since one of the requirements is to use the current steering mechanism of de Vries [3], this formula needs to be adjusted to four segments. In the report of the bachelor thesis group from Engelen [25] et al., a model is created for a staff needle with four rods. This model and the model by Yamada et al. [24] are both used and adjusted to create a model that can predict the deflection behaviour of a tube needle with four segments. This prediction is based on the parameters of the needle itself, like dimensions and material properties. By considering that only ideal deflections occur, the calculations presented below are a simplified approximation of the deflection of the needle tip.

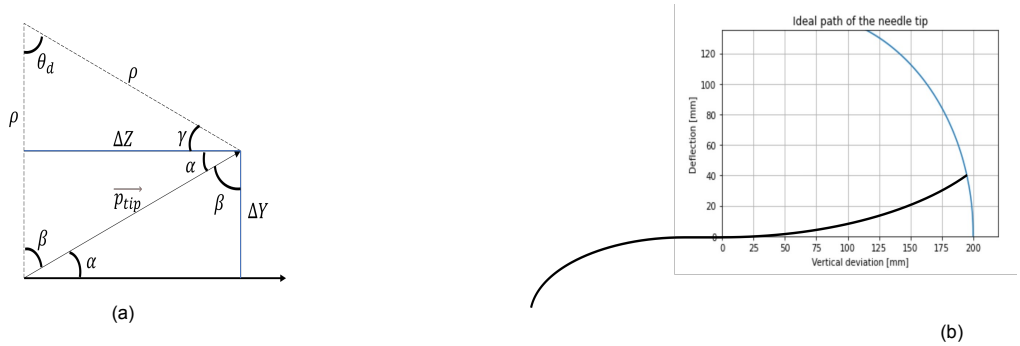

Figure 2.1: a) Visualization of the geometry of the needle tip path of the needle and the corresponding angles. b) Needle tip path graph made with the python model and the visualization of the bending needle.

The location of the needle tip is represented by the vector p_{tip}. Equation 2.1 show the formula for p_{tip}, where ΔZ represents the vertical deviation of the needle and ΔY the deflection. Because the needle bends and the needle length will not change, the tip of the needle will be located a bit closer to the origin, this change in length is called the vertical deviation.

The variable d in equation 2.1 represents the absolute difference between the extensions of the needle segments above or below and left or right u_r and u_l. Since it is assumed that the needle does not have a moment on the neutral line, the extension of the left or right segment is zero. Therefore the variable d is equivalent to the variable u_r.

$$p_{tip} = \begin{bmatrix} \Delta Z \\ \Delta Y \end{bmatrix} = \begin{bmatrix} \rho * sin(\theta_d) + d \\ 2\rho * sin^2(\frac{\theta_d}{2}) \end{bmatrix} \tag{2.1}$$

In equation 2.2 the variable ρ represents the radius of the curvature, and can be calculated using the insertion length (L_n), the distance from the centroid of the needle to the centroid of the upper half of the needle (ω), the angle of the curvature (θ_d) and the elongation of the upper or lower segment (u_r). The movement of the segments is assumed to be a range which includes all inputs untill 0.808mm. This was chosen to provide a path that visualizes the range of the needle for multiple elongations of the segments.

$$\rho = \frac{L_n + u_r + \omega * \theta_d}{\theta_d} \tag{2.2}$$

The variable w represents the distance between the centroid of the needle and the centroid of the upper half of the needle. It can be calculated by using the diameter of the catheter, the radius of the segments, the diameter of the needle and the width of the slots. Further explanation of the variable w can be found in section 2.1.1. All of the parameters used in this model for the prediction of the needle tip path are presented in table 3.3.

Parameter	**Description**
L_n [mm]	Insertion depth
r_n [mm]	Radius of the segments
h [mm]	Distance centroid needle to segments
ω [mm]	Distance centroid needle to centroid upper half
u_r [mm]	Elongation or abridgment of upper or lower segment
d_n [mm]	Outer diameter of the needle
d_c [mm]	Inner diameter of the catheter
S_w [mm]	The width of the slots in the inner needle

Table 2.1: The variables of the steerable needle, that are used in the model for the needle tip path

In figure 2.1a, the values ΔZ and ΔY from equation 2.1 are visualized. The angle α corresponds to the distal angle of the needle. By using the basic geometry rules both ρ and θ_d can be concluded from this figure. This is an isosceles triangle, because both legs have the value ρ. This results in the fact that the angle β and the angle $\alpha + \gamma$ should be the same.

$$\beta + (\gamma + \alpha) + \theta_d = 180° \tag{2.3}$$

$$\alpha + \beta + 90° = 180° \tag{2.4}$$

$$\beta = \gamma + \alpha \tag{2.5}$$

$$\theta_d = 2\alpha = \frac{u_r}{\omega} \tag{2.6}$$

To visualize the curve that resembles the path of the needle tip, the formulas that are stated above are inserted into a python script (Appendix A). The graph in figure 2.1b is created by plotting the vertical deviation against the deflection. The curve presented in this figure represents the needle tip path of a needle with random variables. Needle paths of needles with different dimensions and insertion depths are presented throughout this thesis.

2.1.1. Calculation of the centroid of the upper half of the needle

The variable ω represents the distance between the centroid of the needle and the centroid of upper half of the needle. The stylet has segments that can move, when bending the needle, the segments will expand outward and are stopped by the catheter surrounding them. When calculating the centroid of the upper half, the diameter that is used is in expanded state. Since a steerable needle can be both a staff and a tube, the calculation of the centroid will be explained for both.

2.1.1.1. Wire needle

As discussed above, the segments expand until they reach the catheter. For a steerable wire needle, this means that the distance presented as 'h' maximizes. The variable r_n is the radius of a segments of the stylet, which can be calculated by taking the radius of the stylet, minus half of the slot width.

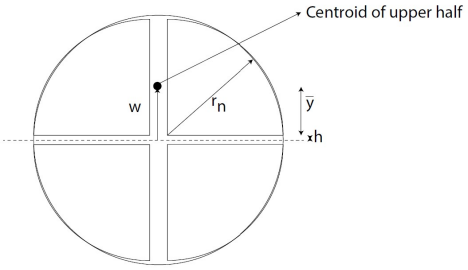

Figure 2.2: Visualisation of the location of the centroid of the upper half of the wire needle [25]

$$\omega = y + h = \frac{4r_n}{3\pi} + h \tag{2.7}$$

$$h = \frac{d_c - 2r_n}{2} \tag{2.8a}$$

$$r_n = \frac{d_n}{2} - \frac{slotwidth}{2} \tag{2.8b}$$

2.1.1.2. Tube needle

For a steerable tube needle the centroid of the upper half lies on other coordinates. In this case the centroid is calculated by using using the formula for the centroid of an arch. The first arch in figure 2.3b has the dimensions of the outer diameter, and the arch in 2.3c of the inner diameter. The diameter of the catheter is used, this is due to the fact that the segments expand until this point, as discussed above.

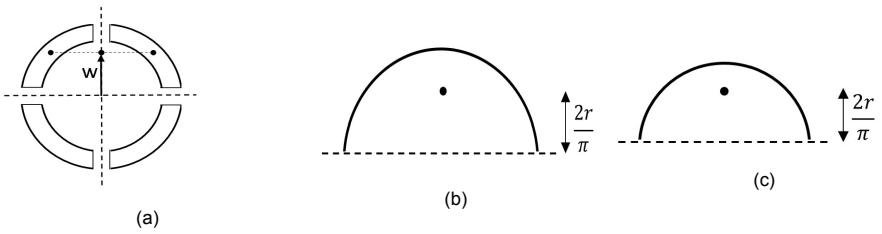

Figure 2.3: Visualisation of the location of the centroid of the upper half for a tube needle

$$\omega = \frac{\left(\frac{2*(d_c/2)}{\pi} + \frac{2((d_c/2)-Wt)}{\pi}\right)}{2} \tag{2.9}$$

2.2. Deflection theory 2 - prediction based on proximal angle

The theory presented in this section is based on an equation that was derived by Nobel [11]. By altering part of this equation, the unknown distal deflection of the needle can be predicted using various known parameters of the needle. The equation is based on the steering mechanism of the needle, meaning there will be a focus on the stylet and not the remaining parts of the needle. The segments slide over one another, as illustrated in figure 2.4b. It is assumed that the force exerted on the proximal side of the needle is perpendicular to the segments, resulting that the moment within these segments will only be experienced by the top and bottom segment. The 'left' and 'right' segment are located on the neutral line. Within the rods of the segments there will be a pull and push motion. This motion shortens one side of the needle, and elongates the other, creating bending. An extended explanation of this motion is given in section 2.3.

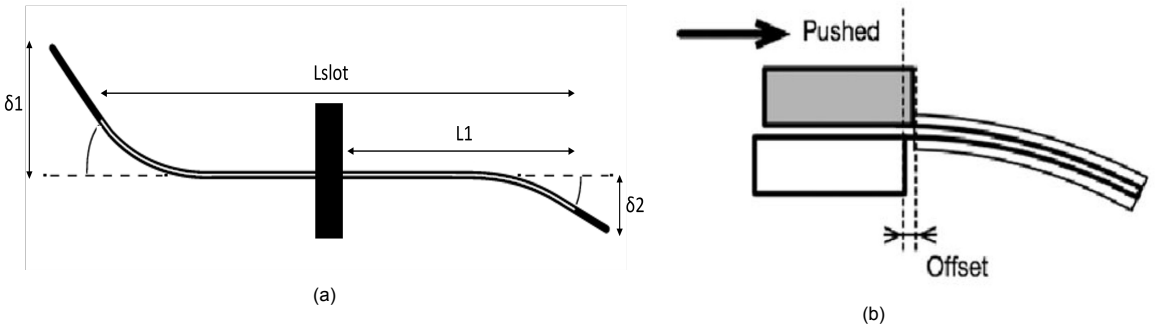

Figure 2.4: Schematic of needle steering: a) Schematic of the parameters of the needle incorporated in the prediction of the deflection based on the proximal angle. b) Schematic of the push mechanism created by the elongation of the segments [24]

In the perfect situation, Nobel [11] claims that the angles θ_1 and θ_2 are the same. However there are losses within the material, and strain must be taken into account. To create an equation that can predict the distal deflection, two assumptions were made to simplify the formula. Firstly, the friction that the needle experiences is neglected and secondly, the needle is viewed as a beam. The derivation of the equation is presented in appendix E.

$$\theta_2 = \frac{R^2 * \theta_1 * L_1 * A}{R^2 * L_1 * A + 4 * I_{stylet} * L_{slot}} \qquad (2.10)$$

$$\theta 2 = \frac{R * \theta_1}{R + (\frac{4EI * L_{slot}}{L_1 RAE})} \qquad (2.11)$$

Parameter	Description
R [m]	Radius of the stylet
θ_1 [m]	Proximal angle
θ_2 [m]	Distal angle
L_1 [m]	Length of the needle from the template until the end of the slot
L_{slot} [m]	Length of the slots
A [m^2]	Area of the stylet
I_{stylet} [m^4]	Second moment of inertia of the stylet
E [GPa]	Young's modulus of the material of the stylet
EI [Nm^2]	Flexural rigidity of the needle

Table 2.2: The variables of the steerable needle, used in the model for the prediction of the distal deflection

The distal deflection of the needle depends on various parameters of the needle. First of all the radius (R) of the needle is important. In addition, the area of the needle, the slot length and the length from the template until the end of the slot are used in the equation. Furthermore, the second moment of inertia in incorporated into the formula, and the deflection that is imposed on the proximal side is also a variable. In section 2.4, the I_{stylet} parameter will be explained further. In case that the second moment of inertia is not known, the equation can also be derived in a different manner, which is explained in appendix E. Equation 2.11 is derived with still the whole parameter flexural rigidity (EI) in it. This prevents possible errors created by the hand calculation of I_{stylet}.

2.3. Deflection theory 3 - prediction based on proximal force

The theory that predicts the distal deflection based on the proximal angle is based on the Euler-Bernoulli beam theory, which is most accurate for small deflections. Therefore a third theory is added, which is based on the proximal force. During the bending process of the needle, there are essentially two types of bending occurring. On the proximal side, a moment bending takes place, whereas at the distal side the needle bends more in a circular or parabolic manner. To predict the distal deflection, these two types of bending need to be translated to each other. This is done by altering theory 1 by adding some newly developed aspects. The needle bends due to the force that is applied on the proximal end (Fp). This force creates a moment (M), which in turn creates forces (F1 and F2) acting on the segments themselves, causing the segments within the stylet to slide past one another (Figure 2.6b). The elongation and abridgment of the segments generates the bending and therefore the deflection of the needle.

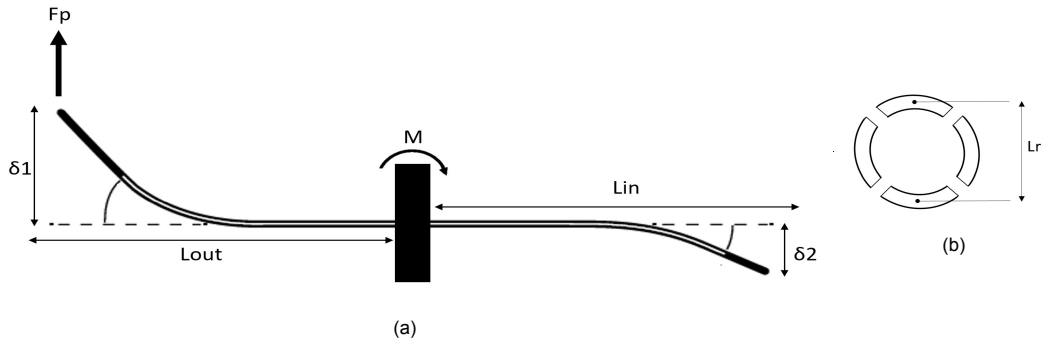

Figure 2.5: Schematic of needle steering: a) Schematic of the parameters of the needle used in the prediction of the deflection based on the proximal force. b) Display of the length between the center of mass of the two opposing segments.

$$M = F_p * L_{out} \qquad (2.12) \qquad F_1 = \frac{M}{2 * L_r} \qquad (2.13) \qquad \delta_s = \frac{F_1 L_{in}}{A_{s1} E} \qquad (2.14)$$

In equation 2.14 the elongation of the segments is presented as δ_s, however this elongation of the segments is the same distance as u_r which was presented in section 2.1. By relating the elongation created by the proximal force to the needle tip path, a theory can be produced that predicts the distal deflection of the needle at a specific force.

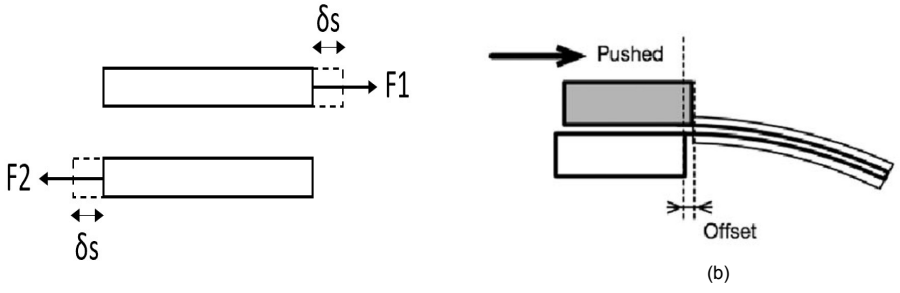

Figure 2.6: Schematic of the movement of the segments: a) Schematic drawing of the forces acting on the segments and how they elongate due to these forces. b) Visualisation of how these elongations of the segments create bending at the distal end of the needle [24]

$$p_{tip} = \begin{bmatrix} \Delta Z \\ \Delta Y \end{bmatrix} = \begin{bmatrix} \rho * sin(\theta_d) + \delta_s \\ 2\rho * sin^2(\frac{\theta_d}{2}) \end{bmatrix} \qquad (2.15)$$

$$\rho = \frac{L_n + \delta_s + \omega * \theta_d}{\theta_d} \qquad (2.16) \qquad \theta_d = \frac{\delta_2}{\omega} \qquad (2.17) \qquad \delta_s = u_r \qquad (2.18)$$

2.4. Second moment of inertia

The second moment of inertia seems to be a key value within multiple crucial equations. Because this parameter has a lot of influence on the behaviour of the needle, it will be investigated within this chapter.

The second moment of inertia, or the second moment of area, is a term in structural engineering. It can either be the planar or polar second moment of inertia. The planar focuses on a beam's resistance to bending, and the polar on a beam's resistance to torsional deflection. The value of the second moment of inertia is completely determined by the geometric values of the part.

The value for the second moment of inertia will be calculated using theory, in combination with the results of a three point bending experiment. The data sheets from a three point bending test provide the values of the normal strain and the standard force applied onto the needle during the experiment. By using the standard formula for the deflection of a beam with two constrains, which is given in equation 2.19, the value for EI can be derived.

$$\delta = \frac{FL^3}{48EI} \tag{2.19}$$

$$EI = \frac{FL^3}{48\delta} \tag{2.20}$$

According to Berg et al. [22] the flexural rigidity (EI) of an item that is constructed of multiple parts can be calculated using the following equation.

$$EI_{needle} = EI_{stylet} + EI_{catheter} \tag{2.21}$$

$$I_{catheter} = \frac{\pi * (D_o^4 - D_i^4)}{64} \tag{2.22}$$

$$I_{stylet} = \frac{EI_{needle} - EI_{catheter}}{E_{stylet}} \tag{2.23}$$

3

Experiment with spring steel needle

The current high dose rate steerable needle prototype made of spring steel, manufactured by M. de Vries is used within an experiment to evaluate the needle tip deflection theory and the theories about the prediction of the distal deflection of the needle. With these results it can be decided which of the models can be used to form the base of the design of the low dose rate steerable needle.

3.1. Materials and method

3.1.1. Set-up

The set up (Figure 3.1) for this experiment is made with any available components, since the lab was closed due to covid. A 3D-printed imitation of the 'standard' needle template (2) is fixed in place, onto a wooden base (3), using a glue clamp (1). On the base, two separate pieces (4) of paper are fixated using tape. These papers will assist in reading the results during the experiment, since they have a protractor drawn on them. The needle is inserted into the needle template at the third row and 7th column. This decision was made because the third row is high enough that the force sensors do not interfere with the results but low enough that the reading is still easy to extract, and because the 7th column is located in the middle of the template. The force sensor (5) that is used during this experiment is a specific load cell from Futek, and is calibrated at 10N. It posses an eye bolt at both ends, one end is used to attach a string while the other end is fixated. This sensor measures the difference in voltage created by the force acting on it, the analog signal conditioner and DAQ will translate these values so that they can be read on the computer using Labview. Lastly, a ruler was used to measure the deflection, vertical deviation and insertion depth.

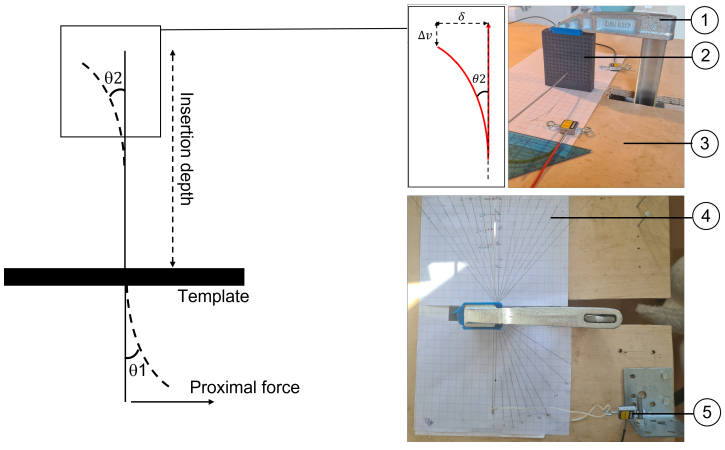

Figure 3.1: Set-up of the needle deflection in air experiment. The figure on the left is a schematic drawing of the set-up. The two figures on the right are pictures of the experiment in reality. θ_2 is the distal angle of the needle, θ_1 is the proximal angle of the needle. δ is the deflection of the needle and Δv is the vertical deviation of the needle. F_p represent the proximal force applied upon the needle.

The needle in this experiment is borrowed from a previous project. Its stylet is made of a spring steel solid wire, engraved with slots, and intended to be used in high dose rate brachytherapy. The dimensions of this needle are presented in table 3.1

Parameter	Description	
L [mm]	Needle length	240
D_n [mm]	Diameter of the stylet	1.40
D_c [mm]	Diameter of the catheter	1.50
S_w [mm]	The width of the slots in the inner needle	0.12
S_L [mm]	Slot length	227

Table 3.1: The variables of the spring steel steerable needle, used in the experiment

3.1.2. Procedure

The needle is inserted into the template, till the desired insertion depth. After which the force sensor is attached, and calibrated by accounting for the offset. After which a force is applied on the needle using the string that is attached to the force sensor. The amount of force applied onto the needle is between 0N and 5N. First small forces are applied under the 1N, to examine if the needle can handle the forces applied onto it, after which larger forces were applied. Per insertion depth it was decided up to which maximum force the experiment was executed. Overall the maximum force was set at 5N, larger force and therefore deflection is possible to evaluate, however due to the fact that the needle was required to be undamaged, this was not performed. By using a small clamp the string is fixated in place to ensure a constant force, while measuring the deflection, vertical deviation, proximal angle and distal angle. This experiment was repeated four times, for different insertion depths (140mm, 120mm, 100mm and 80mm).

3.2. Results

Table 3.2 gives an overview of the deflection for all measured insertion depths. In addition it also gives the forces acting on the needle and the angle that the needle makes during the tests. The results show that an increased insertion depth results in a larger deflection of the needle tip, what is expected from the theory in chapter 2. Furthermore, the angle of the needle on the distal side is a lot smaller then on the proximal side. It appears that as the needle has a shorter insertion depth, that the proximal angle needs to be larger for obtaining the same distal angle. The maximum deflection acquired with this spring steel needle was 27mm laterally over an insertion depth of 140mm. The force required for this deflection was 5.3N.

Insertion depth	Deflection [mm]	Proximal force [N]	Proximal angle [Deg]	Distal angle [Deg]	Vertical deviation [mm]
80mm	2,5	0,225	7,0	2,0	0,04
	4,5	0,408	10,0	3,0	0,13
	5,0	0,408	10,0	3,5	0,16
	5,5	0,623	14,0	4,0	0,19
	7,0	0,623	15,0	5,0	0,31
	8,0	0,837	17,0	5,5	0,40
	9,0	0,753	20,0	6,5	0,51
	10,0	1,016	24,0	7,0	0,63
	13,5	2,109	35,0	9,5	1,15
100mm	4,0	0,350	5,0	2,0	0,08
	6,0	0,424	9,0	3,5	0,18
	7,0	0,608	11,5	4,0	0,25
	7,0	0,633	10,0	4,0	0,25
	8,5	0,822	15,0	4,5	0,36
	9,0	0,613	15,0	5,0	0,41
	10,5	0,766	19,0	5,5	0,55
	11,0	1,082	19,0	6,0	0,61
	14,0	2,241	32,0	8,0	0,98
	17,0	3,472	40,0	10,0	1,46
	20,0	4,764	50,0	11,0	2,02
120mm	5,0	0,260	6,0	2,5	0,10
	5,5	0,424	7,0	2,5	0,13
	7,5	0,618	10,0	3,5	0,23
	8,0	0,470	10,0	3,5	0,27
	8,5	0,516	11,0	4,0	0,30
	10,0	0,648	14,0	4,5	0,42
	12,5	0,812	16,0	6,0	0,65
	16,5	2,272	29,0	7,5	1,14
	19,5	3,012	33,0	9,0	1,59
	22,0	4,483	42,0	10,5	2,03
	24,0	5,826	43,5	11,5	2,42
140mm	6,0	0,429	5,0	2,5	0,13
	7,0	0,403	5,0	3,0	0,18
	8,0	0,602	7,0	3,0	0,23
	8,0	0,444	6,5	3,0	0,23
	10,0	0,557	9,0	4,0	0,36
	12,0	0,751	11,0	4,5	0,52
	15,0	1,052	15,0	6,0	0,81
	17,0	3,584	28,0	6,5	1,04
	21,0	4,187	38,0	8,5	1,58
	27,0	5,305	40,0	11,0	2,63

Table 3.2: Unedited results of the experiment with a steerable spring steel needle in air

3.3. Comparison between theory and practice

3.3.1. Needle tip path

Parameter	Description	Value
L_n [mm]	Insertion depth	140/120/100/80
d_n [mm]	Outer diameter of the stylet	1.40
d_c [mm]	Inner diameter of the catheter	1.50
S_w [mm]	The width of the slots in the inner needle	0.12
ω [mm]	Distance centroid needle to centroid upper half	0.38
u_r[mm]	Elongation or abridgment of upper or lower segment	(0 - 0.81)

Table 3.3: The variables of the spring steel steerable needle, used in the model for the deflection of the needle tip

Figure 3.2 shows the comparison between the deflection of the needle tip that was predicted with the model, and the actual path it traveled during the experiment. For a detailed view of this graph, one can take a look at appendix B. For the first insertion depth (80mm) a visualization of the needle is included to aid reading the graph. As shown in this graph, the paths of the predicted and actual deflection look similar. Meaning that the model can be used to simulate the path of the needle tip, and therefore the deflection of the needle. This model can help with the design of the needle, since it is dependent on the diameter of the catheter, the diameter of the needle, the width of the slots, and the insertion depth.

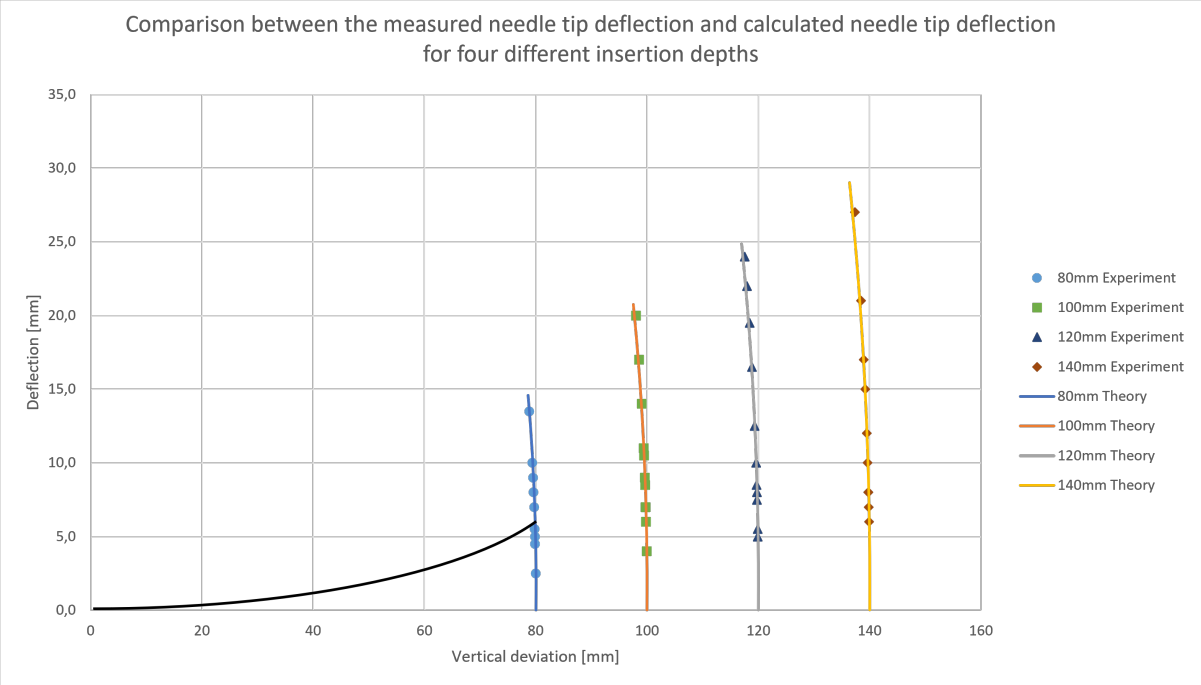

Figure 3.2: Comparison of the needle tip path, for the modelled path (line) and the measured path during the experiment (dots). For four different insertion depths.

3.3.2. Second moment of inertia

The three point bending test measurements of EI during experiment 1, 2 and 3 are 0.00661Nm^2, 0.00703Nm^2 and 0.00719Nm^2 respectively. As an average, 0.00694Nm^2 is used for the value of EI of the steerable spring steel needle.

$$EI_{needle} = EI_{stylet} + EI_{catheter} \tag{3.1}$$

The catheter is a commercially available flexible outer catheter of polyamide (Pro- Guide1 sharp 6F needle, Elekta Instrument AB, Stockholm, Sweden). The type of polyamide that they use is PA6427, which has a young's modulus of approximately 1 GPa. The second moment of inertia of the catheter can be calculated, based on the standard formula for the inertia of a cylinder. For this specific catheter the outer diameter is 2.00mm and the inner diameter 1.50mm.

$$I_{catheter} = \frac{\pi * (D_o^4 - D_i^4)}{64} = 0.5369mm^4 \tag{3.2}$$

$$EI_{catheter} = 0.0005369Nm^2 \tag{3.3}$$

The stylet is made of spring steel wire, which has a young's modulus of 193 GPa [26]. To eventually come to the conclusion of the second moment of inertia of the inner needle or stylet, equation 3.1 is rewritten and filled in with the known variables.

$$I_{stylet} = \frac{EI_{needle} - EI_{catheter}}{E_{stylet}} = 0.034478mm^4 \tag{3.4}$$

The calculated value for the second moment of inertia of the stylet can be used in equation 2.10, this is demonstrated in section 3.3.3.

3.3.3. Deflection prediction

As explained in section 2.2, the distal deflection of the needle during insertion can be predicted beforehand, based on the proximal angle and the parameters of the needle. During the experiment, four different insertion depths were used, which influenced the length L_1. Furthermore the length of the slot was constant, the proximal and distal deflection and the proximal and distal angle of the needle were measured. It should be noted that when the needle deflects it follows a curve, while the angles that were measured assume a straight line from the template to the endpoint. In addition, the distal deflection can also be predicted based on the proximal force, as explained in section 2.3. In table 3.4 the parameters of the spring steel needle are summed up.

Parameter	Description	Value
L [mm]	Needle length	240
D_n [mm]	Diameter of the stylet	1.40
D_c [mm]	Diameter of the catheter	1.50
S_w [mm]	The width of the slots in the inner needle	0.12
L_n [mm]	Insertion depth	140/120/100/80
ω [mm]	Distance centroid needle to centroid upper half	0.38
R [m]	Radius of the stylet	0.0007 m
L_{out} [m]	Length of the proximal side	0.160/0.140/0.120/0.100
L_1 [m]	Length from the template until the end of the slot	0.0785/0.0985/0.1185/0.1385
L_{slot} [m]	Length of the slot	0.227
A [m^2]	Area of the stylet	1.287*10^-6
A_s [m^2]	Area of one segment of the stylet	0.322*10^-6
I_{stylet}[m^4]	Second moment of inertia of the stylet	0.0345*10^-12
EI [Nm^2]	Flexural rigidity of the needle	0.00719
E [GPa]	Young's modulus of the material of the stylet	193

Table 3.4: The variables of the spring steel needle, used in the model for the deflection prediction based on the proximal angle and proximal force

3.3.4. Comparison between the three theories

Table 3.5 presents the results of the comparison between the measured and calculated deflection of the spring steel needle. The first column indicates the insertion depth of the needle during the experiment and the second column shows the measured distal deflection. The following three columns present the calculated distal deflection using the different theories. Theory 3 is based on the proximal force, as explained in section 2.3. Theory 2 is based on the proximal angle, where theory 2.1 uses the value I_{stylet} (equation 2.10) and theory 2.2 uses the entire value EI (equation 2.11), these theories are both explained in section 2.2.

Insertion depth [mm]	Distal deflection measured [mm]	Distal deflection calculated with theory 3 [mm]	Distal deflection calculated with theory 2.1 [mm]	Distal deflection calculated with theory 2.2 [mm]
80mm	2,50	2,45	6,00	5,82
	4,50	4,46	8,59	8,32
	5,00	4,46	8,59	8,32
	5,50	6,80	12,07	11,69
	7,00	6,80	12,94	12,54
	8,00	9,12	14,70	14,25
	9,00	8,21	17,37	16,83
100mm	4,00	5,22	5,81	5,66
	6,00	6,33	10,48	10,20
	7,00	9,06	13,43	13,07
	7,00	9,44	11,66	11,35
	8,50	12,23	17,59	17,11
	9,00	9,13	17,59	17,11
	10,50	11,41	22,41	21,80
120mm	5,00	4,80	8,87	8,67
	5,50	7,81	10,36	10,12
	7,50	11,37	14,84	14,49
	8,00	8,65	14,84	14,49
	8,50	9,49	16,34	15,95
	10,00	11,92	20,87	20,38
	12,50	14,91	23,93	23,36
140mm	6,00	8,96	9,01	8,82
	7,00	8,42	9,01	8,82
	8,00	12,56	12,63	12,36
	8,00	9,28	11,72	11,47
	10,00	11,62	16,26	15,92
	12,00	15,64	19,92	19,50
	15,00	21,84	27,32	26,74

Table 3.5: The comparison between the measured deflection during the experiment and the three theories. Theory 3 = based on proximal force, theory 2.1 = based on proximal angle using I_stylet, theory 2.2 = based on proximal angle using EI.

For the two theories that predict the distal deflection using the proximal angle, theory 2.1 and 2.2, the error between the measured and calculated deflection is 15.1mm ±15.2mm and 14.4mm ±14.6mm respectively. The error between the measured and calculated deflection based on the proximal force is 1.77mm ±1.6mm.

3.4. Discussion

During the experiments it was demonstrated that theory 2 gives abnormal results for larger proximal angles. This can be due to the fact that the Euler–Bernoulli beam theory is only meant for small deflection, or due to measurement of the proximal angle. Because the needle is very flexible and a moment is applied on the proximal end, it is not bending in a straight manner but it bends in a curve. The proximal angle used in the previous equations was measured in a straight line from the template to the endpoint.

According to Avila-Carrasco et al. [19] there is a certain threshold of the positioning error of the seeds under which a significant change of radiation dose can be prevented. This threshold ranges from 2 tot 5mm, confirming the importance of targeting accuracy.

It turns out that the theory for the prediction of the needle tip path, and the distal deflection based on the proximal force are adequate enough. Since they have error values that are still below the threshold mentioned above. The parameters in these two equations will be analysed in chapter 6, this will create a better understand about which parameters need to be changed for a certain application of the steerable needle. Subsequently, in chapter 7 these two theories will be used to design a steerable needle for low dose rate brachytherapy.

4

Needle deflection inside tissue theory

4.1. Introduction

Previously the theory of needle deflection in air is discussed, this will form the basis of the needle theory that is to come. This chapter will discuss the needle deflection in tissue, since the needle eventually will be used in human tissue, this deflection behaviour is important to research. The tissue will affect the deflection of the needle because it applies an extra force onto the needle. What force those are, and how they affect the deflection of the needle will be discussed in this chapter.

4.2. Deflection theory

The deflection of the needle can be calculated using the classic model for a static beam. Since the needle is only fixated at the base or proximal side, by the hand of the surgeon, it can be represented as a cantilever beam. The equations presented below are based on the Euler-Bernoulli beam theory, and can be found in the book mechanics of materials by Hibbeler [27].

$$\delta = \frac{FL^3}{3EI} \qquad (4.1a) \qquad\qquad \delta = \frac{wL^4}{8EI} \qquad (4.1b)$$

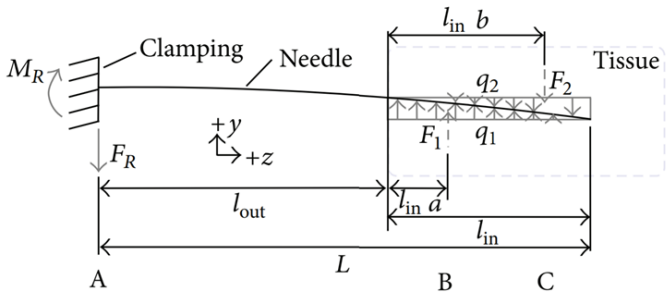

Figure 4.1: Free body diagram of the needle bending in tissue. [8]

As presented in Figure 4.1, the forces that act upon the needle are mainly because of the needle-tissue interactions. The needle exerts a distributed load onto the tissue, that increases as the insertion depth increases. This force is created because the needle works like a loaded spring; as the needle is inserted deeper into the tissue, the deflection increases. But the needle wants to go back to its initial unbent state, but is kept in place by the tissue. The tissue in return acts a force upon the needle to maintain equilibrium and keep the needle in its bent state. These two distributed forces are presented in Figure 4.1 as q1 and q2. According to the classic mechanics of materials, a distributed load can be represented by a resultant force that acts on the geometric center of the area of the distributed load. In this specific case the distributed load is a triangle, meaning that the resultant forces F1 and F2 can be calculated as:

$$F1 = \frac{1}{2} * L_{in} * q1 \qquad (4.2a) \qquad\qquad F2 = \frac{1}{2} * L_{in} * q2 \qquad (4.2b)$$

The specific locations where the resultant forces act upon are located at the centroid of the triangle. Which equals to $\frac{1}{3}$ and $\frac{2}{3}$ of the inserted length. By recalculating these distributed loads to resultant forces, the equations concerning the deflection of the needle will be simplified.

The second order differential equation for the elastic curve of a beam deflection, which is based on equation 4.1, is given in equation 4.3. Where P is the force, EI is the flexural rigidity of the needle, y is the deflection and x is the distance from the base. To specify this even more, E is the young's modulus and I is the area moment of inertia of the needle. The deflection y can be calculated using equation 4.3. How this equation is derived, is explain in appendix E.2.

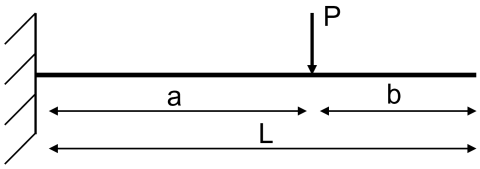

Figure 4.2: Free body diagram of the bending theory for a basic cantilever beam.

$$y = \frac{Px^2(3L - x)}{6EI} \tag{4.3}$$

The length 'x' in this equation would be translated to $(lout + lin * a)$ in the case for F1. For the second force F2, this is changed to $(lout + lin * b)$, because this force has a different point of engagement. Presented below in equations 4.4, 4.5 and 4.6, the classic equation for a cantilever beam is adapted to accommodate the deflection situation of the needle as presented in Figure 4.1.

$$\delta_1 = \frac{F_1(L_{out} + l_{in}a)^2(3L - L_{out} - l_{in}a)}{6EI} \tag{4.4}$$

$$\delta_1 = -\frac{F_2(L_{out} + l_{in}b)^2(3L - L_{out} - l_{in}b)}{6EI} \tag{4.5}$$

$$\delta_{1,2} = \delta_1 + \delta_2 = \frac{F_1(L_{out} + l_{in}a)^2(3L - L_{out} - l_{in}a)}{6EI} - \frac{F_2(L_{out} + l_{in}b)^2(3L - L_{out} - l_{in}b)}{6EI} \tag{4.6}$$

In the equation for the deflection of the needle that has been explained in the paragraph above, there are a few parameters that are still unknown. That is the forces F1 and F2. These two forces can be calculated by drawing a free body diagram of the needle, and use this to obtain the equilibrium conditions.

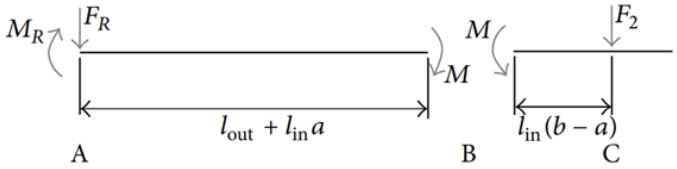

Figure 4.3: Free body diagram of the section of the beam to visualize equations 4.7 and 4.8 [8]

$$-M_R + F_R(L_{out} + l_{in}a) = F_2 L_{in}(b - a) \tag{4.7}$$

$$F_2 = \frac{-M_R + F_R(L_{out} + l_{in}a)}{L_{in}(b - a)} \tag{4.8}$$

In equation 4.8, where F2 is being calculated, there are still 2 unknown parameters. These two are the resultant force and resultant moment at the proximal side of the needle. These two values can be obtained by doing an experiment and testing them. Eventually by drawing another free body diagram of the needle the equilibrium equation can be composed of the three vertical forces. Resulting in equation 4.9.

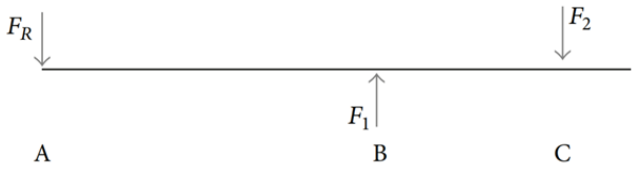

Figure 4.4: Free body diagram to display the force equilibrium of the beam

$$F_1 = F_2 + F_R \tag{4.9}$$

4.2.1. Prediction without moment sensor

The model presented above has great potential if the proximal force and the proximal moment are known. However a moment sensor for such a small range is not available. Therefore the theory presented above is simplified, by creating a resultant force that combines F1 and F2.

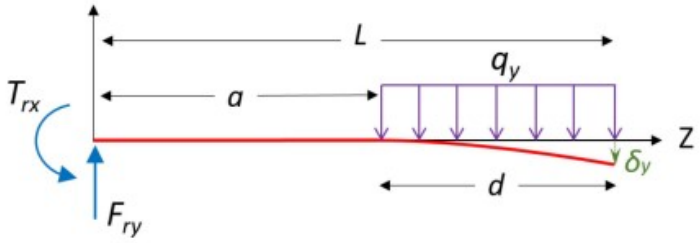

Figure 4.5: Free body diagram of the needle bending inside tissue, used to calculated the deflection without knowing the proximal moment on the needle. [19]

$$\delta_y = \frac{q_y}{24EI}(3L^4 - 4a^3L + a^4) \tag{4.10}$$

If the distributed force 'q_y' is known, then the deflection of the needle in tissue can be predicted. This force is the combination of the force that the tissue exerts onto the needle, and the force that the needle applies onto the tissue. The distributed force could be determined empirically.

5

Material considerations

5.1. Introduction

The material that the needle is composed of influence the flexural rigidity and therefore its ability to bend. In addition, the material also influences a parameter like the yielding of the needle. Which is an unwanted effect that can be prevented when the correct material is chosen. First the axial stress on the needle will be discussed, after which potential candidate materials for the design of the needle are analyzed.

5.2. Yielding

The yield strength indicates at what stress levels the needle will start to experience plastic deformation. To make sure that the needle does not deform permanently during use, the yield strength of the material must be taken into account.
The axial stress, is created by the force acting directly onto the needle tip, and can be calculated using equation 5.1. It will probably be largest during the initial insertion though the skin, or when entering the prostate capsule. According to Podder et al. [7] the maximum axial force they measured are 15.6N and 8.9N for a 17G and 18G needle respectively. The outer and inner diameter of a 17G needle are 1.473mm and 1.067mm respectively. For a 18G needle they are 1.270mm and 0.838mm [28].

$$\sigma = \frac{F}{A} \tag{5.1}$$

$$\sigma_{17G} = \frac{15.6}{(\pi * (0.7365 * 10^{-}3)^2)} = 9.15MPa \tag{5.2a}$$

$$\sigma_{18G} = \frac{8.9}{\pi * (0.635 * 10^{-}3)^2)} = 7.03MPa \tag{5.2b}$$

With materials like nitinol, patented steel wire and stainless steel, the yield strength values are approximately 70-690MPa, 2700-3300MPa, and 190-220MPa respectively. These values are all abundantly larger than the axial load on the needle during insertion. Meaning that the axial stress will not be a bottle neck for the needle design.
Materials used in current steerable needles can form a base on which an estimation can be made for the yield strength. These materials and their values of the yield strength will be discussed in section 5.3.

5.3. Candidate materials

In addition to yielding the material that is used in the needle also affects its flexural rigidity and therefore its bending properties. Materials with a higher young's modulus require more force to bend. The type of material also determines the maximal deflection, for example brittle materials are less suitable for bending then ductile materials. In section 1.4.5 a few materials are mentioned that are used in existing steerable needles. Meaning they are for sure bio-compatible, and therefore suitable to be inserted into the patients body. Furthermore, the mass density of the material is also of importance for the steerable needle. In order for the ultrasound probe to detect the needle inserted into the prostate, the mass density

of the material of the needle should differ from the mass density of the human tissue. The larger the difference in this mass density between the two materials, the clearer the image will be. Rigid standard needles used for brachytherapy are often made from stainless steel, which has a mass density between 7870 and 8000 kg/m^3 according to CES Edupack database. A few examples of human tissue densities that might be involved during brachytherapy in the prostate, are fat, muscle and prostate tissue, which have a mass density of 991 kg/m^3, 1090 kg/m^3 and 1045 kg/m^3 respectively [29]. The current LDR needles are qualified for ultrasound, and are made of stainless steel [4][5]. When choosing a material for the steerable needle, the ratio between the material and the tissue should resemble that of stainless steel and tissue, i.e. 7:1.
Using the program CES Edupack, a graph is created that presents the young's modulus and yield strength of materials. The graph is zoomed in on patented steel, since this is a good candidate for a steerable needle but is not available in tube form. The aim was made to search for a material that has comparable properties to patented steel.

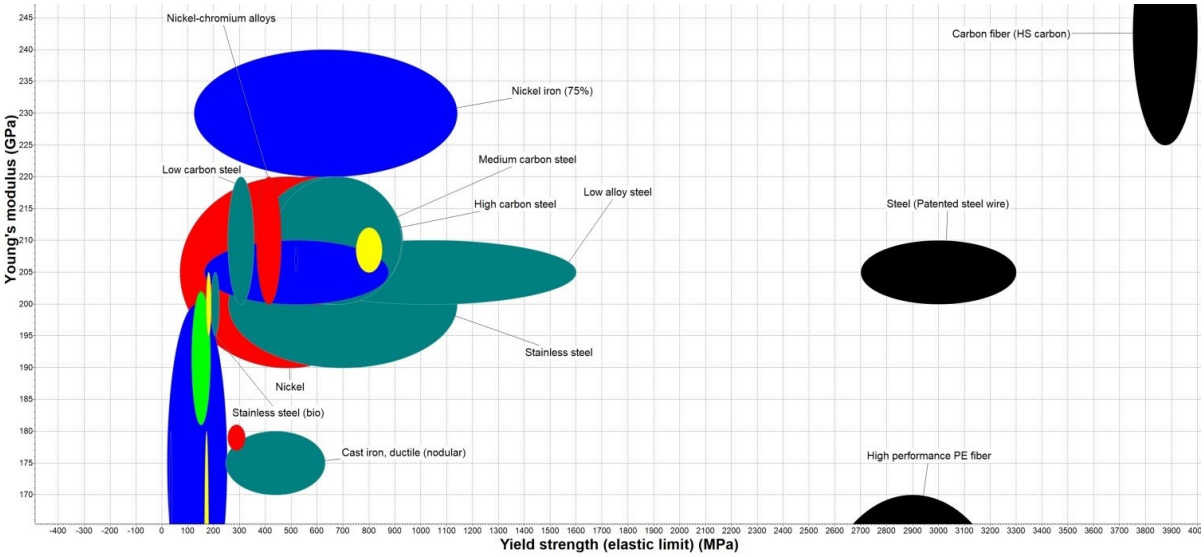

Figure 5.1: Cambridge engineering selector (CES) material selection graph. With on the y-axis the young's modulus in GPa, and on the x-axis the yield strength in MPa. In search of a material with properties comparable to patented steel wire.

Table 5.1 presents the material properties of the previously mentioned materials. The most important property in these tables is the young's modulus (E), because it influences the flexural rigidity of the needle and therefore also multiple other parameters which will be discussed in chapter 6.

	Youngs modulus	**Yield strength**	**Mass density**	**Price**	**Guidance for MRI safety**
unit	Gpa	MPa	kg/m^3	EUR/kg	
Patented steel	200-210	2.7e3 – 3.3e3	7.85e3 – 7.9e3	0,645 - 0,716	Caution
Nitinol (martensitic)	28 - 41	70 - 140	6,41e3 - 6,54e3	15,9 - 18,2	Low risk
Nitinol (austenitic)	41 - 83	195 - 690	6,41e3 - 6,54e3	15,9 - 18,1	Low risk
Stainless steel (bio)	195 - 205	190 - 220	7,87e3 - 8e3	4,91 - 5,41	Caution
Titanium (bio)	100 - 105	276 - 360	4,51e3	12,8 - 14,3	Low risk
Nickel-chromium	200 - 220	365 - 460	8,3e3 - 8,5e3	11,3 - 14,3	Low risk
Nickel-iron (75%)	220 - 240	125 - 1,14e3	8,6e3 - 8,85e3	20 - 23,9	-
Nickel	190 - 220	70 - 900	8,83e3 - 8,95e3	6,7 - 9,02	Caution
Carbon fiber	225 - 260	3,75e3 - 4e3	1,8e3 - 1,84e3	21,4 - 28,6	Low risk
Tungsten	310 - 370	490 - 1,22e3	1,69e4 - 1,86e4	52,9 - 58,5	Low risk

Table 5.1: Overview of the potential materials for the steerable needle and their most important properties.

6

Parameter influence on needle behaviour

6.1. Introduction

As explained in 1.3, this thesis also aims to determine the parameters that influence the behaviour of the needle and how they do so. In this chapter the various parameters of the deflection prediction models are presented, and for each it is clarified how the needle behaviour is influenced by them. First the diameter of the needle is discussed, followed by the wall thickness which is on its turn also dependent on the diameter of both the needle and, if applicable, the catheter(s). In addition, the flexural rigidity is investigated. Furthermore, the slots that are engraved in the stylet are treated, including their length, width and how far they are located from the end of the needle. Finally, the insertion depth of the needle is looked into. For all these parameters, certain behaviours are examined; like the deflection, the total bending, the angle that the needle makes both proximal and distal and the second moment of inertia.

For the comparison of the various parameters, the deflection and vertical deviation of the needle are used quite often. However, some times these two cannot be compared with each other directly, because the equation in dependent on the elongation of the segments, ur. Therefore, the value ur and the total bending is used as the values that can be compared. The composition of the total bending is explained below.

$$\delta = \sqrt{\Delta Z^2 + \Delta Y^2} \tag{6.1}$$

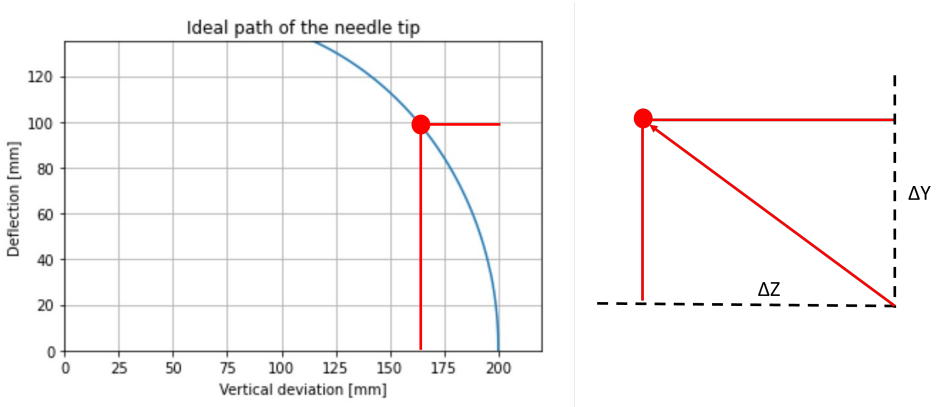

Figure 6.1: Visualisation of the explanation of the total bending of the needle.

The total bending of the needle tip, is the direct line from the initial starting point of the needle, to the location of the tip during bending. This value of total bending is therefore calculated with Pythagorean's theorem, as shown in equation 6.1. Figure 6.1 shows how this total bending value is related to the graph of the path of the needle tip, and therefore how it corresponds to the previously presented vertical deviation and deflection of the needle.

6.2. Diameter

The size of the individual parts that the needle is composed of, is one of the most important parameters. This includes the outer and inner diameter of the outer catheter, the stylet and the inner catheter. The diameters of these components influence the bending of the needle according to equations 2.8a, 2.8b in combination with 2.1. In addition, the diameter also influences the second moment of inertia and therefore the flexural rigidity and the needles ability to bend. For now the focus will be on the diameter, and the second moment of inertia will be discussed in section 6.3.

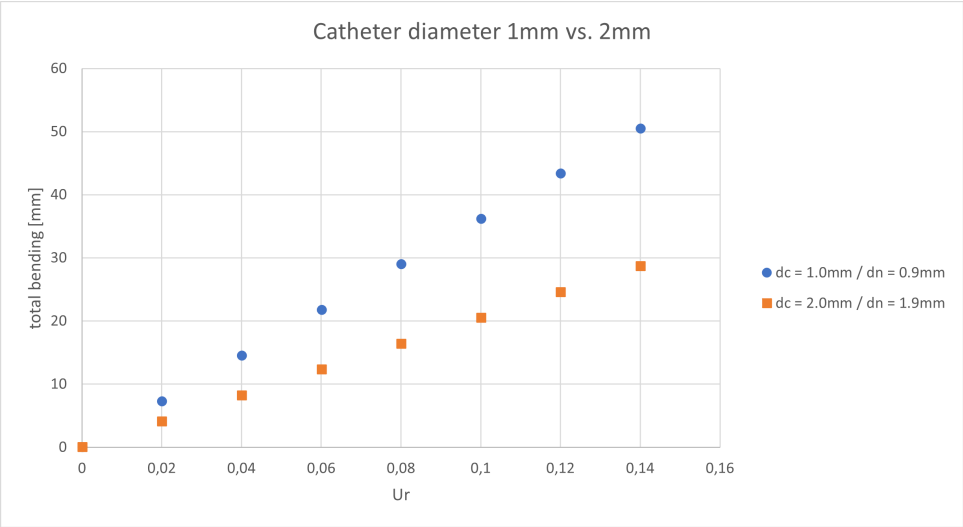

Figure 6.2: Comparison of the total bending of the needle with a smaller and larger diameter to find the influence of the parameter. Portraying two values for the inner diameter of the catheter: 1.0mm and 2.0mm.

As can be seen in graph 6.2, the total bending of the needle will be larger if the needle has a smaller diameter, in the case that distance between the catheter and the stylet is kept constant. This is to be expected since the diameter affects the second moment of inertia which in turn affects the bending of the needle.

The diameter of the needle also has an effect in the deflection theory based on the proximal force, which is described in section 2.3. In these equations the radius of the stylet is used instead of the diameter, but the influence will stay the same. In addition to the influence of 'R', the diameter also influences the 'area' variable in this equation. Confirming the important role the diameter plays in predicting the bending of the needle.

6.2.1. Wall thickness

The wall thickness of the individual components of the needle affects the second moment of inertia. The outer catheter as well as the stylet and the inner catheter all have a wall thickness that can influence the behaviour of the needle. Because the stylet is the actual part of the needle that is responsible for the steering, this component is used as the example. The wall thickness also affects the value for the centroid of the upper half of the needle. This parameter will be discussed the next paragraph.

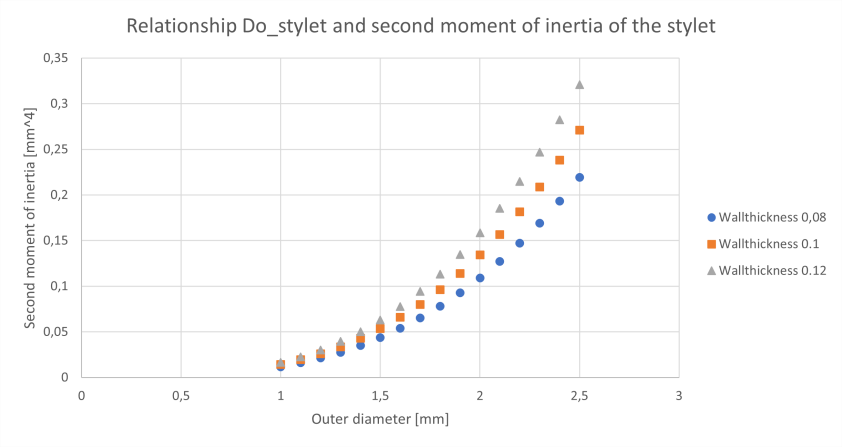

Figure 6.3: Comparison of the value of the second moment of inertia with different wall thicknesses, to find the influence of this parameter. Including three values for the wall thickness: 0.08mm, 0.1mm and 0.12mm.

Graph 6.3 shows the relation between the second moment of inertia and the outer diameter of the stylet. In this scenario the outer diameter of the stylet in changed, all the other parameters are kept constant. In addition to this, the wall thickness is changes by the changing outer diameter. First of all it shows that a larger diameter of the stylet results in a larger second moment of inertia, which in turn will result in less bending of the needle. Secondly, the second moment of inertia is larger for a needle with a thicker wall. Therefore, a needle with a thicker wall will bend less, then a needle with a thinner wall. It should be noted that at some point, when the wall thickness is increase too much, the needle will cease to bend. The same is true for a wall thickness that is too small, because the needle cannot withstand the forces needed for steering.

6.2.2. Centroid of the upper half

The distance from the centroid of the needle to the centroid of the upper half (ω) is dependent on the diameter and wall thickness of the needle as described in equation 2.7. Therefore the influence that this parameter has on the distal deflection is also affected by a change in diameter. As can be seen in graph 6.4 the distal deflection decreases with a larger distance for 'ω'.

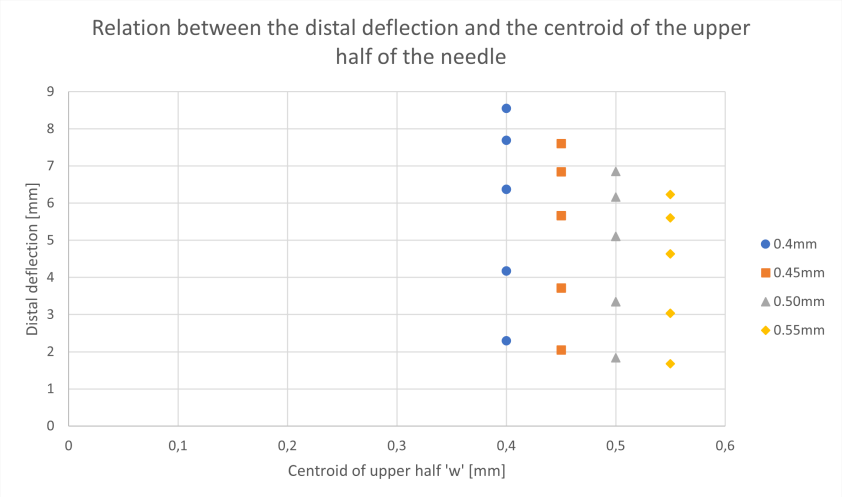

Figure 6.4: Comparison of the distal deflection calculated with the theory based on the proximal force, for four different values of the centroid of the upper half of the needle. The four values used are: 0.40mm, 0.45mm, 0.50mm and 0.55mm.

6.3. Flexural rigidity

The flexural rigidity is composed of the young's modulus and the second moment of inertia. This parameter is important because it can be found in multiple equations in this thesis. The young's modulus (E), is a fixed value, and is dependent on the material that is used in the needle. The young's modulus is also individual a parameter in equation 2.14. The second moment of inertia (I), is influences by the diameter of the components of the needle. Both the inner and outer diameter of the inner catheter, the outer catheter and stylet are important factors as explained in chapter 2.4. The second moment of inertia itself influences other variables of the needle. Like for example the deflection of the needle is dependent on the second moment of inertia, and so is the axial strength.

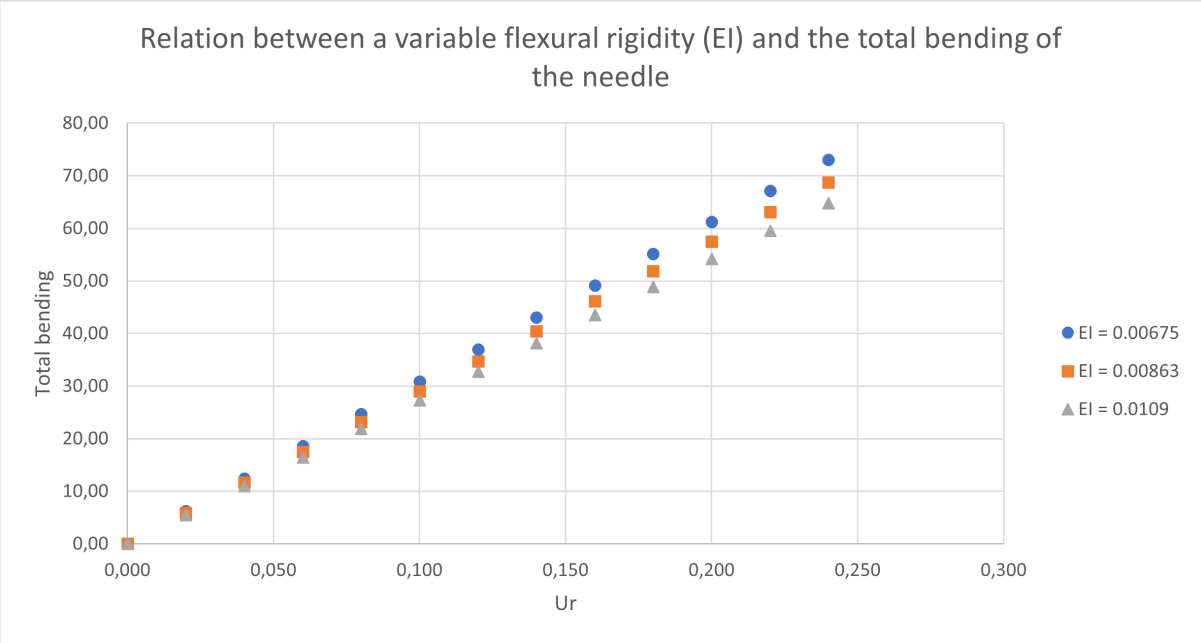

Figure 6.5: Comparison of the total bending of the needle with three different values for the flexural rigidity.

That the bending increases with a smaller value for the flexural rigidity is confirmed in graph 6.5. A needle with a smaller value for EI is weaker, and less rigid and therefore more prone to deflection. Here the total bending is plotted for three needles with different values for the flexural rigidity. It shows that the needle with the smallest value (0.00675), bends the furthest (73mm) compared with 69mm and 65mm for the two larger needles.

6.4. Slots

The slots that are engraved in the stylet of the needle affect its flexibility and creates the ability to steer. In this section the relations of the slots are investigated, including their width and distance from the end of the needle to the start/end of the slots.

6.4.1. Slot width

The width of the slots affects the second moment of inertia, which in turn affects the deflection of the needle. The slot width is represented in the deflection theory 1 (2.8b), but also indirectly in deflection theory 3 (2.14) due to the affect that the slot width has on the area of the segments and the centroid of the upper half.

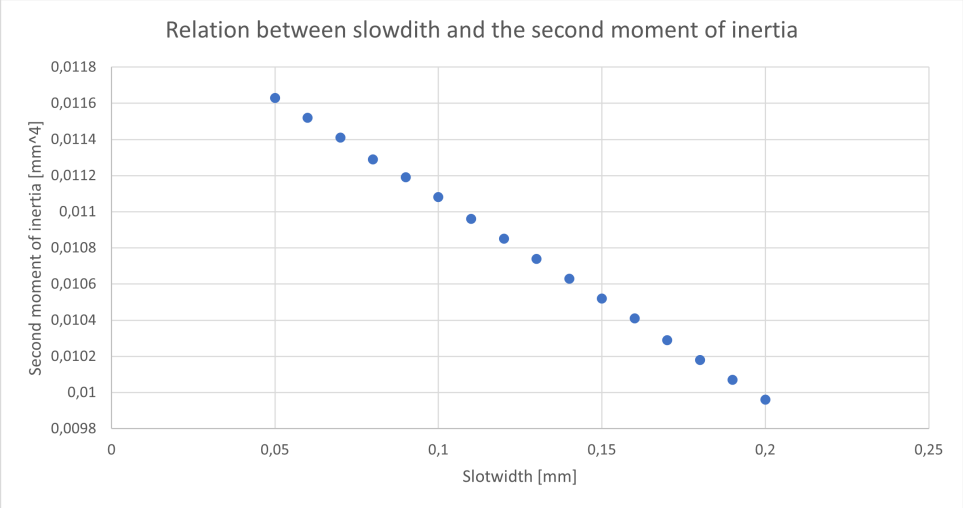

Figure 6.6: Relationship between the slot width and the second moment of inertia of the stylet for a constant size of the stylet. Outer diameter = 1.40mm and inner diameter = 1.28mm

Graph 6.6 displays the relation between the slot width and the second moment of inertia. This graph was made by calculating the second moment of inertia of the stylet when altering the slot width. It clearly shows that with larger slot widths, the second moment of inertia of the needle decreases. Which is exactly what would be expected according to the equations. The second moment of inertia, which is influenced by the slot width, affect the flexural rigidity of the needle as explained in section 6.3. So the a larger slot width causes the needle to deflect further.

6.4.2. Slot distance from the end of the needle

According to equation 2.14, the elongation of the segments of the needle is dependent on the proximal force, the area of a segment, the young's modulus of the material of the segment and the length L_1. The latter is determined as the insertion depth of the needle minus the length L_3, which is the distance between the end of the slot and the end of the needle. It was investigated if this distance would have a major impact on the distal deflection of the needle. As can be seen in graph 6.8 the distal deflection increases as the length L1 increases. With about 14mm of difference between the length L1, the deflection increases with 2mm.

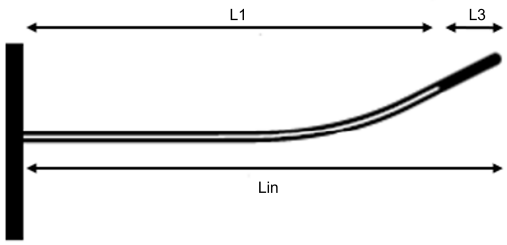

Figure 6.7: Schematic of the two lengths represented as L1 and L3

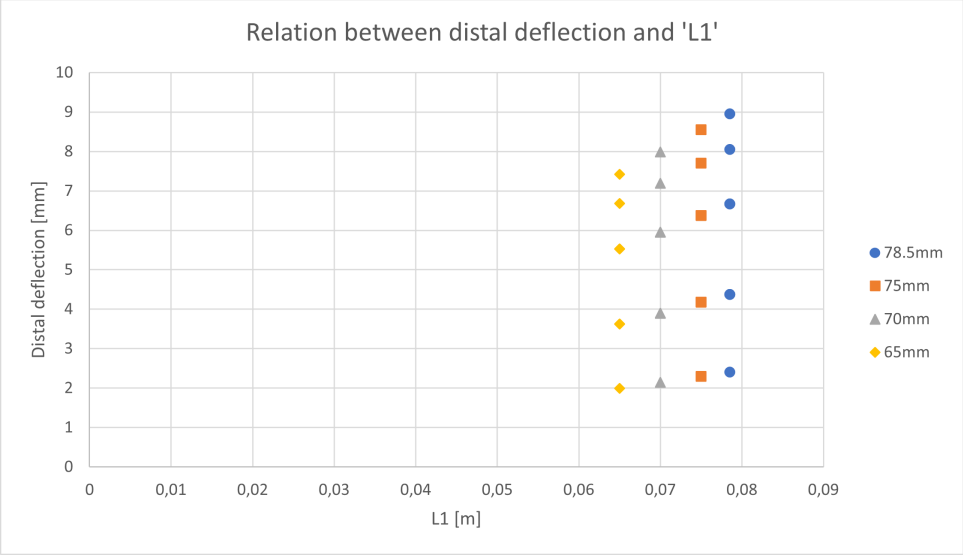

Figure 6.8: Comparison of the distal deflection calculated with the theory based on the proximal force, with four different lengths for L1.

6.5. Insertion depth

The insertion depth of the needle is another parameter that has a major influence on the behaviour of the needle. In this section these behavioural changes will be discussed. Starting with the effect on the deflection of the needle, followed by the needle tip path, the total bending and the distal deflection.

In the basic Euler-Bernoulli formula for deflection 4.1a, the length is already incorporated. This length in this equation represents the distance from where the needle is fixed until its end, aka from the template and thus from where the needle is inserted.

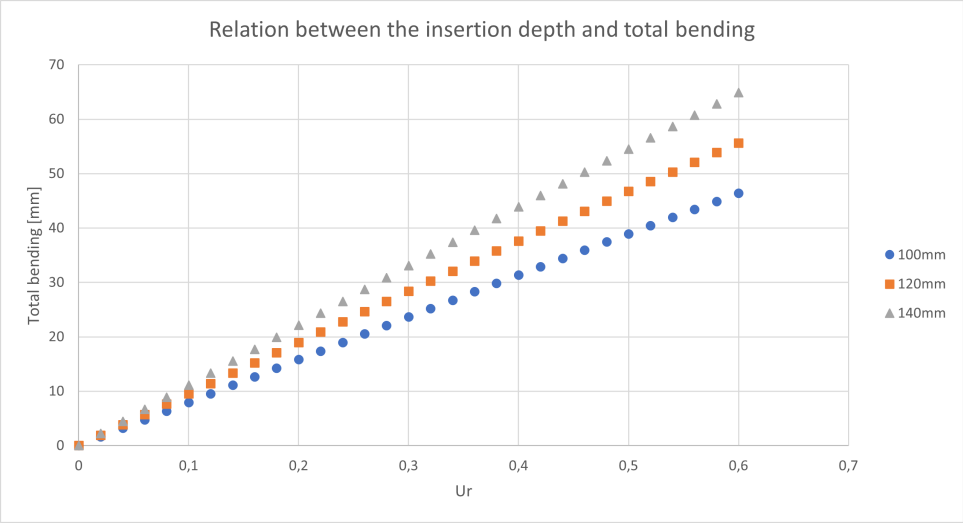

Figure 6.9: Comparison of the total bending of the needle with three different insertion depths. Using a constant slot width: Sw = 0.12mm, catheter diameter: Dc = 2.00mm, and needle diameter: Dn = 1.40mm

Graph 6.9 shows the total bending of a needle with different insertion depths. The total bending increases with insertion depth, at the same proximal action.

From this graph, it can be concluded that the needle deflects more when the insertion depth is more. This makes sense when equation 4.1a is used. As can be seen in this equation, the length is to the power of three, resulting in a larger deflection for a longer length.

7

Needle designs

7.1. Introduction

Based on the previously discussed theory about the deflection of the needle and the influence of the individual parameters, a large number of potential concepts are developed. Only a select few will be discussed in this chapter, the remaining concepts can be found in appendix C.2. These concepts are selected on how well they match the criteria of the needle and on the availability of their components. First the general material and dimension choices will be discussed, followed by the explanation of the concepts for a low dose rate nitinol needle, concepts for a smaller nitinol needle and the final needle design.

7.2. General design choices

7.2.1. Material choice

From table 5.1 it can be concluded that patented steel and spring steel are both satisfactory materials for the development of the stylet for a steerable needle. These two materials have already been used for previous designs of a steerable needle, confirming that they would perform sufficiently. However both materials are only available as a wire form, and not the desired tube. Therefore different materials were chosen. Both nitinol and carbon fiber are potential candidates for the steerable needle and have promising properties, they could possibly provide a new perspective into using alternative materials for steering. Nitinol would be a candidate for brachytherapy procedures using ultrasound, because the mass density of this material differs enough from the human tissue. The ratio between the mass density of nitinol and human tissue is roughly 1:6. Carbon fiber however would probably be a better candidate for MRI, since it only has a ratio of 1:1.5. However, the slot for the steering of the needle cannot be engraved in carbon fiber using EDM. It is possible with laser cutting, but a location to execute this process was not found in time. Therefore, the material of the concepts are all focused on nitinol. For future research the carbon fiber concepts that are presented in appendix C.2 could be tested.

7.2.2. Dimensions

For the design of the steerable needle for low dose rate brachytherapy in the prostate, the first step will be to determine the required inner lumen. As presented in chapter 1.5 the requirement for the inner lumen of the needle is 0.96mm for the stranded seeds. Including the margin taken to ensure that the seeds can fit through the curve of the needle, the inner lumen must be at least 1.10mm. In addition, the length of the needle must be longer then 150mm, to ensure insertion into the prostate.

7.3. Concepts for steerable tube needles

All concepts are based on the previous theory with regards to material and dimensions. Three concepts were made with this in mind. The appendix C.2 can be consulted for further information about these concepts. All concepts are bound by the availability of the materials. Unfortunately the materials needed for concept 1 were not available, therefore only concept 2 and 3 will be discussed below.

7.3.1. Concepts nitinol LDR needle

Concepts 2 and 3 both have the same outer catheter made of polyimide, which has a Young's modulus of 4GPa. This type of plastic is transparent with a light amber colour. Furthermore, the stylet for these two needles are both made of nitinol, and have the same outer diameter. The difference between the two is their inner diameter which differs 0.055mm. Due to a smaller inner diameter for concept 2, the inner catheter must be smaller as well. The inner catheter for concept 2 is made of the same material as its outer catheter, i.e. polyimide, but with different dimensions. For concept 3, a standard 5F catheter is used, which is made from polyamide. All of the dimensions mentioned above, and additional details on the needle design are presented in table 7.1. The parameters that differ between the two concepts are made bold for clarification purposes.

		Concept 2	**Concept 3**
Outer catheter	Outer diameter [mm]	1.90	1.90
	Inner diameter [mm]	1.88	1.88
	Wall thickness [mm]	0.02	0.02
	Material (E-modulus) [GPa]	Polyimide (~4)	Polyimide (~4)
Stylet	Outer diameter [mm]	1.80	1.80
	Inner diameter [mm]	**1.67**	**1.725**
	Wall thickness [mm]	**0.13**	**0.075**
	Material (E-modulus) [GPa]	Nitinol (28-83)	Nitinol (28-83)
	Slot width [mm]	0.12	0.12
Inner catheter	Outer diameter [mm]	**1.57**	**1.667** (5F)
	Inner diameter [mm]	**1.47**	**1.43**
	Wall thickness [mm]	**0.1**	**0.24**
	Material (E-modulus) [GPa]	Polyamide (~1)	Polyamide (~1)
EI		0,00618 Nm^2	0,00388 Nm^2

Table 7.1: Dimensions and properties of concept 2 and concept 3.

After investigating the nitinol tube (without slots), and examining its bending, it seems that this tube would be too flexible to provide steering. This is due to the thin wall thickness of the stylet of both concepts. By adding slots this unwanted flexibility would only be enhanced. Especially when testing in tissue stimulant, the incapability of steering will be amplified due to the increasing forces acting on the needle. Based on the same principle as concept 2 and concept 3, two new concepts were designed, with a larger wall thickness but the same materials.

7.3.2. Concepts nitinol needle

In order for the wall thickness to be larger, space elsewhere in the needle needs to be sacrificed. There are two solutions to this problem, either the outer diameter of the needle needs to be increased above 2mm, or the inner lumen of the needle needs to decrease. Due to the available materials it was decided to choose the latter. Because of this, the inner lumen of the two concepts presented below are not large enough for the radioactive seeds to pass though. However, the proof of principle for a steerable tube can still be provided.

		Concept 7	**Concept 8**
Outer cathter	Outer diameter [mm]	1.90	1.90
	Inner diameter [mm]	1.88	1.88
	Wall thickness [mm]	0.02	0.02
	Material (E-modulus) [GPa]	Polyimide (~4)	Polyimide (~4)
Stylet	Outer diameter [mm]	**1.60**	**1.67**
	Inner diameter [mm]	**1.08**	**1.37**
	Wall thickness [mm]	**0.52**	**0.30**
	Material (E-modulus) [GPa]	Nitinol (28-83)	Nitinol (28-83)
	Slot width [mm]	0.12	0.12
Inner catheter	Outer diameter [mm]	1.00	1.00
	Inner diameter [mm]	0.70	0.70
	Wall thickness [mm]	0.30	0.30
	Material (E-modulus) [GPa]	Teflon (~0.575)	Teflon (~0.575)
	EI	0,0125 Nm^2	0,0104 Nm^2

Table 7.2: Dimensions and properties of concept 7 and concept 8.

The outer catheter for concept 7 and 8 are the same as for concept 2 and 3. The stylet however is made from a nitinol tube with a significantly larger wall thickness. The wall thickness for concept 7 is four times larger then for concept 2. The inner catheter for concept 7 and concept 8 are the same, they are made of PTFE and are very small in order for them to fit inside of the stylet. All dimensions for concept 7 and 8 are presented in table 7.2

7.4. Final design nitinol needle

Eventually only one nitinol needle will be made. It was decided to manufacture concept 7 because this design has the largest wall thickness and therefore more rigidity. In addition to the dimensions of the tubes that are used in this design, there are more aspects to the needle that need to be designed. The needle should have a sharp tip to be able to cut through tissue, especially the skin and the prostate capsule and known to be tough. Since this needle has an open end a conical tip was not possible, therefore it was decided to create a tip that looks like the tip of a standard rigid LDR brachytherapy needle. These needles have a beveled tip of approximately 20 degrees. The slots of the needle will be kept at 0.12mm, just like the previous designed needles by de Vries [3]. This width is a consequence of the manufacturing method; the slots are created by using wire-cut electrical discharge machining (EDM). With this method, two different width are possible; 0.12mm and 0.28mm. The latter is to big for the small dimensions of the needle, and would leave the needle with barely any rigidity, preventing the needle from steering. The decision on the length of the slot was made to create a needle that will be flexible enough to create the needed curves, but at the same time create a little niche at the beginning and end of the needle for the inner catheter to fit into.

Outer catheter	Length [mm]	205
	Outer diameter [mm]	1.90
	Inner diameter [mm]	1.88
	Young's modulus [GPa]	~4
Stylet	Length [mm]	200
	Outer diameter [mm]	1.60
	Inner diameter [mm]	1.08
	Young's modulus [GPa]	28-83
	Slot width [mm]	0.12
	Bevel tip [mm]/[°C]	5 / 20
Inner catheter	Length [mm]	200
	Outer diameter [mm]	1.00
	Inner diameter [mm]	0.70
	Young's modulus [GPa]	~0.575

Table 7.3: Dimensions and properties of the final design of the steerable needle

Concept 7 was simulated in SolidWorks to visualise the design and to provide the drawings of the design for the instrument maker. Figure 7.1 shows the render image that was reacted in SolidWorks after assigning the materials of the individual parts.

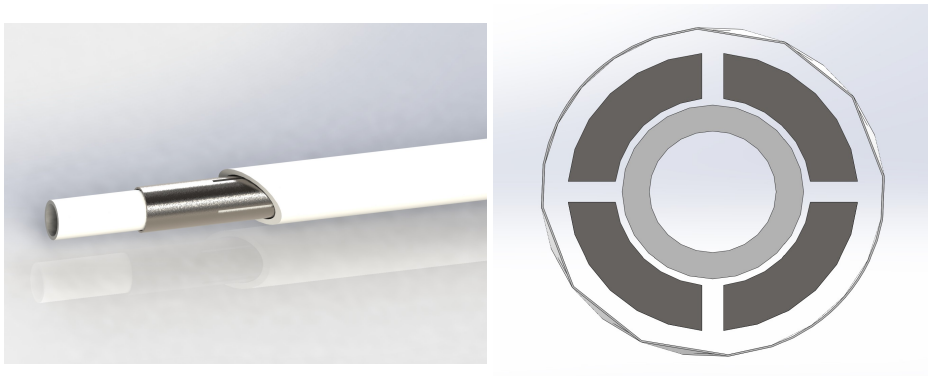

(a) (b)

Figure 7.1: SolidWorks images of the designed steerable needle: a) Render image of the final design. b) Cross section of the final design

One of the major adjustments that had to be made in order for the needle to be manufactured on time, is the omission of a large enough lumen for the radioactive seeds. Nonetheless, the needle that is produced is enough to verify the predicting models presented previously in this thesis. By implementing these models, eventually a needle can be designed that is suitable for the radioactive seeds to pass though.

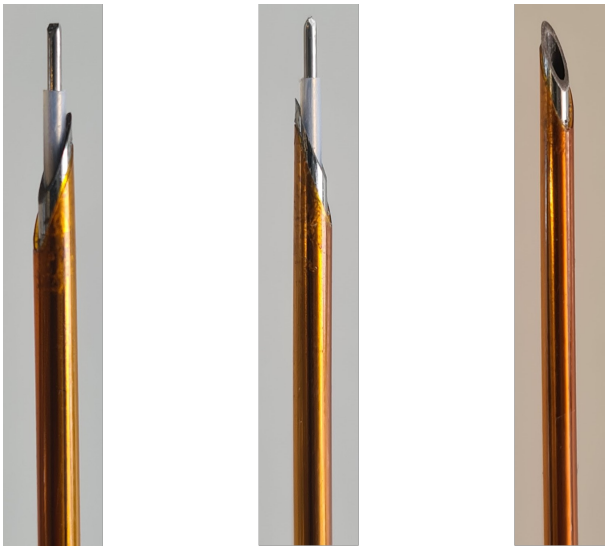

Figure 7.2: Pictures of the manufactured steerable nitinol tube needle:
a) Right side view b) Left side view c) Isometric view

In figure 7.2 three views of the manufactured nitinol steerable needle are shown. The beveled orange tube is the outer catheter, the beveled metal tube the stylet, the white tube the inner catheter and the metal rod in the middle is inserted to show that the needle is indeed hollow.

8

Experimental evaluation of nitinol needle

8.1. Introduction

The final design of the nitinol steerable needle was manufactured into a prototype with help from Mario van der Wel, to provide an additional substantiation for the validate of the prediction models presented earlier in this thesis, and to provide a proof of principal. Three experiments are performed to examine the behaviour of the steerable tube needle. A three point bending test to verify the second moment of inertia, an experiment in air to compare with the previous experiment and validate the two air theories and an experiment in tissue to test the function of the needle, and thereby provide a proof of principle and to validate the theory about deflection in tissue.

8.2. Three point bending test

To confirm the calculated value for the flexural rigidity, a three point bending test is performed. The value for EI that comes forward from this experiment can be used in the further validation of the needle in both air and tissue. Figure 8.1 shows the experiment set-up of the three point bending test. The distance between the two supports is 60mm. The pre-load on the needle is set at 0.05N, and the travel speed is set at 4mm/minute. The total displacement that the needle will undergo is 2mm.

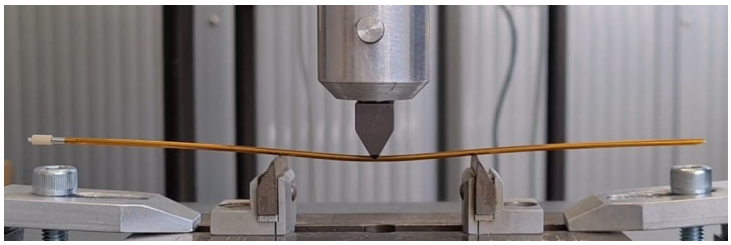

Figure 8.1: Picture of the experimental set up of the three point bending test with the nitinol steerable needle.

The three point bending test measurements of EI during experiment 1, 2 and 3 are 0.032Nm^2, 0.0036Nm^2 and 0.0035Nm^2 respectively. As an average, 0.0035Nm^2 is used for the value of EI of the nitinol needle. Equation 8.1 that was also presented in chapter 2.4 will be used to calculate the second moment of inertia of the stylet.

$$EI_{needle} = EI_{stylet} + EI_{catheter} \tag{8.1}$$

The catheter is a commercially available flexible outer tube of Polyimide. Which has a young's modulus of approximately 4GPa. The second moment of inertia of the catheter can be calculated, based on the standard formula for the inertia of a cylinder. For this specific needle the outer diameter is 1.90mm and the inner diameter 1.88mm.

$$I_{outercatheter} = \frac{\pi * (D_o^4 - D_i^4)}{64} = 0.03mm^4 \tag{8.2}$$

$$EI_{outercatheter} = 0.00012Nm^2 \tag{8.3}$$

The inner catheter of this needle design is made of Teflon, which has a young's modulus of 0.575GPa. The outer diameter is 1.00mm and an inner diameter 0.70mm.

$$I_{innercatheter} = \frac{\pi * (D_o^4 - D_i^4)}{64} = 0.04mm^4 \tag{8.4}$$

$$EI_{innercatheter} = 0.000021Nm^2 \tag{8.5}$$

The stylet is made of a nitinol tube, which has a young's modulus of 50GPa. To eventually come to the conclusion of the second moment of inertia of the inner needle or stylet, equation 8.1 is rewritten and filled in with the known variables.

$$I_{stylet} = \frac{EI_{needle} - EI_{catheter}}{E_{stylet}} = 0.07105mm^4 \tag{8.6}$$

The value that is calculated for the second moment of inertia of the stylet, can be used in the calculation of the distal deflection based on the proximal angle. These results for the nitinol needle can be found in appendix H.4.

8.3. Validation in air

The aim of the validation of the nitinol needle in air is to compare the designed and manufactured needle to the previously performed experiment with the spring steel needle, and to validate the two deflection theories.

8.3.1. Materials and method

8.3.1.1. Set-up

The set up (Figure 8.2) for this experiment is made with any available components, since the lab was closed due to covid. A 3D-printed imitation of the 'standard' needle template (2) is fixed in place, onto a wooden base (3), using a glue clamp (1). On the base, two separate pieces (4) of paper are fixated using tape. These papers will assist in reading the results during the experiment, since they have a protractor drawn on them. The needle is inserted into the needle template at third row and 7th column. This decision was made because the third row is high enough that the force sensors do not interfere with the results but low enough that the reading is still easy to extract, and because the 7th column is located in the middle of the template. The force sensor (5) that is used during this experiment is a specific load cell from Futek, and is calibrated at 10N. It posses an eye bolt at both ends, one end is used to attach a string while the other end is fixated. This sensor measures the difference in voltage created by the force acting on it, the analog signal conditioner and DAQ will translate these values so that they can be read on the computer using Labview. Lastly, a ruler was used to measure the deflection, vertical deviation and insertion depth.

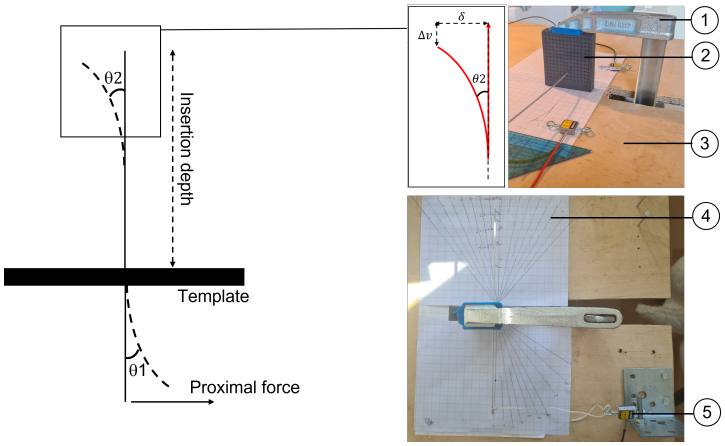

Figure 8.2: Set-up of the needle deflection in air experiment. The figure on the left is a schematic drawing of the set-up. The two figures on the right are pictures of the experiment in reality. θ_2 is the distal angle of the needle, θ_1 is the proximal angle of the needle. δ is the deflection of the needle and Δv is the vertical deviation of the needle. F_p represent the proximal force applied upon the needle.

8.3.1.2. Procedure

The needle is inserted into the template, till the desired insertion depth. After which the force sensor is attached, and calibrated by accounting for the offset. A force was applied to the proximal force sensor by pulling on the string. This was repeated five times. The force that was applied, was not identical during every measurement. The goal was to apply forces between 0N and 1.5N. Larger forces and therefore larger deflections are possible to evaluate, however due to the fact that the needle was required to be undamaged, this was not performed to prevent the risk of permanent deformation. When the desired force had been applied, the proximal side would be fixated using the piece of sting and the clamp after which the deflection, vertical deviation and both angles were measured. This experiment was repeated four times, for different insertion depths (140mm, 120mm, 100mm and 80mm). The whole experiment was performed twice to account for possible measurement errors. Resulting in 40 trails.

8.3.2. Results

The unedited results of the experiment with the nitinol needle in air can be found in appendix H. In the upcoming section, the results of the two models will be compared with the results of the experiment in air. First the needle tip path model will be discussed, second the method to predict the distal deflection based on the proximal force will be elaborated.

8.3.3. Needle tip path

The needle tip path during the experiments is composed of the deflection of the needle and the vertical deviation. The theoretical needle tip path is made by insertion the variables presented in table 8.1 into the needle tip path prediction model.

Parameter	Description	Value
L_n [mm]	Length of the catheter	140/120/100/80
d_n [mm]	Diameter of the needle	1.88
d_c [mm]	Diameter of the catheter	1.60
S_w [mm]	The width of the slots in the inner needle	0.12
ω [mm]	Distance centroid needle to centroid upper half	0.52

Table 8.1: The variables of the nitinol steerable needle, used in the model for the deflection of the needle tip

In graph 8.3 the needle tip paths of four different insertion depths are shown. The lines form the needle tip path of the model, and the dots are experimental values. The horizontal line in the graph is a visualisation of the needle, to help understand the graph.

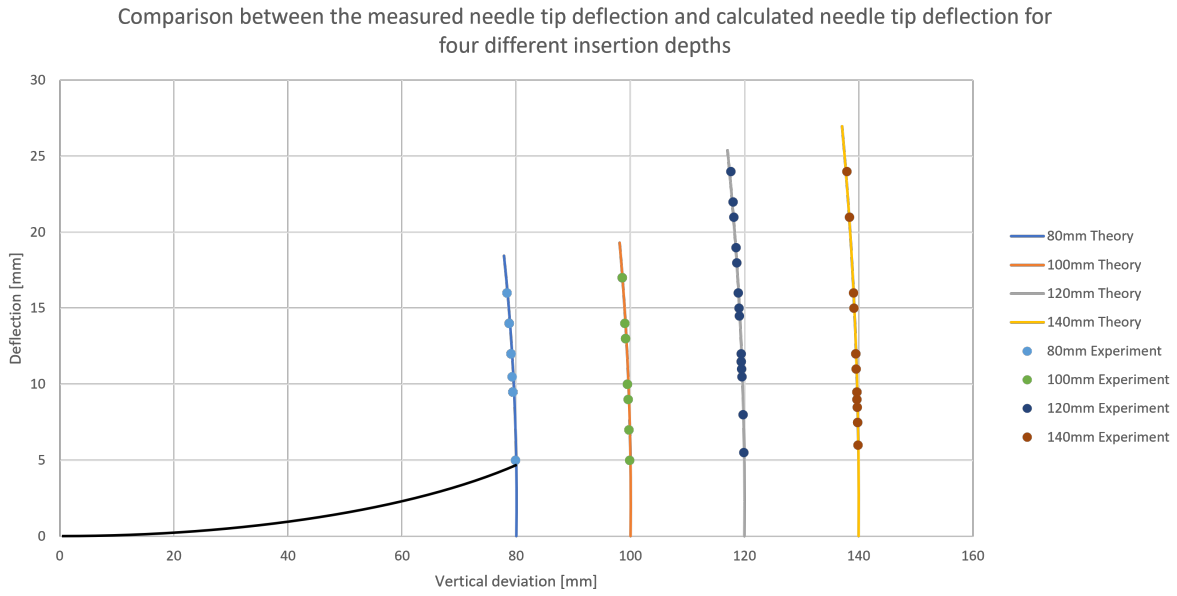

Figure 8.3: Needle tip path of the nitinol steerable needle, calculated using the model. For four different insertion depths.

8.3.4. Deflection prediction with proximal force

The proximal force that was measured during the experiment, is used in the model to check the error between the predicted distal deflection and the measured distal deflection. The variables that are used in the model are presented in table 8.2. The parameter u_r is the elongation of the segments, which is determined using the proximal force and equation 2.14.

Parameter	Description	Value
L_n = L_1 [mm]	Length from the template until the end of the slot	140/120/100/80
d_n [mm]	Diameter of the needle	1.88
d_c [mm]	Diameter of the catheter	1.60
S_w [mm]	The width of the slots in the inner needle	0.12
ω [mm]	Distance centroid needle to centroid upper half	0.52
u_r[mm]	Elongation or abridgment of upper or lower segment	δ_s
L_r [m]	Length between the center of mass of two segments	1.62×10^{-3}
L_{out} [mm]	Length of the proximal side	120/100/80/60
A_s [m^2]	Area of one segment	0.24×10^{-6}
E [GPa]	Young's modulus of stylet material	50

Table 8.2: The variables of the nitinol steerable needle

The data that was created by the experiments and by the model is presented in table 8.3. The first column shows how far the needle is inserted through the template, the second column presents the force that was applied on the proximal side. The third and fourth column display the measured and calculated distal deflection. The last column shows the difference between the measured and calculated deflection. The mean error between the measured and calculated deflection is found to be 2.75mm with a standard deviation of 2.99mm. These results will be debated in the discussion.

Insertion depth	Proximal angle [Deg]	Distal deflection measured [mm]	Distal deflection calculated [mm]	Δ [mm]
80mm	0,214	5,0	4,0	0,97
	0,403	9,5	7,6	1,93
	0,403	9,5	7,6	1,93
	0,419	9,5	7,9	1,63
	0,521	10,5	9,8	0,72
	0,618	12,0	11,6	0,42
	0,618	12,0	11,6	0,42
	0,751	14,0	14,0	0,04
	0,812	14,0	15,2	1,16
	0,812	16,0	15,2	0,84
100mm	0,128	5,0	3,1	1,87
	0,209	7,0	5,1	1,87
	0,306	9,0	7,5	1,50
	0,352	10,0	8,6	1,38
	0,403	13,0	9,9	3,15
	0,449	14,0	11,0	3,02
	0,516	10,0	12,6	2,60
	0,551	13,0	13,5	0,46
	0,602	17,0	14,7	2,31
	0,715	17,0	17,4	0,39
120mm	0,194	5,5	5,5	0,03
	0,322	8,0	9,1	1,07
	0,429	11,0	12,1	1,08
	0,434	11,5	12,2	0,72
	0,434	12,0	12,2	0,22
	0,500	16,0	14,1	1,93
	0,505	11,5	14,2	2,72
	0,511	10,5	14,4	3,87
	0,628	14,5	17,6	3,13
	0,628	18,0	17,6	0,37
	0,654	15,0	18,3	3,34
	0,735	21,0	20,6	0,41
	0,756	19,0	21,2	2,15
	0,817	24,0	22,8	1,16
	0,848	22,0	23,7	1,67
140mm	0,271	6,0	7,8	1,79
	0,301	7,5	8,7	1,17
	0,368	7,5	10,6	3,08
	0,408	9,5	11,7	2,25
	0,424	8,5	12,2	3,69
	0,439	9,0	12,6	3,63
	0,536	11,0	15,4	4,40
	0,623	12,0	17,9	5,87
	0,628	9,5	18,0	8,52
	0,628	15,0	18,0	3,02
	0,771	12,0	22,1	10,06
	1,001	16,0	28,5	12,49
	1,113	21,0	31,6	10,60
	1,271	24,0	35,9	11,92

Table 8.3: The comparison between the measured deflection during the experiment and the deflection calculated with the model based on the proximal force.

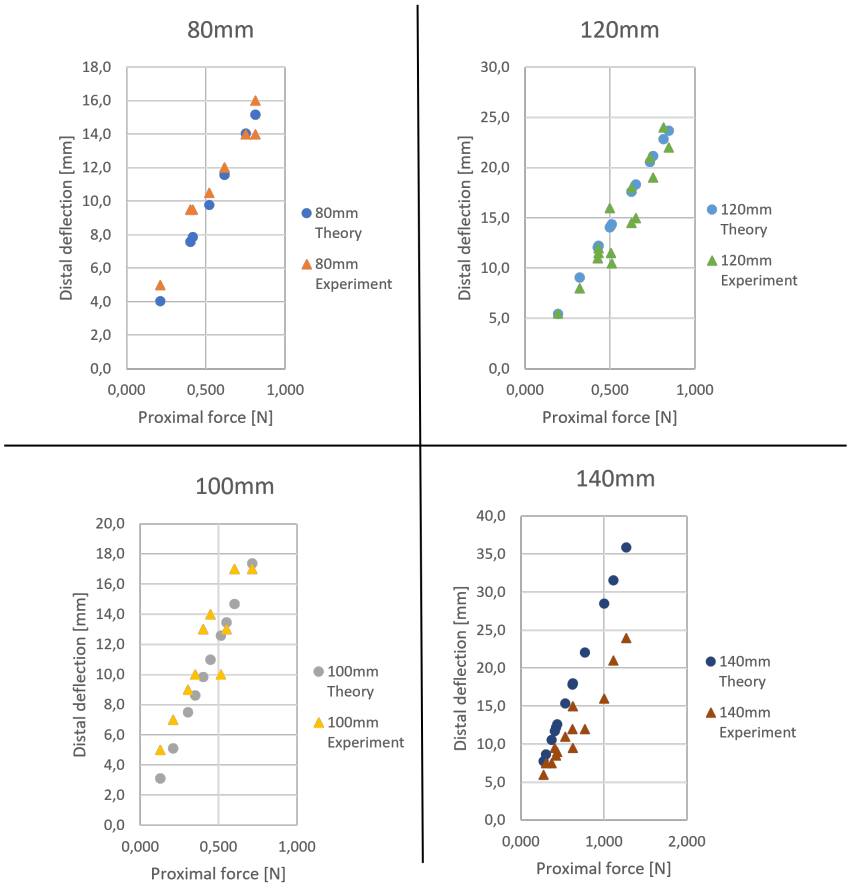

Figure 8.4: Comparison of the distal deflection of the needle between the model and the experimental values. For four different insertion depths.

Figure 8.4 presents the comparison between the predicted and measured distal deflection, when the proximal force is kept the same. It shows that the calculated value for the distal deflection lies close to the measured values. Adding to the proof that the distal deflection theory is an adequate tool to predict the needle deflection in air. There are some outliers in the prediction of the distal deflection for 140mm insertion depth these will be analyzed in the discussion.

8.4. Validation in tissue stimulant

As the needle is eventually going to be used in tissue, a tissue stimulant is made to test the steerable nitinol needle with a lumen. The aim of this experiment is to confirm that the needle meets the requirements and to provide a proof of principal. In addition, the theory for deflection in tissue will be evaluated, and it will be investigated if the theory of deflection in air can also be translated into deflection in tissue.

8.4.1. Materials and methods

8.4.1.1. Set-up

In contrast to the experiment performed in air, the tests in tissue stimulant will be dynamic instead of static. To ensure that the needle insertion speed does not affect the results as a dependent variable, a linear stage is used. This lead to the task to design and make a fixation mechanism to attach the needle and the force sensor to the moving linear slide. In order to make the force sensor move along side with the needle, an individual part was created using laser-cutting and 3D-printing.

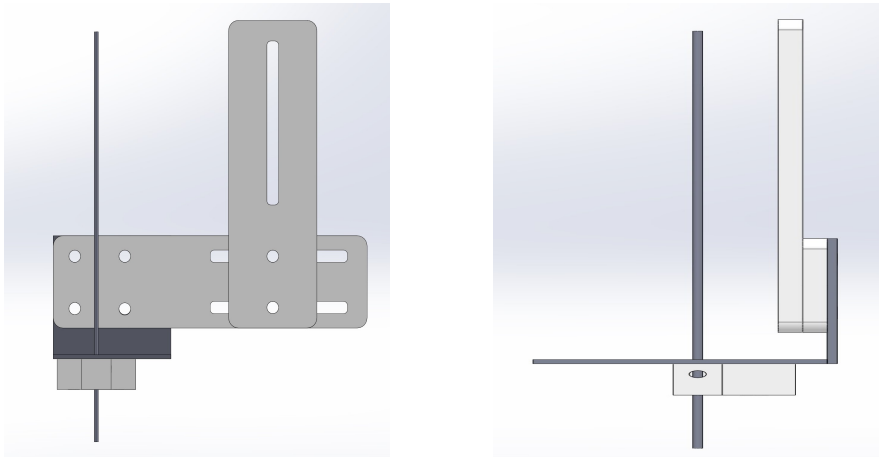

(a) (b)

Figure 8.5: SolidWorks simulation of the fixation mechanism for the needle and force sensor used in the tissue experiments. a) Front view. b) Side view.

First of all, a corner plate is used to create a connection to the linear slide (Gamma 60x60x2mm). Holes are drilled into the corner plate at the correct dimensions to align with the linear slide, and it is attached with M6 bolts. From here the other elements are added. The needle holder is 3D-printed and attached to the corner plate using two M6 bolts. The needle holder is 15mm, which corresponds with the needle template that is used for brachytherapy procedures. To prevent the needle from falling through the needle holder due to gravity, a small bolt (M3) is inserted and lightly tightened against the needle. In addition, two PMMA slides are manufactured, one vertical and one horizontal. The vertical PMMA slide is created to ensure the ability to experiment with various insertion depths. The horizontal PMMA slide is made to enable various forces to be applied on the proximal side of the needle during insertion. Both mechanism work with a M6 nut and bolt, which is tightened and therefore clenches the slides in place.

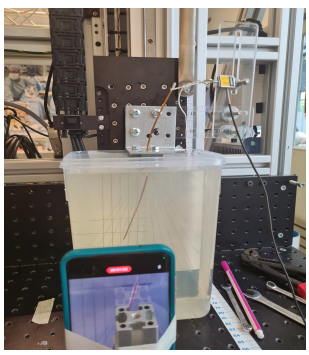

Figure 8.6: Picture of the experiment set up for the needle in tissue.

8.4.1.2. Tissue stimulant

Prostate tissue is known to be relatively stiff compared to other tissues in the body. For example, fat has a density of 991 kg/m^3 and prostate tissue is 1045 kg/m^3 [30]. In addition, cancerous or diseased tissue is also known to be stiffer then healthy tissue. Combining these two facts, results in a tissue stimulant that has to be stiff. In order to create a tissue stimulant that represents both these tissues, it was decided to make two phantoms. One that represents healthy prostate tissue and one that represents cancerous prostate tissue.

Two tissue stimulants are made from Dr. Oetker gelatin and are used at room temperature ($\sim$ 20°C). To simulate the two types of tissues, the gelatin is made with the corresponding densities. The first sample: ”Tissue1”, has 7% wt., which equals to a density of 1040 kg/m^3. The second sample: ”Tissue2”, has 10% wt., which equals to a density of 1056 kg/m^3. These gelatin tissue stimulants are made in a container with dimensions $\sim$ 16x10xx21, this container is transparent to ensure an easy reading of the needle deflection. A figure of the containers is included in appendix J.2

8.4.1.3. Procedure

The needle is inserted and fixated into the needle holder, at the desired insertion depth, with the bevel facing to the right. The needle is inserted into the tissue stimulant for 10mm. Once the needle in already inserted into the tissue stimulant, the desired force is applied to the proximal side of the needle, using the string, force sensor and the horizontal PMMA slide. The linear stage is set to 5mm/s as its insertion speed, the remaining settings of the linear stage can be found in appendix D. After the needle is inserted until the desired insertion depth, the deflection is documented. This is all documented by a camera that records the live insertion of the needle. The vertical deviation and proximal and distal angles can be derived from the deflection of the needle. The experiment was repeated 12 times; i.e. for insertion depths 80mm, 100mm, 120mm and 140mm, and for proximal forces 0.4N, 0.6N and 0.8N. In addition the experiments are done in both tissue 1 and tissue 2. Every experimental condition was repeated to account for possible measurement errors.

8.4.2. Results

Table 8.4 presents the raw data from the experiments in tissue 1 and tissue 2, for a visualisation of this data one can look at the graph in appendix H.7. During the experiments, an extreme was tested, to show the capabilities of the nitinol needle. A proximal force of 2N was applied, after which an insertion of 140mm followed. Resulting in a distal deflection of 51mm in tissue 2.

	Tissue 1 (7%)			**Tissue 2 (10%)**	
Insertion depth [mm]	Proximal force [N]	Distal deflection measured [mm]		Proximal force [N]	Distal deflection measured [mm]
80mm	0,414	19		0,403	20
	0,429	23		0,419	21
	0,613	26		0,618	28
	0,654	27		0,618	29
	0,812	28		0,802	31
	0,863	29		0,807	32
100mm	0,434	25		0,424	35
	0,439	22		0,424	30
	0,602	30		0,602	40
	0,654	30		0,602	36
	0,807	37		0,802	40
	0,832	34		0,822	45
120mm	0,429	25		0,424	28
	0,434	22		0,439	36
	0,608	32		0,623	41
	0,613	34		0,628	38
	0,817	35		0,802	45
	0,832	37		0,812	47
140mm	0,414	28		0,408	26
	0,424	28		0,424	31
	0,608	36		0,597	39
	0,659	36		0,613	42
	0,842	39		0,791	42
	0,842	39		0,807	46

Table 8.4: Unedited results of the experiment in tissue. For both tissue 1 and 2, and for four different insertion depths.

8.4.3. Needle tip path

The needle tip path during the experiments is composed of the deflection of the needle and the vertical deviation. The theoretical needle tip path is made by insertion of the variables presented in table 8.2 into the needle tip path prediction model.

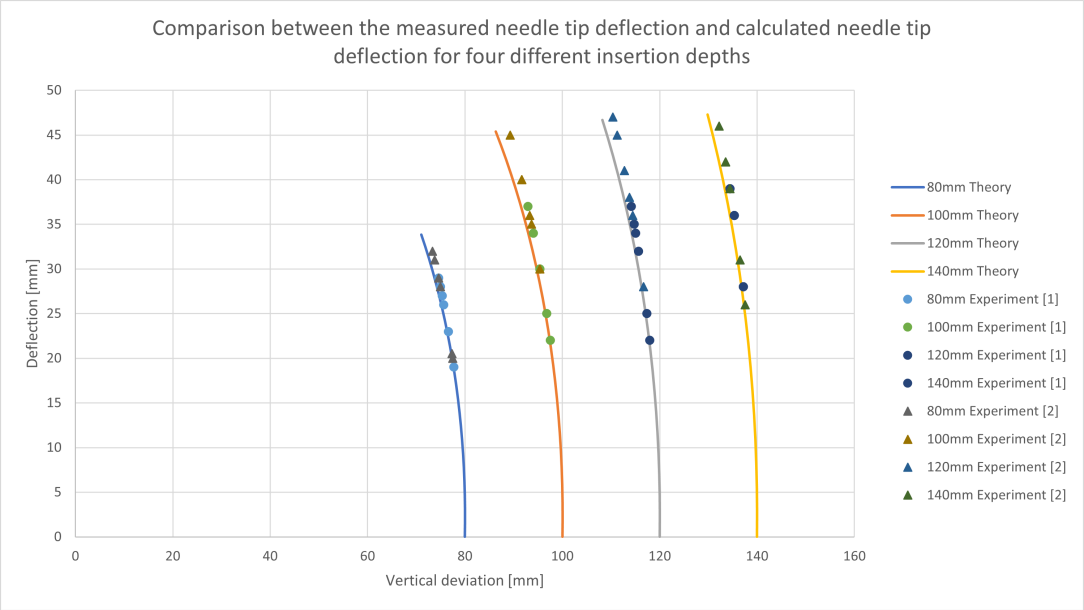

Figure 8.7: Needle tip path of the nitinol needle in tissue. Three categories are presented in this graph: The needle tip path according to the model (line), the values for tissue 1 (dots) and the values for tissue 2 (triangles)

8.4.4. Distal deflection prediction in tissue

As discussed in chapter 4 the distal deflection of the needle can be estimated even if the moment on the proximal side is not known. However for this theory to work, the influence of the tissue onto the needle needs to be known. In this case, the influence of the tissue on the needle is empirically determined. The first three results from each kind of force, is used to determine what the distributed force of the tissue is. This is done by using equation 8.7.

$$\delta_y = \frac{q_y}{24EI}(3L^4 - 4a^3L + a^4) \tag{8.7}$$

In this equation L is 200mm, which is the length of the entire needle. The other parameter is EI which is 0.0035 Nm^2 and the length 'a' is variable with the different insertion depths. The deflection of the needle, δ_y, is known from the experiments, leaving only the distributed force to be an unknown variable. For the first three results the value for q_y is calculated as an distributed force. With these values the deflection for all insertion depths are calculated. Because the value for q is a distributed force, the resultant force on the needle inside the tissue can be calculated for every desired insertion depth.

Tissue 1 (7%)			**Tissue 2 (10%)**	
Proximal force [N]	Distributed distal force [N]		Proximal force [N]	Distributed distal force [N]
0,4	0,45		0,4	0,5
0,6	0,6		0,6	0,7
0,8	0,7		0,8	0,8

Table 8.5: Overview of the distributed forces acting on the needle inside tissue 1 and tissue 2.

When looking at the distributed forces, it already stands out that the force acting on the needle within the tissue increases with the force that is applied on the proximal end. In addition, the force acting on the needle inside the tissue is also larger for tissue 2, which is the stiffer tissue.

A second theory for the prediction of the needle deflection in tissue is created by converting the deflection theory in air based on the proximal force to accommodate tissue predictions. However, it should be noted that this equation and theory does not take into account that the needle has a beveled tip. A bevel tip can steer the needle on its own, and induces a significant amount of additional bending during insertion. The amount of additional bending is approximated by performing a test. In this test the needle is inserted into the tissue in a straight manner, without a proximal force applied onto it. The deflection that the needle experiences in this test, is assumed to be the amount of steering caused by the bevel. This value will be inserted into the equations (equation 8.8) as a constant 'x'. For tissue 1 the additional deflection of the needle is 15mm and for tissue 2 it is 20mm.

$$p_{tip} = \begin{bmatrix} \Delta Z \\ \Delta Y \end{bmatrix} = \begin{bmatrix} \rho * sin(\theta_d) + \delta_s \\ 2\rho * sin^2(\frac{\theta_d}{2}) + x \end{bmatrix} \tag{8.8}$$

8.4.4.1. Tissue 1 (7%)

In table 8.6 the deflection of the nitinol needle in tissue 1 is compared with the two calculated deflections of the models. As can be seen in this table, the fourth column presents the calculated deflection for the theory that uses the distributed force, the fifth column shows the difference between the calculated deflection and the measured deflection. The mean error between the calculated and measured deflection values is 1.48mm ±1.18mm. The sixth and seventh column present the same values as discussed above, however these values belong to the prediction based on the proximal force. The mean error for this prediction is 1.62mm ±1.39mm.

				Theory distributed force			**Theory proximal force**	
Insertion depth	Proximal force [N]	Distal deflection measured [mm]		Distal deflection calculated [mm]	Δ [mm]		Distal deflection calculated +15mm [mm]	Δ [mm]
80mm	0,414	19		19,5	0,48		22,8	3,78
	0,429	23		19,5	3,52		23,1	0,06
	0,613	26		26,0	0,03		26,5	0,49
	0,654	27		26,0	1,03		27,2	0,25
	0,812	28		30,3	2,30		30,2	2,16
	0,863	29		30,3	1,30		31,1	2,09
100mm	0,434	25		22,0	2,97		25,6	0,61
	0,439	22		22,0	0,03		25,7	3,73
	0,602	30		29,4	0,62		29,7	0,32
	0,654	30		29,4	0,62		30,9	0,93
	0,807	37		34,3	2,73		34,6	2,42
	0,832	34		34,3	0,27		35,2	1,17
120mm	0,429	25		23,8	1,19		27,1	2,08
	0,434	22		23,8	1,81		27,2	5,22
	0,608	32		31,7	0,25		32,1	0,07
	0,613	34		31,7	2,25		32,2	1,79
	0,817	35		37,0	2,04		37,8	2,84
	0,832	37		37,0	0,04		38,2	1,25
140mm	0,414	28		24,9	3,07		26,9	1,09
	0,424	28		24,9	3,07		27,2	0,81
	0,608	36		33,2	2,75		32,4	3,55
	0,659	36		33,2	2,75		33,9	2,10
	0,842	39		38,8	0,21		39,1	0,06
	0,842	39		38,8	0,21		39,1	0,06

Table 8.6: Comparison between the measured deflection during the experiments and the calculated deflection using the models in tissue 1. Both the theory based on the distributed force, and the theory based on the proximal force are presented in this table.

8.4.4.2. Tissue 2 (10%)

In table 8.7 the deflection of the nitinol needle in tissue 1 is compared with the two calculated deflections of the models. Same as for tissue 1, the first presented calculated distal deflection belongs to the theory that uses the distributed force, and the second one applies the proximal force theory. For the distributed force model, the error between the measured and calculated distal deflection is 3.27mm ±2.56mm. For the other model the error is 3.35mm ±2.01mm.

				Theory distributed force			**Theory proximal force**	
Insertion depth	Proximal force [N]	Distal deflection measured [mm]		Distal deflection calculated [mm]	Δ [mm]		Distal deflection calculated +15mm [mm]	Δ [mm]
80mm	0,403	20		21,6	1,64		27,6	7,57
	0,419	21		21,6	1,14		27,9	7,37
	0,618	28		30,3	2,30		31,6	3,58
	0,618	29		30,3	1,30		31,6	2,58
	0,802	31		34,6	3,63		35,0	3,98
	0,807	32		34,6	2,63		35,1	3,07
100mm	0,424	35		24,5	10,52		30,4	4,63
	0,424	30		24,5	5,52		30,4	0,37
	0,602	40		34,3	5,73		34,7	5,32
	0,602	36		34,3	1,73		34,7	1,32
	0,802	40		39,2	0,83		39,5	0,54
	0,822	45		39,2	5,83		39,9	5,06
120mm	0,424	28		26,5	1,54		31,9	3,94
	0,439	36		26,5	9,54		32,4	3,64
	0,623	41		37,0	3,96		37,5	3,51
	0,628	38		37,0	0,96		37,6	0,37
	0,802	45		42,3	2,67		42,4	2,57
	0,812	47		42,3	4,67		42,7	4,30
140mm	0,408	26		27,7	1,70		31,7	5,73
	0,424	31		27,7	3,30		32,2	1,19
	0,597	39		38,8	0,21		37,1	1,87
	0,613	42		38,8	3,21		37,6	4,41
	0,791	42		44,3	2,33		42,6	0,63
	0,807	46		44,3	1,67		43,1	2,92

Table 8.7: Comparison between the measured deflection during the experiments and the calculated deflection using the models in tissue 2. Both the theory based on the distributed force, and the theory based on the proximal force are presented in this table.

9

Additional substantiation provided by tungsten needle

9.1. Introduction

Previously in this thesis, two needles are tested. The spring steel wire needle in chapter 3 and the nitinol tube needle in chapter 8. Both are used to verify the model for the prediction of the behaviour of the needle. To provide an extra confirmation of the reliability of the model and parameter influence, an additional needle is tested in air. This needle is borrowed from a previous project, it is also a wire needle, without an inner lumen, it is made out of tungsten and has other dimensions then the previous two needles.

9.2. Dimensions

The dimensions of the needle, and the additional parameters that are used in the model for the prediction of the deflection are presented in table 9.1. These variables are also used in the model for the needle tip path.

Parameter	Description	Value
L [mm]	Needle length	240
D_n [mm]	Diameter of the stylet	1.40
D_c [mm]	Diameter of the catheter	1.50
S_w [mm]	The width of the slots in the inner needle	0.12
L_n [mm]	Insertion depth	140/120/100/80
ω [mm]	Distance centroid needle to centroid upper half	0.38
R [m]	Radius of the stylet	0.0007 m
L_{out} [m]	Length of the proximal side	0.160/0.140/0.120/0.100
L_1 [m]	Length from the template until the end of the slot	0.0785/0.0985/0.1185/0.1385
L_{slot} [m]	Length of the slot	0.227
A [m^2]	Area of the stylet	1.287×10^{-6}
A_s [m^2]	Area of one segment of the stylet	0.322×10^{-6}
I_{stylet}[m^4]	Second moment of inertia of the stylet	0.019×10^{-12}
EI [Nm^2]	Flexural rigidity of the needle	0.0082
E [GPa]	Young's modulus of the material of the stylet	401

Table 9.1: The variables of the tungsten needle, used in the model for the deflection of the needle tip and model for the prediction of the distal deflection.

9.3. Needle tip path

The needle tip path during the experiments, with the tungsten needle, is composed of the deflection of the needle and the vertical deviation. The theoretical needle tip path is made by insertion of the variables presented in table 9.1 into the needle tip path prediction model.

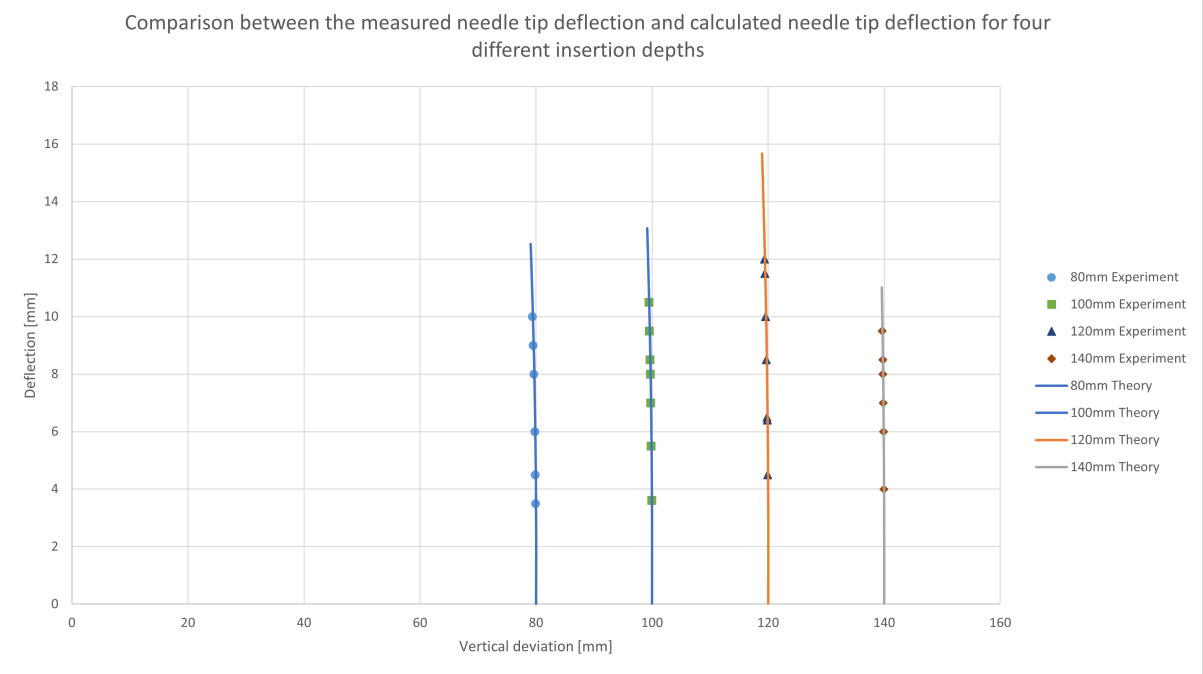

Figure 9.1: Comparison of the needle tip path of the tungsten needle between the model and the measured tip location.

The comparison between the needle tip path of the tungsten needle, the spring steel needle and the nitinol needle is presented in a graph in appendix I.3.

9.4. Distal deflection prediction based on proximal force

The distal deflection of the tungsten needle is measured during the experiment in air. In addition it is also calculated using the model for the prediction of the distal deflection based on the proximal force. Table 9.2 presents the results from both the measured and the calculated deflection. The last column displays the difference between the two. The mean error between the calculated and predicted distal deflection is 1.76mm with a standard deviation of 1.4mm.

Insertion depth	Proximal force [N]	Distal deflection measured [mm]	Distal deflection calculated [mm]	Δ [mm]
80mm	0,414	4,5	2,30	2,20
	0,618	6,0	3,43	2,57
	0,827	8,0	4,59	3,41
	0,400	3,5	2,22	1,28
	0,700	6,0	3,89	2,11
	1,675	10,0	9,28	0,72
	1,287	9,0	7,14	1,86
100mm	0,643	5,5	4,88	0,62
	1,052	8,0	7,98	0,02
	0,802	8,5	6,09	2,41
	0,400	3,6	3,04	0,56
	0,817	7,0	6,20	0,80
	1,251	9,5	9,48	0,02
	1,562	10,5	11,83	1,33
120mm	0,424	4,5	3,97	0,53
	0,613	6,5	5,74	0,76
	0,802	8,5	7,51	0,99
	0,424	6,4	3,97	2,43
	0,802	10,0	7,51	2,49
	1,516	11,5	14,17	2,67
	1,823	12,0	17,00	5,00
140mm	0,403	4,0	4,28	0,28
	0,623	6,0	6,62	0,62
	0,822	8,0	8,73	0,73
	0,403	7,0	4,28	2,72
	1,026	8,5	10,90	2,40
	1,455	9,5	15,43	5,93

Table 9.2: Comparison between the measured and calculated distal deflection of the tungsten needle. The calculated distal deflection is determined with the theory based on the proximal force.

10

Theoretical design for the low dose rate brachytherapy steerable needle

10.1. Introduction

In the requirements (section 1.5) it was stated that the steerable needle should ”allow radioactive seeds to pass though in single-file”, and ”allow the radioactive seeds to pass though the curvature of 30mm over 150mm”. Due to the unavailability of some materials, this requirement was not met. In order to provide a solution for this requirement, a theoretical design will be made of a needle that is compatible for LDR brachytherapy. This needle is designed with the model that was created and proofed within this thesis.

10.2. Dimensions

For the design of the steerable needle for low dose rate brachytherapy in the prostate, the first step will be to determine the required inner lumen. As presented in chapter 1.5; the requirement for the inner lumen of the needle is 0.96mm for the stranded seeds. Including the margin taken to ensure that the seeds can fit through the curve of the needle, the inner lumen must be 1.10mm. In addition, the length of the needle must be longer then 150mm, to ensure insertion into the prostate.

From this starting point the needle design will be build up further outward. The nitinol needle that was made for this thesis, shows promising results. Therefore the choice was made to design the LDR needle with similar dimensions.

Outer catheter	Length [mm]	205
	Outer diameter [mm]	2.00
	Inner diameter [mm]	1.98
	Young’s modulus [GPa]	4
Stylet	Length [mm]	200
	Outer diameter [mm]	1.92
	Inner diameter [mm]	1.40
	Young’s modulus	28-83 GPa
	Slot width [mm]	0.12
	Bevel tip [mm]	5 / 20 °C
Inner catheter	Length [mm]	200
	Outer diameter [mm]	1.35
	Inner diameter [mm]	1.10
	Young’s modulus [GPa]	0.575

Table 10.1: Dimensions of the theoretical design for the low dose rate brachytherapy steerable needle.

10.3. Predicted bending

Like all the other needles presented in this thesis, the theoretical needle for LDR will also be analyzed by prediction the distal deflection of the needle. The parameters that are used within the two models are presented in table 10.2.

Parameter	Description	Value
L [mm]	Needle length	240
D_n [mm]	Diameter of the stylet	1.92
D_c [mm]	Diameter of the catheter	1.98
S_w [mm]	The width of the slots in the inner needle	0.12
L_n [mm]	Insertion depth	140/120/100/80
ω [mm]	Distance centroid needle to centroid upper half	0.55
R [m]	Radius of the stylet	0.00096 m
L_{out} [m]	Length of the proximal side	0.160/0.140/0.120/0.100
L_1 [m]	Length from the template until the end of the slot	0.075/0.095/0.115/0.135
L_{slot} [m]	Length of the slot	0.190
A [m^2]	Area of the stylet	1.294×10^{-6}
A_s [m^2]	Area of one segment of the stylet	0.323×10^{-6}
E [GPa]	Young's modulus of the material of the stylet	50
L_r [m]	Length between the center of mass of two segments	0.00146

Table 10.2: Variables of the theoretical designed needle, used in the prediction models.

10.3.1. Needle tip path prediction

Since this needle is not made, the comparison with experiments is not possible. However, the two models can be compared with each other. In graph 10.1 the needle tip path that is created by the model that predicts the needle tip path is presented as a line, whereas the model that predicts the distal deflection based on the proximal force is presented as dots.

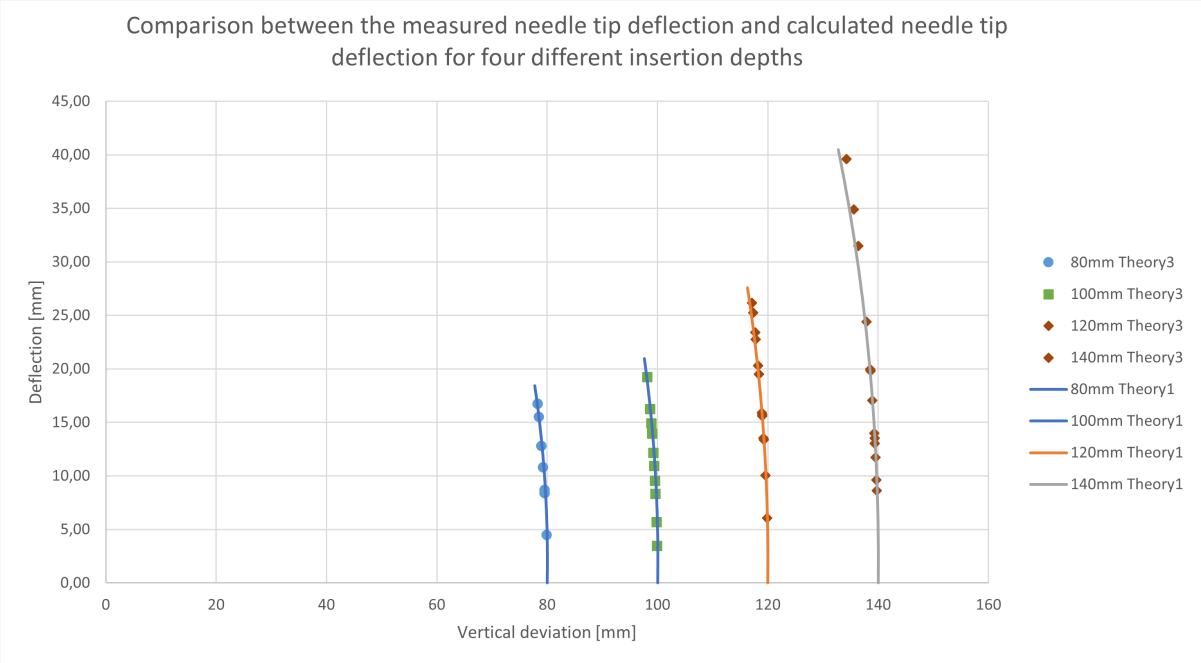

Figure 10.1: Needle tip path of the theoretical designed LDR needle. Using the model for the needle tip path (theory 1), and using the model for the prediction of the distal deflection based on the proximal force (theory 3).

10.3.2. Distal deflection prediction based on proximal force

For the verification of the model that predicts the distal deflection based on proximal force, there is also no experimental data. However, it was decided that there could be a comparison with the previously presented nitinol needle. Since both needles are quite similar, it would be interesting to see how the bending of the needle changes, with the adjustment of a few parameters.

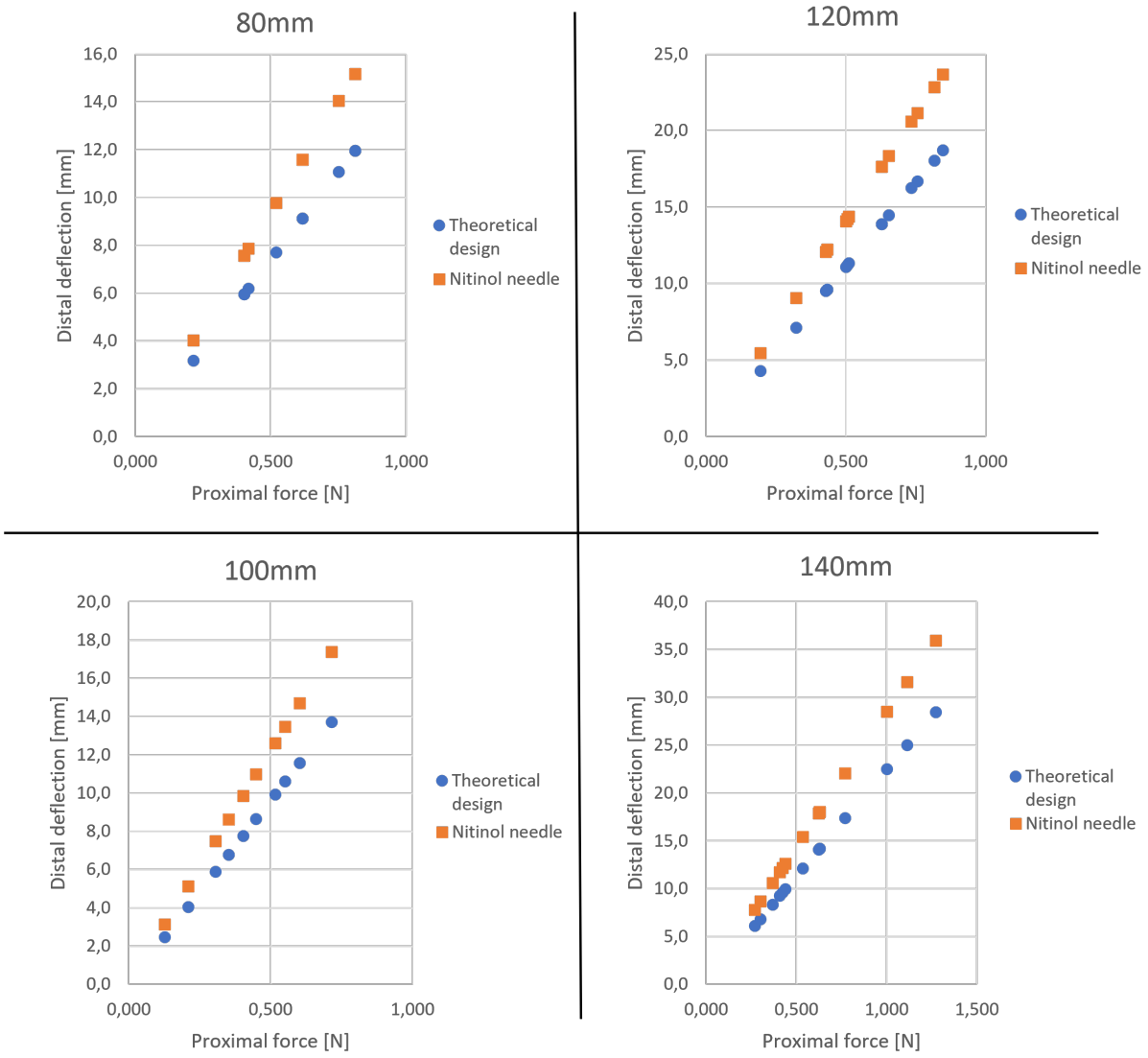

Figure 10.2: Comparison of the distal deflection between the theoretical needle design and the nitinol needle design. For four different insertion depths.

In the four graph 10.2 it stands out that the nitinol needle that was developed in this thesis bends more compared to the theoretical LDR needle for the same amount of proximal force applied. An explanation for this will be given in the discussion.

11 Discussion

This work presents a novel steerable needle for low dose rate brachytherapy and an additional model to predict the distal deflection of the needle. Multiple deflection prediction theories are developed and tested using a borrowed spring steel needle. The theory that predicts the needle tip path and the theory that predicts the distal deflection based on the proximal force are proven to be accurate. The individual parameters from these two models are analyzed, creating a foundation for the design of the steerable needle. Various concepts are developed, resulting in a final design of a nitinol steerable needle with an inner lumen. This nitinol needle is tested in numerous experiments, both in air and in tissue stimulant, to provide a proof of principle and to verify the correctness of the prediction models.

11.1. Discussion

In the upcoming chapter the findings of this thesis are discussed, and the evidence critically examined. After which a few recommendations for future research are considered, and the conclusion of this thesis will be drawn.

11.1.1. Steps forward

The aim of this thesis was to develop a steerable needle for low dose rate brachytherapy of the prostate. In addition the influence of the design parameters on the steering capabilities of the needle needed to be analyzed. To the authors' best knowledge, this is the first steerable needle with this specific compliant mechanism that has an inner lumen through which an object can be inserted. In addition, the needle is completely parametrically designed, providing a very specific solution for the problem. This can also be useful for other projects and needle designs. If a needle is presented and the properties are known, then by using the model the deflection can be predicted. Hereby it can be concluded if a needle is qualified for a specific task. In addition, the model could possibly be reversed. Creating a model that can design a needle based on the procedure it is going to be used for. If a certain amount of bending is needed, then the needle could be reversed engineered with this model. Both the model and the design for the steerable needle for LDR, could be used for other practices. Needles have unwanted deflection everywhere in the body, and anatomical variations form problems in other locations than the prostate. For example, a steerable needle could be a contribution to liver ablation, or could aid in the treatment of brain tumors with holmium.

11.1.2. Evidence examination

The python model showed a close relation between its predicted needle tip path, and the path the needle tip takes during all the experiments. The experiment of the nitinol needle in air demonstrates the validation of the deflection model. The prediction mean error was found to be 2.75mm ±2.99mm. For the experiment condition where the needle was inserted 140mm, the error at larger forces was unacceptably large. This could be caused by limitations of the strain formula, which is supposed to be applied only to small elongations. The experiment of the nitinol needle in tissue demonstrates the steering of the needle up to 51mm laterally at 140mm insertion. Providing a proof of principle and data which can be compared with the deflection prediction model. The needle bends further in tissue 2, this is the stiffer tissue. Due to the tissue being stiffer, there will be a larger force exceeded onto the needle. The two prediction models

of the deflection in tissue turned out to have a mean error of 1.48mm ±1.18mm and 1.62mm ±1.39 in tissue 1. For tissue 2 this was 3.27mm ±2.56mm and 3.35mm ±2.01mm. The threshold to prevent a significant change of radiation dose (2mm to 5mm), is mostly not exceeded.

During the experiments in tissue stimulant, gelatin was used. It should be noted that gelatin has some shortcomings when it is directly compared with tissue. First of all, it is homogeneous, the temperature of gelatin affects the consistency, and the density of the batch is an estimation. Furthermore, during all experiments, the camera that is used is often moved, which could cause inaccurate readings of the deflection. The equations that are used in the prediction models are simplifications of the reality, meaning they are all based on certain assumptions. In the equation for the calculation of the elongation of the segments, the friction is not taken into account and neither is the complexity of the geometry of the needle, it is viewed as a beam. Furthermore, it is assumed that the segments elongate and the abridgment of the segments is equal, which in practice might not be the case. Causing variable 'd' in equation 2.1 to change. In addition, the parameters used in the formula for the prediction of the deflection based on the proximal force, are focused on the stylet. Both the inner and the outer catheter are not included, which could cause deviations in the results. It was decided to make this choice because the catheters are so flexible and weak, that they will bend with whatever bending the stylet will perform. The deflection of the needle is only examined in one plane, instead of multiple. In reality the needle has unwanted deflection in other planes, which could cause the deflection of the needle to differ with the prediction model.
In spite of these assumptions and shortcomings, the needle designed in this thesis meets twelve out of fourteen requirements, which is presented in table 11.1 The remaining two are related to the fact that the radioactive seeds do not fit through the inner lumen. However, the requirements were met in a theoretical manner.

Requirements	
..allow radioactive seeds to pass through in single-file (not-stranded/stranded)	
..have a minimal length of 150mm to be inserted inside the patient	✓
..be able to acquire a lateral deflection of 30mm when the needle is inserted 150mm	✓
..allow the radioactive seeds to pass through the curvature of 30mm over 150mm	
..allow omnidirectional needle tip movement	✓
..have an outer diameter between 14G (2.108mm) and 18G (1.270mm)	✓
..use the current compliant active steering mechanism	✓
..not undergo plastic deformation	✓
..allow the seed(s) to be inserted in 1 action	✓
..be operable in the limited workspace between the legs of the patient in lithotomy position	✓
..be compatible with ultrasound	✓
..be hand operated, either 1 or 2 hands	✓
..be manually operable	✓
..be compatible with the existing template	✓

Table 11.1: Overview of the requirements that are met in this thesis.

11.1.3. Recommendations

There is still further research needed on the steerable needle for LDR. First and foremost, the needle that was designed theoretically needs to be manufactured to test if the radioactive seeds can indeed pass through its inner lumen. Furthermore, the experiments in tissue stimulant have some shortcomings as explained above, it is recommended to test the needle in animal tissue to examine if the needle is rigid enough. Moreover, part of the theory about the prediction of the distal deflection in tissue could not be tested since the moment sensor that was available was in the wrong range. When the correct moment sensor is used, and in combination with an analysis on the deflection induced by the bevel tip, this theory could have the potential of accurately predicting the deflection in tissue. Lastly, it could be researched if the idea of a hollow steerable needle could be used in other treatments.

11.2. Conclusion

This thesis presents the design of a steerable needle for low dose rate brachytherapy and the development of a model for the prediction of the deflection of the needle. Two models are presented, one to predict the needle tip path, and another to predict the distal deflection based on the proximal force with an average error of 2mm. By analyzing the developed model for every individual variable, a specific needle can be designed for a specific problem. In this thesis, a nitinol steerable hollow needle is designed for LDR, which can insert radioactive seeds into the prostate. This needle meets twelve of the fourteen requirements and has a range of 51mm laterally over 140mm insertion. The needle has the potential to overcome multiple challenges of the low dose rate brachytherapy procedure and to create more inclusiveness for patients.

A

Python model code

A.1. Needle tip path

```
import pandas as pd
import matplotlib.pyplot as plt
import numpy as np
import math

Ln = 100
slotwidth = 0.12
dc = 1.40
dn = 1.28
rn = (dn/2) - (slotwidth/2)
print('rn = ', rn)

h = (dc - (2*rn))/2
print('h = ', h)

w = ((4*rn)/(3*np.pi)) + h
print('w=', w)

ur = np.arange(0.0001, 0.808, 0.02)
deltad = (ur/w)
d = ur

rho = ((Ln + ur + (w*deltad))/deltad)
print('rho =', rho)

Z = ((rho*(np.sin(deltad)))+ d)

Y = ((2*rho)*((np.sin(0.5*deltad))**2))

deltaZ = 200 - Z
absolute = np.sqrt(deltaZ**2 + Y**2)

plt.plot(Z,Y)
plt.title('Ideal path of the needle tip')
plt.xlabel('Z-Axis [mm]')
plt.ylabel('Y-Axis [mm]')
plt.grid(True)
t =  'Z' : Z,
'Y' : Y,
'ur': ur,
'absolute':absolute
```

table = pd.DataFrame(t)
table
writer = pd.ExcelWriter('pandas$_{t}able.xlsx', engine =' xlsxwriter')
$table.to_{e}xcel(writer, sheet_{n}ame =' Sheet1', startrow = 1, header = False, index = False)$
$workbook = writer.book$
$worksheet = writer.sheets['Sheet1']$
$(max_{r}ow, max_{c}ol) = table.shape$
$column_{s}ettings = ['header' : columnforcolumnintable.columns]$
$worksheet.add_{t}able(0, 0, max_{r}ow, max_{c}ol - 1, 'columns' : column_{s}ettings)$
$worksheet.set_{c}olumn(0, max_{c}ol - 1, 12)$
$writer.save()$

B

Needle tip path of spring steel needle (a closer look)

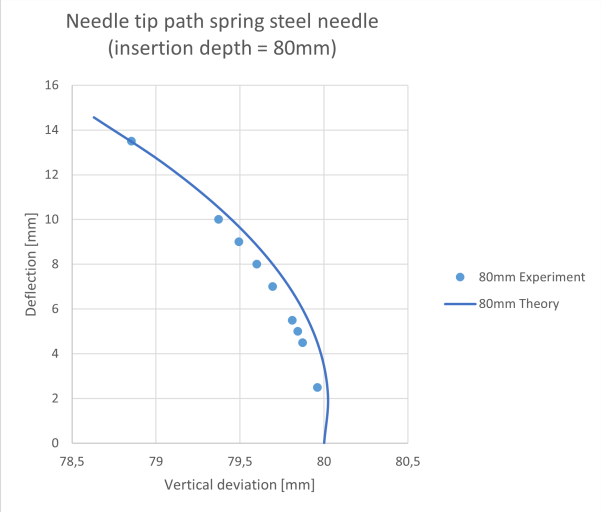

Figure B.1: Needle tip path experiment values compared with model for 80mm insertion.

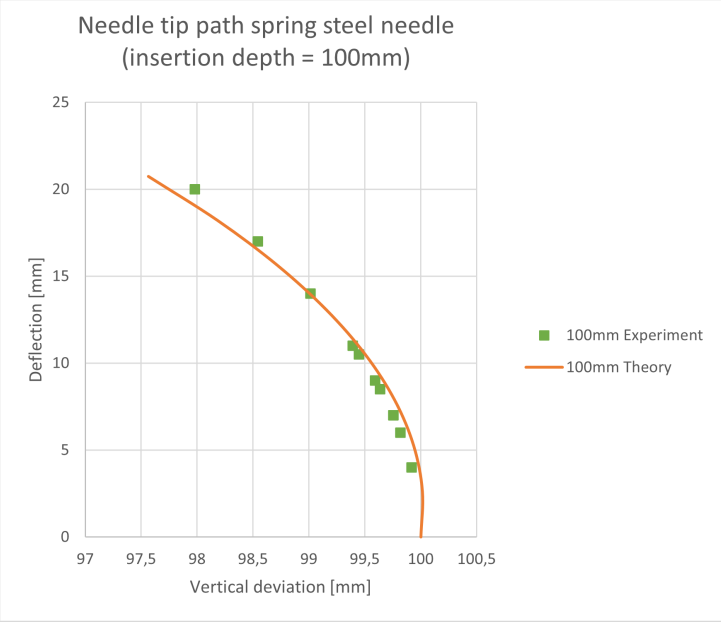

Figure B.2: Needle tip path experiment values compared with model for 100mm insertion.

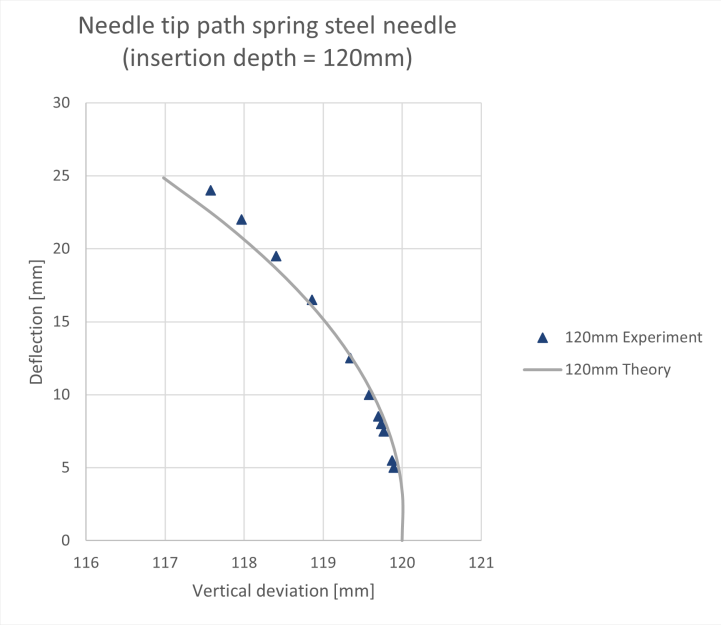

Figure B.3: Needle tip path experiment values compared with model for 120mm insertion.

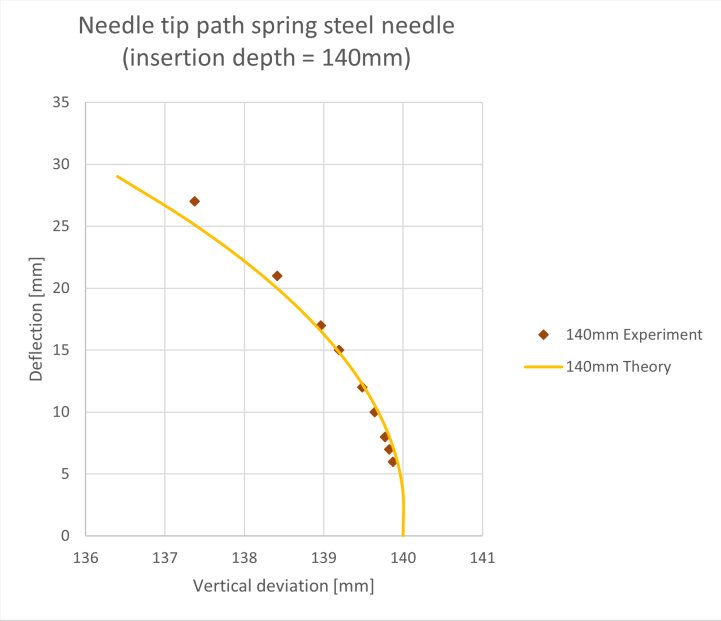

Figure B.4: Needle tip path experiment values compared with model for 140mm insertion.

C

Design concepts

C.1. Available nitinol tubes

Outer diameter [mm]	Inner diameter [mm]	Wall thickness [mm]
1,2	1,1	0,1
1,524	1,41	0,114
1,8	1,725	0,075
1,8	1,67	0,13
1,956	1,871	0,094
2,5	2,35	0,15
0,724	0,42	0,304
0,86	0,71	0,15
1,37	1,29	0,08
1,67	1,37	0,3
1,296	1,076	0,22
1,6	1,08	0,52
0,58	0,35	0,23
0,61	0,34	0,27
1,4	1,12	0,28

Table C.1: Overview of the dimensions of the available nitinol tubes.

C.2. Concept design of steerable needles

		LDR	LDR	LDR	Holmium	Holmium	Holmium	
		Concept 1	**Concept 2**	**Concept 3**	**Concept 4**	**Concept 5**	**Concept 6**	**Concept 7**
Outer catheter	Outer diameter	2.00mm (6F)	1.90mm	1.90mm	0.9906mm	1.67mm (5F)	1.57mm	1.90mm
	Inner diameter	~1.50mm	1.88mm	1.88mm	0.9398mm	~1.43mm	1.47mm	1.88mm
	Wall thickness	~0.50mm	0.02mm	0.02mm	0.0254mm	~0.24mm	0.10mm	0.02mm
	Material (E-modulus)	Polyamide (~1GPa)	Polyimide (~4GPa)	Polyimide (~4GPa)	Polyimide (~4GPa)	Polyamide (~1GPa)	Polyimide (~4GPa)	Polyimide (~4GPa)
Stylet	Outer diameter	1.37mm	1.80mm	1.80mm	0.86mm	1.40mm	1.40mm	1.60mm
	Inner diameter	1.29mm	1.67mm	1.725mm	0.71mm	1.12mm	1.12mm	1.08mm
	Wall thickness	0.08mm	0.13mm	0.075mm	0.15mm	0.28mm	0.28mm	0.52mm
	Material (E-modulus)	Nitinol (~50GPa)	Nitinol (~50GPa)	Nitinol (~50GPa)	Nitinol (~50GPa)	Nitinol (~50GPa)	Nitinol (~50GPa)	Nitinol (~50GPa)
	Slot width	0.12mm	0.12mm	0.12mm	0.12mm	0.12mm	0.12mm	0.12mm
Inner catheter	Outer diameter	1.1684mm	1.57mm	1.667mm (5F)	~0.6604mm	1.016mm	1.016mm	1.00mm
	Inner diameter	1.1176mm	1.47mm	1.43mm	~0.4191mm	0.8636mm	0.8636mm	0.70mm
	Wall thickness	0.0254mm	0.1mm	0.24mm	0.1016mm	0.0762mm	0.0762mm	0.30mm
	Material (E-modulus)	Polyamide (~1GPa)	Polyamide (~1GPa)	Polyamide (~1GPa)	Polyamide (~1GPa)	Polyimide (~4GPa)	Polyimide (~4GPa)	Teflon (~0.58 GPa)
	EI	0,00219	0,00618	0,00388	0,000634	0,00517	0,0051	0,0125

Table C.2: Dimensions of concepts 1 up to 7.

			LDR	LDR	LDR	LDR		
		Concept 8	**Concept 9**	**Concept 10**	**Concept 11**	**Concept 12**	**Concept 13**	**Concept 14**
Outer cathter	Outer diameter	1.90mm	1.90mm	1.90mm	1.90mm	2.794mm	2.50mm	1.80mm
	Inner diameter	1.88mm	1.88mm	1.88mm	1.88mm	2.54mm	2.35mm	1.67mm
	Wall thickness	0.02mm	0.02mm	0.02mm	0.02mm	0.26mm	0.15mm	0.13mm
	Material (E-modulus)	Polyimide (~4GPa)	Polyimide (~4GPa)	Polyimide (~4GPa)	Polyimide (~4GPa)	PEEK (3.85GPa)	Nitinol (~50GPa)	Nitinol (~50GPa)
Stylet	Outer diameter	1.67mm	1.80mm	1.80mm	1.70mm	2.5mm	2.0mm	1.5mm
	Inner diameter	1.37mm	1.67mm	1.725mm	1.50mm	1.5mm	1.0mm	0.7mm
	Wall thickness	0.30mm	0.13mm	0.075mm	0.2mm	1mm	1mm	0.8mm
	Material (E-modulus)	Nitinol (~50GPa)	Nitinol (~50GPa)	Nitinol (~50GPa)	RVS (200GPa)	Carbon (248GPa)	Carbon (248GPa)	Carbon (248GPa)
	Slot width	0.12mm	0.12mm	0.12mm	0.12mm	0.28mm	0.28mm	0.28mm
Inner catheter	Outer diameter	1.00mm	1.41mm	1.41mm	1.41mm	1.41mm	0.64mm	0.64mm
	Inner diameter	0.70mm	1.07mm	1.07mm	1.07mm	1.07mm	0.30mm	0.30mm
	Wall thickness	0.30mm	0.34mm	0.34mm	0.34mm	0.34mm	0.34mm	0.34mm
	Material (E-modulus)	Teflon (~0.58 GPa)	Teflon (~0.58 GPa)	Teflon (~0.58 GPa)	Teflon (~0.58 GPa)	Teflon (~0.58 GPa)	Teflon (~0.58 GPa)	Teflon (~0.58 GPa)
	EI	0,0104	0,0068	0,0042	0,0293	0,3873	0,1627	0,0475

Table C.3: Dimensions of concept 8 up to 14

D

Linear stage settings

	Insertion depth	Initial position	Start bending position	Insertion
10%	80mm	103	93	-69
	100mm	123	113	-89
	120mm	143	133	-109
	140mm	163	153	-129
7%	80mm	105	95	-69
	100mm	125	115	-89
	120mm	145	135	-109
	140mm	165	155	-129

Table D.1: Settings of the linear stage used during the nitinol needle experiments in tissue stimulant.

E

Derivation of equations

E.1. Derivation deflection prediction based on proximal angle

$$\Delta S = (r + \frac{R}{2})\theta - (r - \frac{R}{2})\theta = R\theta \quad \text{(E.1)}$$

$$\theta_2 = \frac{-PL^3}{2EI} \quad \text{(E.2)}$$

$$F = \frac{PL_1}{R} \quad \text{(E.3)}$$

$$\Delta S_{strain} = 2 * \frac{FL_{slot}}{AE} \quad \text{(E.4)}$$

$$\delta_1 = tan^{-1}(\frac{\delta_1}{L_{out}}) \quad \text{(E.5)}$$

Fill in equations E.1, E.2, E.3, E.4 and E.5 into the equation E.6

$$\frac{\Delta S}{\theta_1} = \frac{\Delta S + \Delta S_{strain}}{\theta_2} \quad \text{(E.6)}$$

$$\delta_2 = \frac{R^2 * tan^{-1}(\frac{\delta_1}{L_{out}}) * L_1 * A}{R^2 * L_1 * A + 4 * I_{stylet} * L_{slot}} \quad \text{(E.7)}$$

$$A = (\pi * R^2) - (4 * (Sw * R_n) - (Sw * Sw) \quad \text{(E.8)}$$

E.2. Derivation equation deflection is tissue

$$M = EI\frac{d^2y}{dx^2} = Px \quad \text{(E.9a)} \qquad EI\frac{dy}{dx} = \frac{1}{2}Px^2 \quad \text{(E.9b)} \qquad EIy = \frac{1}{6}Ps^2(3L - x) \quad \text{(E.9c)}$$

$$y = \frac{Pa^2(3L - a)}{6EI} \tag{E.10}$$

$$\delta_1 = \frac{F_1(L_{out} + l_{in}a)^2(3L - L_{out} - l_{in}a)}{6EI} \tag{E.11}$$

$$\delta_1 = -\frac{F_2(L_{out} + l_{in}b)^2(3L - L_{out} - l_{in}b)}{6EI} \tag{E.12}$$

$$\delta_{1,2} = \delta_1 + \delta_2 = \frac{F_1(L_{out} + l_{in}a)^2(3L - L_{out} - l_{in}a)}{6EI} - \frac{F_2(L_{out} + l_{in}b)^2(3L - L_{out} - l_{in}b)}{6EI} \tag{E.13}$$

E.3. Derivation of deflection prediction based on proximal force

$$M = F_p * L_{out} \tag{E.14}$$

$$F_1 = \frac{F_p * L_{out}}{2 * L_r} \tag{E.15}$$

$$\delta_s = \frac{F_p * L_{out}}{2 * L_r} * \frac{L_{in}}{A_{s1}E} \tag{E.16}$$

F

Needle tip path comparison for all 3 needles

F.1. 80mm insertion depth

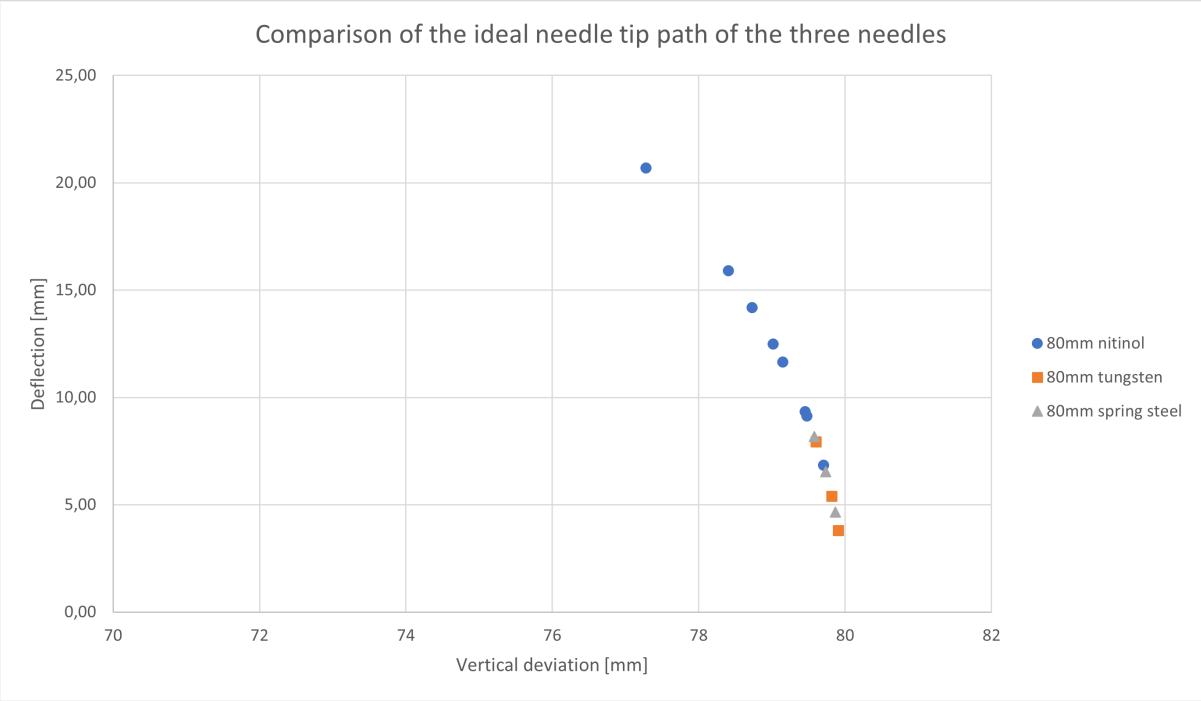

Figure F.1: Comparison of the needle tip path measured during the experiments of three different needles, for insertion depth 80mm.

F.2. 100mm insertion depth

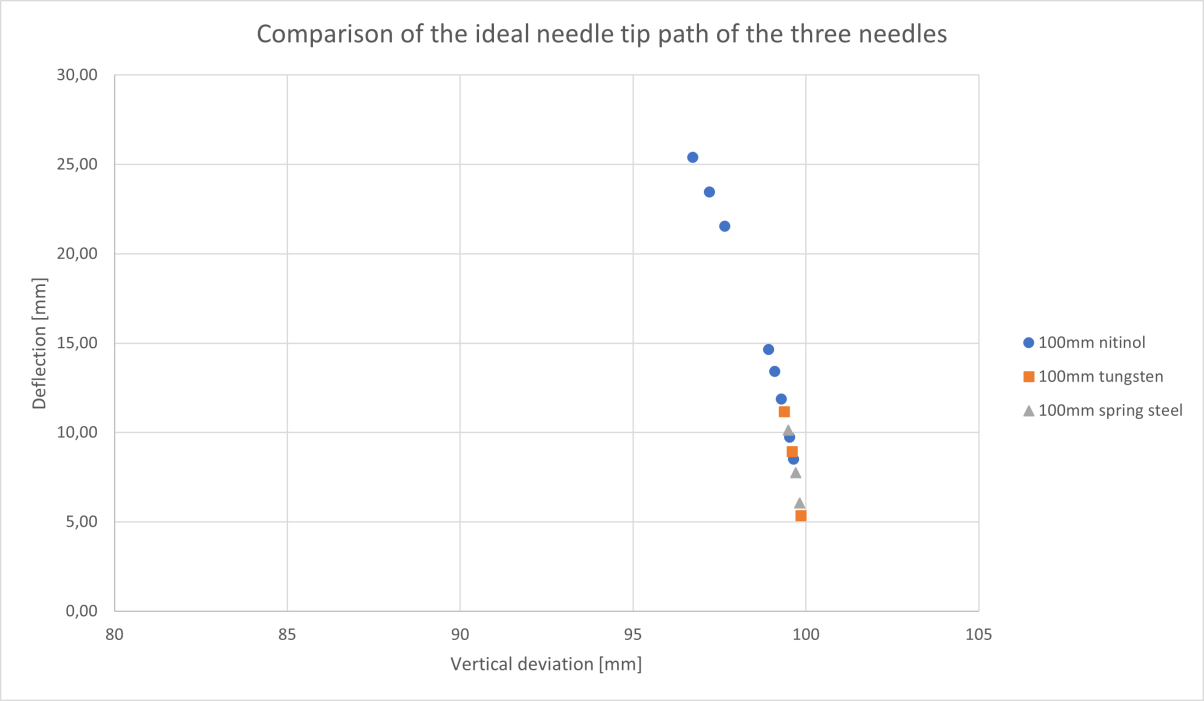

Figure F.2: Comparison of the needle tip path measured during the experiments of three different needles, for insertion depth 100mm.

F.3. 120mm insertion depth

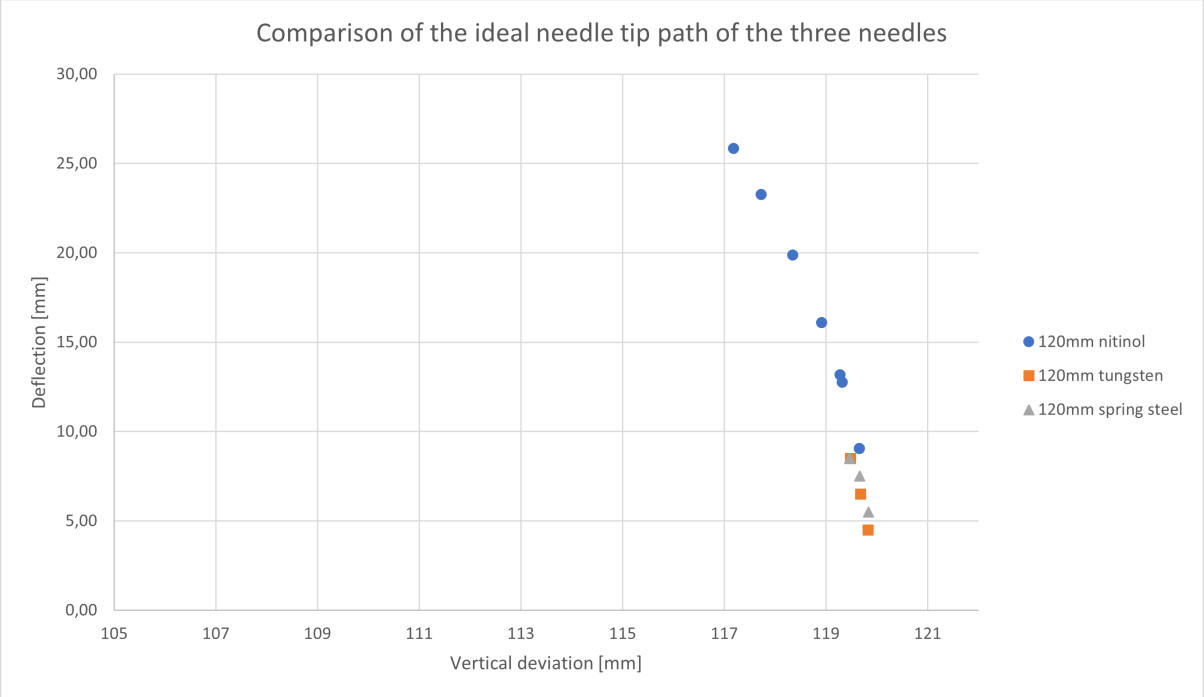

Figure F.3: Comparison of the needle tip path measured during the experiments of three different needles, for insertion depth 120mm.

F.4. 140mm insertion depth

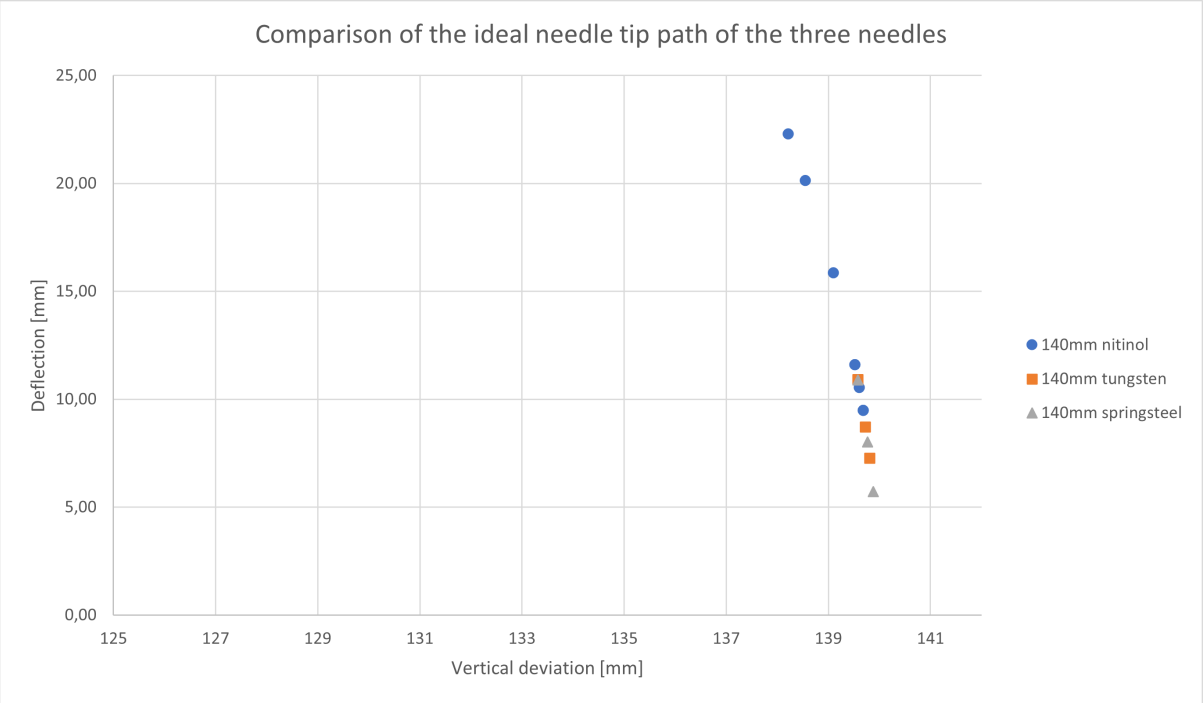

Figure F.4: Comparison of the needle tip path measured during the experiments of three different needles, for insertion depth 140mm.

G

Results spring steel needle

G.1. Results distal deflection based on proximal angle with Istylet

Insertion depth	Proximal angle [Deg]	Distal deflection measured [mm]	Distal deflection calculated [mm]	Δ [mm]
80mm	7,0	2,5	6,00	3,5
	10,0	4,5	8,59	4,1
	10,0	5,0	8,59	3,6
	14,0	5,5	12,07	6,6
	15,0	7,0	12,94	5,9
	17,0	8,0	14,70	6,7
	20,0	9,0	17,37	8,4
	24,0	10,0	20,99	11,0
	35,0	13,5	31,42	17,9
100mm	5,0	4,0	5,81	1,8
	9,0	6,0	10,48	4,5
	11,5	7,0	13,43	6,4
	10,0	7,0	11,66	4,7
	15,0	8,5	17,59	9,1
	15,0	9,0	17,59	8,6
	19,0	10,5	22,41	11,9
	19,0	11,0	22,41	11,4
	32,0	14,0	38,94	24,9
	40,0	17,0	50,07	33,1
	50,0	20,0	65,55	45,6
120mm	6,0	5,0	8,87	3,9
	7,0	5,5	10,36	4,9
	10,0	7,5	14,84	7,3
	10,0	8,0	14,84	6,8
	11,0	8,5	16,34	7,8
	14,0	10,0	20,87	10,9
	16,0	12,5	23,93	11,4
	29,0	16,5	44,72	28,2
	33,0	19,5	51,57	32,1
	42,0	22,0	68,17	46,2
	43,5	24,0	71,13	47,1
140mm	5,0	6,0	9,01	3,0
	5,0	7,0	9,01	2,0
	7,0	8,0	12,63	4,6
	6,5	8,0	11,72	3,7
	9,0	10,0	16,26	6,3
	11,0	12,0	19,92	7,9
	15,0	15,0	27,32	12,3
	28,0	17,0	52,66	35,7
	38,0	21,0	74,36	53,4
	40,0	27,0	79,03	52,0

Table G.1: Results of the distal deflection measured and calculated based on proximal angle with Istylet.

G.2. Results distal deflection based on proximal angle with EI

Insertion depth	Proximal angle [Deg]	Distal deflection measured [mm]	Distal deflection calculated [mm]	Δ [mm]
80mm	7,0	2,5	5,82	3,3
	10,0	4,5	8,32	3,8
	10,0	5,0	8,32	3,3
	14,0	5,5	11,69	6,2
	15,0	7,0	12,54	5,5
	17,0	8,0	14,25	6,2
	20,0	9,0	16,83	7,8
	24,0	10,0	20,33	10,3
	35,0	13,5	30,37	16,9
100mm	5,0	4,0	5,66	1,7
	9,0	6,0	10,20	4,2
	11,5	7,0	13,07	6,1
	10,0	7,0	11,35	4,3
	15,0	8,5	17,11	8,6
	15,0	9,0	17,11	8,1
	19,0	10,5	21,80	11,3
	19,0	11,0	21,80	10,8
	32,0	14,0	37,82	23,8
	40,0	17,0	48,55	31,5
	50,0	20,0	63,39	43,4
120mm	6,0	5,0	8,67	3,7
	7,0	5,5	10,12	4,6
	10,0	7,5	14,49	7,0
	10,0	8,0	14,49	6,5
	11,0	8,5	15,95	7,5
	14,0	10,0	20,38	10,4
	16,0	12,5	23,36	10,9
	29,0	16,5	43,59	27,1
	33,0	19,5	50,24	30,7
	42,0	22,0	66,27	44,3
	43,5	24,0	69,12	45,1
140mm	5,0	6,0	8,82	2,8
	5,0	7,0	8,82	1,8
	7,0	8,0	12,36	4,4
	6,5	8,0	11,47	3,5
	9,0	10,0	15,92	5,9
	11,0	12,0	19,50	7,5
	15,0	15,0	26,74	11,7
	28,0	17,0	51,46	34,5
	38,0	21,0	72,54	51,5
	40,0	27,0	77,07	50,1

Table G.2: Results of the distal deflection measured and calculated based on proximal angle with EI.

G.3. Results distal deflection based on proximal force

Insertion depth	Proximal force [N]	Distal deflection measured [mm]	Distal deflection calculated [mm]	Δ [mm]
80mm	0,225	2,5	2,45	0,05
	0,408	4,5	4,46	0,04
	0,408	5,0	4,46	0,54
	0,623	5,5	6,80	1,30
	0,623	7,0	6,80	0,20
	0,837	8,0	9,12	1,12
	0,753	9,0	8,21	0,79
100mm	0,350	4,0	5,22	1,22
	0,424	6,0	6,33	0,33
	0,608	7,0	9,06	2,06
	0,633	7,0	9,44	2,44
	0,822	8,5	12,23	3,73
	0,613	9,0	9,13	0,13
	0,766	10,5	11,41	0,91
120mm	0,260	5,0	4,80	0,20
	0,424	5,5	7,81	2,31
	0,618	7,5	11,37	3,87
	0,470	8,0	8,65	0,65
	0,516	8,5	9,49	0,99
	0,648	10,0	11,92	1,92
	0,812	12,5	14,91	2,41
140mm	0,429	6,0	8,96	2,96
	0,403	7,0	8,42	1,42
	0,602	8,0	12,56	4,56
	0,444	8,0	9,28	1,28
	0,557	10,0	11,62	1,62
	0,751	12,0	15,64	3,64
	1,052	15,0	21,84	6,84

Table G.3: Results of the distal deflection measured and calculated based on proximal force.

H

Results nitinol needle

H.1. Air - raw data

Insertion depth	Deflection [mm]	Vertical deviation [mm]	Proximal force [N]	Proximal angle [Degrees]	Distal angle [Degrees]
80mm	10,5	0,5	0,521	22	7,5
	14	2	0,751	30	10
	14,5	3	1,118	34	10,5
	18	2,5	1,343	38	13
	24,5	5	1,573	49	19
100mm	10	0	0,516	16	5
	14	0,5	0,776	22	7,5
	24	0,5	1,179	35	13,5
	26,5	2	1,322	38	15
	28	2,5	1,562	41	16
120mm	10,5	0	0,511	11	4,5
	14,5	0,5	0,735	16	6
	20,5	1	1,139	24	9,5
	24	2	1,333	28	11
	27	3	1,511	31	12,5
140mm	8,5	0	0,505	9	3
	12	1,5	0,771	11	4,5
	15,5	2,5	1,113	15	6
	18,5	3	1,312	19	7,5
	23	3	1,573	21	9

Table H.1: Unedited data from the experiments in air with the nitinol needle.

H.2. Air - distal angle comparison

L1 [m]	Lout [m]	Delta_1 [mm]	Calculated Delta_2 [mm]	Measured Delta_2 [mm]
0,075	0,12	47,9	10,9	10,5
0,075	0,12	68,4	14,9	14
0,075	0,12	79,9	16,9	14,5
0,075	0,12	92,6	19,0	18
0,075	0,12	136,3	24,8	24,5
0,095	0,1	28,2	11,4	10
0,095	0,1	39,8	15,8	14
0,095	0,1	69,0	25,4	24
0,095	0,1	77,0	27,7	26,5
0,095	0,1	85,6	30,0	28
0,115	0,08	15,3	10,5	10,5
0,115	0,08	22,5	15,3	14,5
0,115	0,08	35,0	23,1	20,5
0,115	0,08	41,7	27,1	24
0,115	0,08	47,2	30,1	27
0,135	0,06	9,3	10,9	8,5
0,135	0,06	11,4	13,3	12
0,135	0,06	15,7	18,2	15,5
0,135	0,06	20,1	23,1	18,5
0,135	0,06	22,5	25,6	23

Table H.2: Comparison of the measured and calculated distal angle, using the experiment and the theory based on the proximal angle.

H.3. Tissue - raw results

H.3.0.1. Tissue 1

Lin [mm]	L_out [mm]	Angle proximal [deg]	Angle distal [deg]	Deflection [mm]	Vertical deviation [mm]	F_proximal [N]
80	120	13	14	19	2,2	0,414
		18	18	27	4,4	0,654
		21	21	29	5,1	0,863
		13	15	23	3,2	0,429
		17	16,5	26	4,1	0,613
		20	18	28	4,8	0,812
100	100	10	12,5	22	2,4	0,439
		14	16	30	4,4	0,654
		18	17,5	34	5,6	0,832
		10	12,5	25	3,1	0,434
		13	15,5	30	4,4	0,602
		17	18,5	37	6,6	0,807
120	80	7	10	25	2,6	0,429
		10	14	34	4,7	0,613
		12	16	37	5,6	0,832
		6	8	22	2,0	0,434
		8	13,5	32	4,2	0,608
		11	15	35	5,0	0,817
140	60	5	10	28	2,8	0,424
		8	14	36	4,6	0,608
		10	16	39	5,3	0,842
		5	9,5	28	2,8	0,414
		7	12,5	36	4,6	0,659
		10	14	39	5,3	0,842

Table H.3: Unedited results of the experiment with the nitinol needle performed in tissue stimulant Tissue 1 (7%).

H.3.0.2. Tissue 2

Lin [mm]	L_out [mm]	Angle proximal [deg]	Angle distal [deg]	Deflection [mm]	Vertical deviation [mm]	F_proximal [N]
80	120	11	14	20,5	2,6	0,419
		16	18	28	4,8	0,618
		20	21	31	5,8	0,802
		10	13,5	20	2,5	0,403
		16	18,5	29	5,1	0,618
		21	23	32	6,2	0,807
100	100	10	17,5	35	5,9	0,424
		13	20	40	7,7	0,602
		18	23	45	9,7	0,822
		10	15	30	4,4	0,424
		14	18	36	6,3	0,602
		18	21	40	7,7	0,802
120	80	7	14	36	5,3	0,439
		11	16	41	6,8	0,623
		14	18	47	8,9	0,812
		6	13	28	3,2	0,424
		9	15	38	5,9	0,628
		14	19	45	8,2	0,802
140	60	6	11	31	3,4	0,424
		8	15	42	6,2	0,613
		10	18	46	7,4	0,807
		3	8	26	2,4	0,408
		5	10	29	3,0	0,597
		8	14,5	42	6,2	0,791

Table H.4: Unedited results of the experiment with the nitinol needle performed in tissue stimulant Tissue 2 (10%).

Parameter	**Value**
R [m]	0.0008 m
θ_1 [Deg]	Variable
L_{out} [m]	0.160 / 0.140 / 0.120 / 0.100
L_1 [m]	0.075 / 0.095 / 0.115 / 0.135
L_{slot} [m]	0.190
A [m^2]	$0.96973*10^{-6}$
I_{stylet}[m^4]	$0.07105*10^{-12}$
EI [Nm^2]	0.0034893
E [GPa]	50

Table H.5: The variables of the nitinol needle, used in the model for the prediction of the distal deflection

H.4. Results distal deflection based on proximal angle with Istylet

Insertion depth	Proximal angle [Deg]	Distal deflection measured [mm]	Distal deflection calculated [mm]	Δ [mm]
80mm	11,50	5,00	7,46	2,46
	18,50	9,50	12,05	2,55
	15,00	9,50	9,74	0,24
	16,50	9,50	10,73	1,23
	22,00	10,50	14,37	3,87
	20,00	12,00	13,04	1,04
	22,50	12,00	14,71	2,71
	25,00	14,00	16,38	2,38
	24,50	14,00	16,05	2,05
	28,00	16,00	18,41	2,41
100mm	6,00	5,00	5,47	0,47
	10,00	7,00	9,14	2,14
	11,00	9,00	10,05	1,05
	12,50	10,00	11,44	1,44
	16,00	10,00	14,68	4,68
	15,00	13,00	13,75	0,75
	18,00	13,00	16,55	3,55
	16,50	14,00	15,15	1,15
	21,00	17,00	19,37	2,37
	21,50	17,00	19,84	2,84
120mm	5,00	5,50	5,97	0,47
	9,00	8,00	10,76	2,76
	11,00	10,50	13,17	2,67
	10,50	11,00	12,56	1,56
	11,00	11,50	13,17	1,67
	11,50	11,50	13,77	2,27
	10,00	12,00	11,96	0,04
	15,00	14,50	18,02	3,52
	15,00	15,00	18,02	3,02
	12,50	16,00	14,98	1,02
	15,00	18,00	18,02	0,02
	18,50	19,00	22,31	3,31
	17,50	21,00	21,08	0,08
	20,00	22,00	24,17	2,17
	20,00	24,00	24,17	0,17
140mm	5,00	6,00	7,44	1,44
	7,50	7,50	11,17	3,67
	6,00	7,50	8,93	1,43
	9,00	8,50	13,41	4,91
	9,00	9,00	13,41	4,41
	10,00	9,50	14,91	5,41
	7,50	9,50	11,17	1,67
	9,00	11,00	13,41	2,41
	10,00	12,00	14,91	2,91
	10,00	12,00	14,91	2,91
	10,00	15,00	14,91	0,09
	15,00	16,00	22,48	6,48
	15,00	21,00	22,48	1,48
	20,00	24,00	30,17	6,17

Table H.6: Nitinol distal deflection prediction based on proximal angle with Istylet

H.5. Results distal deflection based on proximal angle with EI

Insertion depth	Proximal angle [Deg]	Distal deflection measured [mm]	Distal deflection calculated [mm]	Δ [mm]
80mm	11,50	5,00	7,53	2,53
	18,50	9,50	12,17	2,67
	15,00	9,50	9,84	0,34
	16,50	9,50	10,83	1,33
	22,00	10,50	14,51	4,01
	20,00	12,00	13,17	1,17
	22,50	12,00	14,85	2,85
	25,00	14,00	16,55	2,55
	24,50	14,00	16,21	2,21
	28,00	16,00	18,60	2,60
100mm	6,00	5,00	5,52	0,52
	10,00	7,00	9,21	2,21
	11,00	9,00	10,14	1,14
	12,50	10,00	11,54	1,54
	16,00	10,00	14,81	4,81
	15,00	13,00	13,87	0,87
	18,00	13,00	16,69	3,69
	16,50	14,00	15,28	1,28
	21,00	17,00	19,54	2,54
	21,50	17,00	20,02	3,02
120mm	5,00	5,50	6,01	0,51
	9,00	8,00	10,84	2,84
	11,00	10,50	13,27	2,77
	10,50	11,00	12,66	1,66
	11,00	11,50	13,27	1,77
	11,50	11,50	13,88	2,38
	10,00	12,00	12,06	0,06
	15,00	14,50	18,16	3,66
	15,00	15,00	18,16	3,16
	12,50	16,00	15,10	0,90
	15,00	18,00	18,16	0,16
	18,50	19,00	22,49	3,49
	17,50	21,00	21,24	0,24
	20,00	22,00	24,36	2,36
	20,00	24,00	24,36	0,36
140mm	5,00	6,00	7,49	1,49
	7,50	7,50	11,25	3,75
	6,00	7,50	8,99	1,49
	9,00	8,50	13,51	5,01
	9,00	9,00	13,51	4,51
	10,00	9,50	15,02	5,52
	7,50	9,50	11,25	1,75
	9,00	11,00	13,51	2,51
	10,00	12,00	15,02	3,02
	10,00	12,00	15,02	3,02
	10,00	15,00	15,02	0,02
	15,00	16,00	22,64	6,64
	15,00	21,00	22,64	1,64
	20,00	24,00	30,39	6,39

Table H.7: Nitinol distal deflection prediction based on proximal angle with EI

H.6. Comparison between the three deflection theories

Insertion depth [mm]	Distal deflection measured [mm]	Distal deflection calculated with theory 3 [mm]	Distal deflection calculated with theory 2.1 [mm]	Distal deflection calculated with theory 2.2 [mm]
80mm	5,00	4,03	7,46	7,53
	9,50	7,87	12,05	12,17
	9,50	7,57	9,74	9,84
	9,50	7,57	10,73	10,83
	10,50	9,78	14,37	14,51
	12,00	11,58	13,04	13,17
	12,00	11,58	14,71	14,85
	14,00	15,16	16,38	16,55
	14,00	14,04	16,05	16,21
	16,00	15,16	18,41	18,60
100mm	5,00	3,13	5,47	5,52
	7,00	5,13	9,14	9,21
	9,00	7,50	10,05	10,14
	10,00	8,62	11,44	11,54
	10,00	12,60	14,68	14,81
	13,00	9,85	13,75	13,87
	13,00	10,98	16,55	16,69
	14,00	13,46	15,15	15,28
	17,00	14,69	19,37	19,54
	17,00	17,39	19,84	20,02
120mm	5,50	5,47	5,97	6,01
	8,00	9,07	10,76	10,84
	10,50	14,37	13,17	13,27
	11,00	12,08	12,56	12,66
	11,50	12,22	13,17	13,27
	11,50	12,22	13,77	13,88
	12,00	17,63	11,96	12,06
	14,50	14,22	18,02	18,16
	15,00	14,07	18,02	18,16
	16,00	17,63	14,98	15,10
	18,00	18,34	18,02	18,16
	19,00	21,15	22,31	22,49
	21,00	20,59	21,08	21,24
	22,00	22,84	24,17	24,36
	24,00	23,67	24,17	24,36
140mm	6,00	7,79	7,44	7,49
	7,50	10,58	11,17	11,25
	7,50	12,19	8,93	8,99
	8,50	8,67	13,41	13,51
	9,00	12,63	13,41	13,51
	9,50	18,02	14,91	15,02
	9,50	11,75	11,17	11,25
	11,00	22,06	13,41	13,51
	12,00	18,02	14,91	15,02
	12,00	15,40	14,91	15,02
	15,00	28,49	14,91	15,02
	16,00	17,87	22,48	22,64
	21,00	31,60	22,48	22,64
	24,00	35,92	30,17	30,39

Table H.8: Comparison between the measured deflection of the nitinol needle and three calculated distal deflections. Theory 3 = based on proximal force, theory 2.1 = based on proximal angle using I_stylet, theory 2.2 = based on proximal angle using EI.

H.7. Results in tissue nitinol needle

H.7.1. Visualisation of the results in tissue

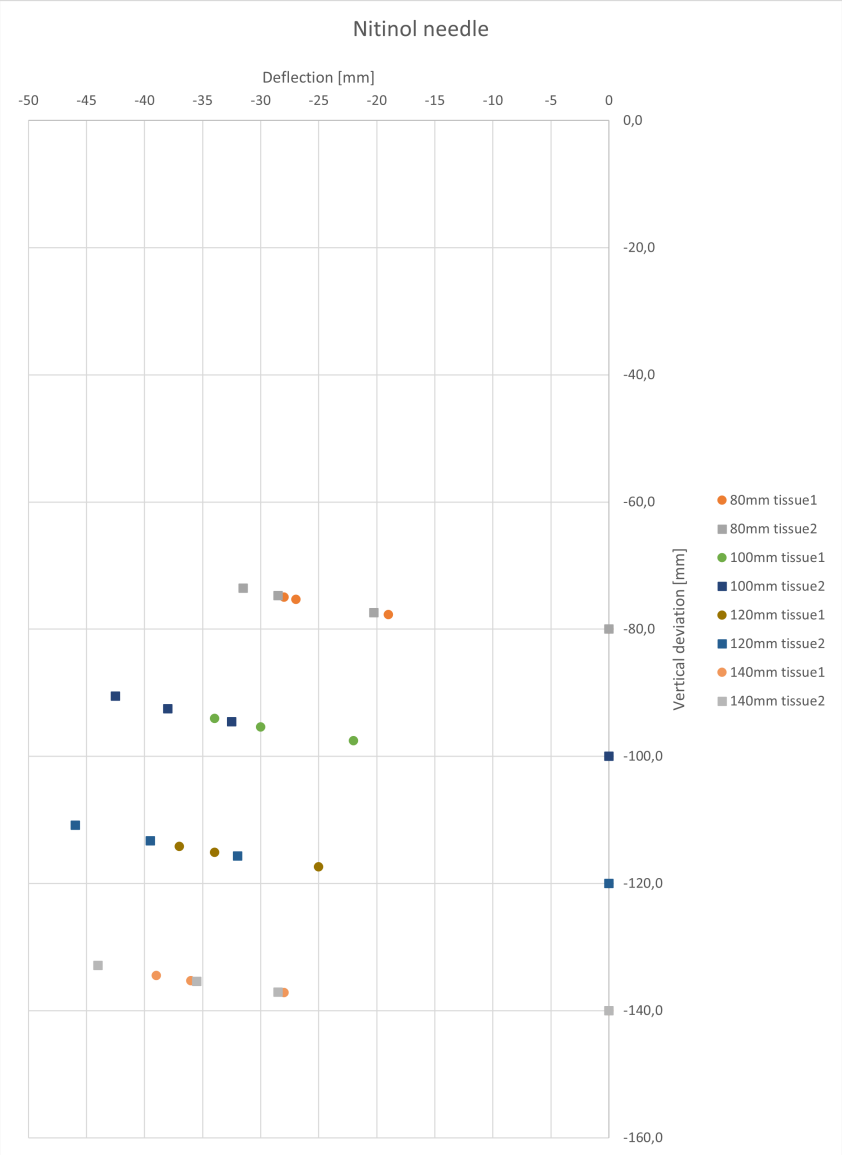

Figure H.1: Graph presenting the location of the needle tip during the experiment in tissue 1 and tissue 2.

H.7.2. Distributed force
H.7.2.1. Tissue 1

Insertion depth [mm]	Proximal force [N]	qy [N/m]	Distal deflection measured [mm]	Distal deflection calculated [mm]	Δ [mm]
80mm	0,414	0,45	19	19,5	0,48
	0,429	0,45	23	19,5	3,52
	0,613	0,6	26	26,0	0,03
	0,654	0,6	27	26,0	1,03
	0,812	0,7	28	30,3	2,30
	0,863	0,7	29	30,3	1,30
100mm	0,434	0,45	25	22,0	2,97
	0,439	0,45	22	22,0	0,03
	0,602	0,6	30	29,4	0,62
	0,654	0,6	30	29,4	0,62
	0,807	0,7	37	34,3	2,73
	0,832	0,7	34	34,3	0,27
120mm	0,429	0,45	25	23,8	1,19
	0,434	0,45	22	23,8	1,81
	0,608	0,6	32	31,7	0,25
	0,613	0,6	34	31,7	2,25
	0,817	0,7	35	37,0	2,04
	0,832	0,7	37	37,0	0,04
140mm	0,414	0,45	28	24,9	3,07
	0,424	0,45	28	24,9	3,07
	0,608	0,6	36	33,2	2,75
	0,659	0,6	36	33,2	2,75
	0,842	0,7	39	38,8	0,21
	0,842	0,7	39	38,8	0,21

Table H.9: Results of the calculated deflection based on the distributed force theory in tissue 1.

H.7.2.2. Tissue 2

Insertion depth [mm]	Proximal force [N]	qy [N/m]	Distal deflection measured [mm]	Distal deflection calculated [mm]	Δ [mm]
80mm	0,403	0,5	20	21,6	1,64
	0,419	0,5	21	21,6	1,14
	0,618	0,7	28	30,3	2,30
	0,618	0,7	29	30,3	1,30
	0,802	0,8	31	34,6	3,63
	0,807	0,8	32	34,6	2,63
100mm	0,424	0,5	35	24,5	10,52
	0,424	0,5	30	24,5	5,52
	0,602	0,7	40	34,3	5,73
	0,602	0,7	36	34,3	1,73
	0,802	0,8	40	39,2	0,83
	0,822	0,8	45	39,2	5,83
120mm	0,424	0,5	28	26,5	1,54
	0,439	0,5	36	26,5	9,54
	0,623	0,7	41	37,0	3,96
	0,628	0,7	38	37,0	0,96
	0,802	0,8	45	42,3	2,67
	0,812	0,8	47	42,3	4,67
140mm	0,408	0,5	26	27,7	1,70
	0,424	0,5	31	27,7	3,30
	0,597	0,7	39	38,8	0,21
	0,613	0,7	42	38,8	3,21
	0,791	0,8	42	44,3	2,33
	0,807	0,8	46	44,3	1,67

Table H.10: Results of the calculated deflection based on the distributed force theory in tissue 2.

H.7.3. Proximal force
H.7.3.1. Tissue 1

Insertion depth	Proximal force [N]	Elongation δs [mm]	Distal deflection measured [mm]	Distal deflection calculated [mm]	Δ [mm]		Distal deflection calculated +15mm [mm]	Δ [mm]
80mm	0,414	0,101	19	7,8	11,2		22,8	3,78
	0,429	0,105	23	8,1	14,9		23,1	0,06
	0,613	0,150	26	11,5	14,5		26,5	0,49
	0,654	0,160	27	12,2	14,8		27,2	0,25
	0,812	0,198	28	15,2	12,8		30,2	2,16
	0,863	0,211	29	16,1	12,9		31,1	2,09
100mm	0,434	0,111	25	10,6	14,4		25,6	0,61
	0,439	0,112	22	10,7	11,3		25,7	3,73
	0,602	0,153	30	14,7	15,3		29,7	0,32
	0,654	0,167	30	15,9	14,1		30,9	0,93
	0,807	0,205	37	19,6	17,4		34,6	2,42
	0,832	0,212	34	20,2	13,8		35,2	1,17
120mm	0,429	0,105	25	12,1	12,9		27,1	2,08
	0,434	0,106	22	12,2	9,8		27,2	5,22
	0,608	0,149	32	17,1	14,9		32,1	0,07
	0,613	0,150	34	17,2	16,8		32,2	1,79
	0,817	0,200	35	22,8	12,2		37,8	2,84
	0,832	0,203	37	23,2	13,8		38,2	1,25
140mm	0,414	0,089	28	11,9	16,1		26,9	1,09
	0,424	0,091	28	12,2	15,8		27,2	0,81
	0,608	0,130	36	17,4	18,6		32,4	3,55
	0,659	0,141	36	18,9	17,1		33,9	2,10
	0,842	0,180	39	24,1	14,9		39,1	0,06
	0,842	0,180	39	24,1	14,9		39,1	0,06

Table H.11: Results of the calculated deflection based on the proximal force theory in tissue 1.

H.7.3.2. Tissue 2

Insertion depth	Proximal force [N]	Elongation δs [mm]	Distal deflection measured [mm]	Distal deflection calculated [mm]	Δ [mm]		Distal deflection calculated +15mm [mm]	Δ [mm]
80mm	0,403	0,099	20	7,6	12,4		27,6	7,57
	0,419	0,102	21	7,9	12,6		27,9	7,37
	0,618	0,151	28	11,6	16,4		31,6	3,58
	0,618	0,151	29	11,6	17,4		31,6	2,58
	0,802	0,196	31	15,0	16,0		35,0	3,98
	0,807	0,197	32	15,1	16,9		35,1	3,07
100mm	0,424	0,108	35	10,4	24,6		30,4	4,63
	0,424	0,108	30	10,4	19,6		30,4	0,37
	0,602	0,153	40	14,7	25,3		34,7	5,32
	0,602	0,153	36	14,7	21,3		34,7	1,32
	0,802	0,204	40	19,5	20,5		39,5	0,54
	0,822	0,209	45	19,9	25,1		39,9	5,06
120mm	0,424	0,104	28	11,9	16,1		31,9	3,94
	0,439	0,107	36	12,4	23,6		32,4	3,64
	0,623	0,152	41	17,5	23,5		37,5	3,51
	0,628	0,154	38	17,6	20,4		37,6	0,37
	0,802	0,196	45	22,4	22,6		42,4	2,57
	0,812	0,198	47	22,7	24,3		42,7	4,30
140mm	0,408	0,087	26	11,7	14,3		31,7	5,73
	0,424	0,091	31	12,2	18,8		32,2	1,19
	0,597	0,128	39	17,1	21,9		37,1	1,87
	0,613	0,131	42	17,6	24,4		37,6	4,41
	0,791	0,169	42	22,6	19,4		42,6	0,63
	0,807	0,173	46	23,1	22,9		43,1	2,92

Table H.12: Results of the calculated deflection based on the proximal force theory in tissue 2.

Results tungsten needle

I.1. Results distal deflection based on proximal angle with Istylet

Insertion depth	Proximal angle [Deg]	Distal deflection measured [mm]	Distal deflection calculated [mm]	Δ [mm]
80mm	6,0	4,5	6,23	1,73
	8,5	6,0	8,84	2,84
	12,5	8,0	13,06	5,06
	5,0	3,5	5,18	1,68
	10,0	6,0	10,41	4,41
	23,0	10,0	24,54	14,54
	19,0	9,0	20,08	11,08
100mm	10,5	5,5	14,44	8,94
	16,0	8,0	22,21	14,21
	12,5	8,5	17,24	8,74
	5,0	3,6	6,84	3,24
	14,0	7,0	19,36	12,36
	17,5	9,5	24,37	14,87
	20,0	10,5	28,02	17,52
120mm	5,5	4,5	9,38	4,88
	7,5	6,5	12,81	6,31
	9,5	8,5	16,26	7,76
	5,0	6,4	8,52	2,12
	10,0	10,0	17,13	7,13
	16,5	11,5	28,60	17,10
	19,0	12,0	33,14	21,14
140mm	5,0	4,0	10,22	6,22
	6,0	6,0	12,27	6,27
	7,5	8,0	15,36	7,36
	5,0	7,0	10,22	3,22
	9,5	8,5	19,51	11,01
	12,5	9,5	25,79	16,29

Table I.1: Results of the distal deflection measured and calculated based on proximal angle with I_{stylet}.

I.2. Results distal deflection based on proximal angle with EI

Insertion depth	Proximal angle [Deg]	Distal deflection measured [mm]	Distal deflection calculated [mm]	Δ [mm]
80mm	6,0	4,5	6,10	1,60
	8,5	6,0	8,65	2,65
	12,5	8,0	12,78	4,78
	5,0	3,5	5,08	1,58
	10,0	6,0	10,19	4,19
	23,0	10,0	24,01	14,01
	19,0	9,0	19,65	10,65
100mm	10,5	5,5	14,19	8,69
	16,0	8,0	21,81	13,81
	12,5	8,5	16,93	8,43
	5,0	3,6	6,72	3,12
	14,0	7,0	19,01	12,01
	17,5	9,5	23,93	14,43
	20,0	10,5	27,51	17,01
120mm	5,5	4,5	9,24	4,74
	7,5	6,5	12,61	6,11
	9,5	8,5	16,01	7,51
	5,0	6,4	8,39	1,99
	10,0	10,0	16,87	6,87
	16,5	11,5	28,15	16,65
	19,0	12,0	32,61	20,61
140mm	5,0	4,0	10,08	6,08
	6,0	6,0	12,11	6,11
	7,5	8,0	15,16	7,16
	5,0	7,0	10,08	3,08
	9,5	8,5	19,25	10,75
	12,5	9,5	25,44	15,94

Table I.2: Results of the distal deflection measured and calculated based on proximal angle with EI.

I.3. Comparison of the needle tip path of the three different needles

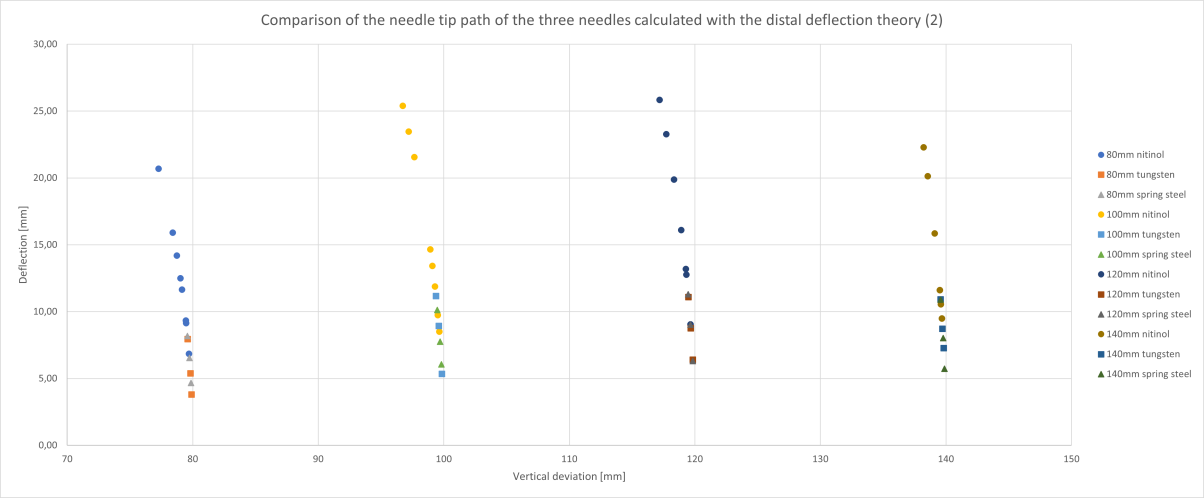

Figure I.1: All three needle tip paths plotted into one graph to point out the difference between their amount of bending.

J

Experiment set-up

J.1. Experiment in air

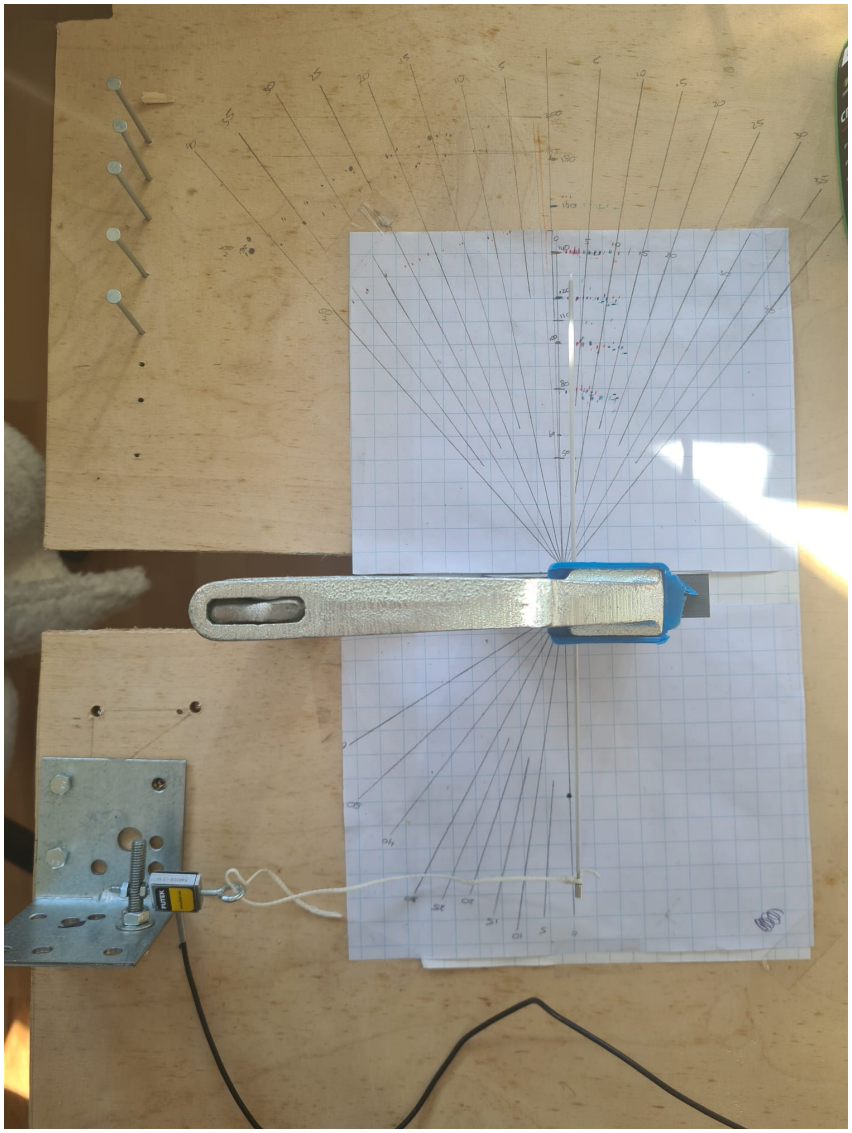

Figure J.1: Overview of the experiment set up in air.

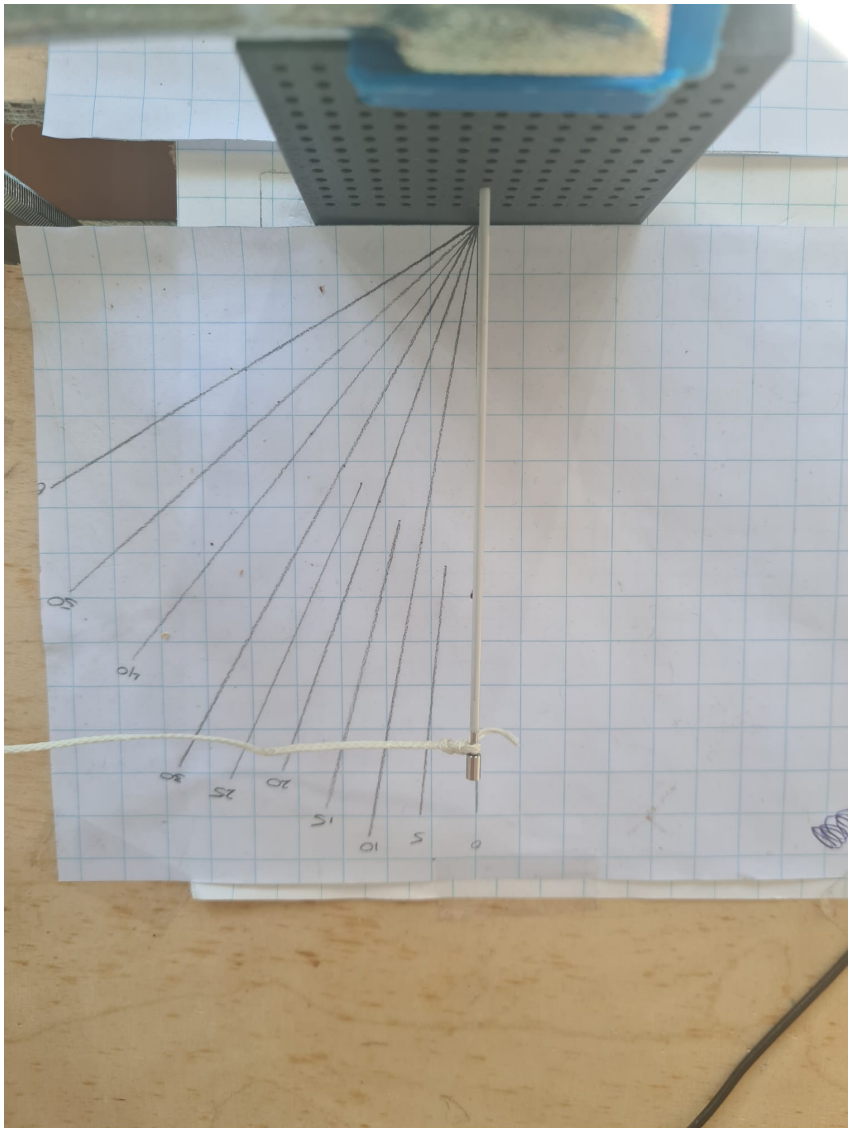

Figure J.2: Zoomed in on the proximal side of the experiment set up in air.

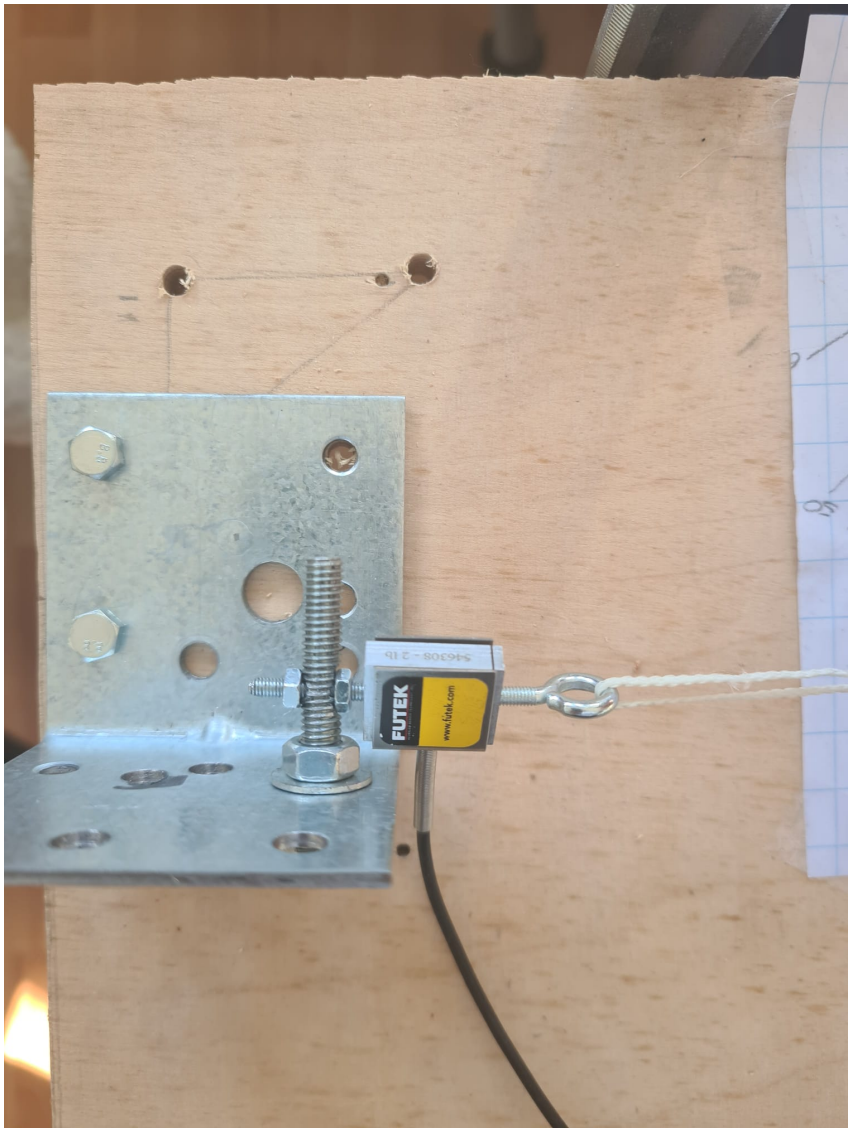

Figure J.3: Zoomed in on the fixation of the force sensor during the experiment in air.

J.2. Experiment in tissue stimulant

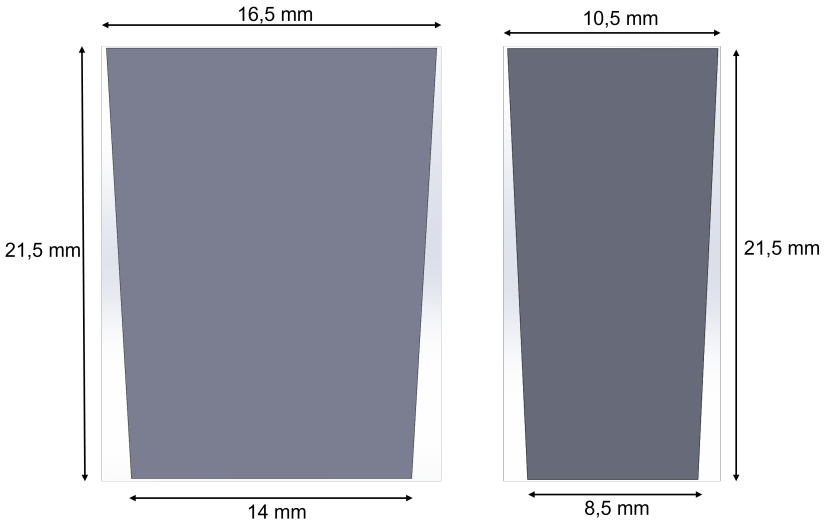

Figure J.4: Schematic of the measurements of the tissue simulant trays.

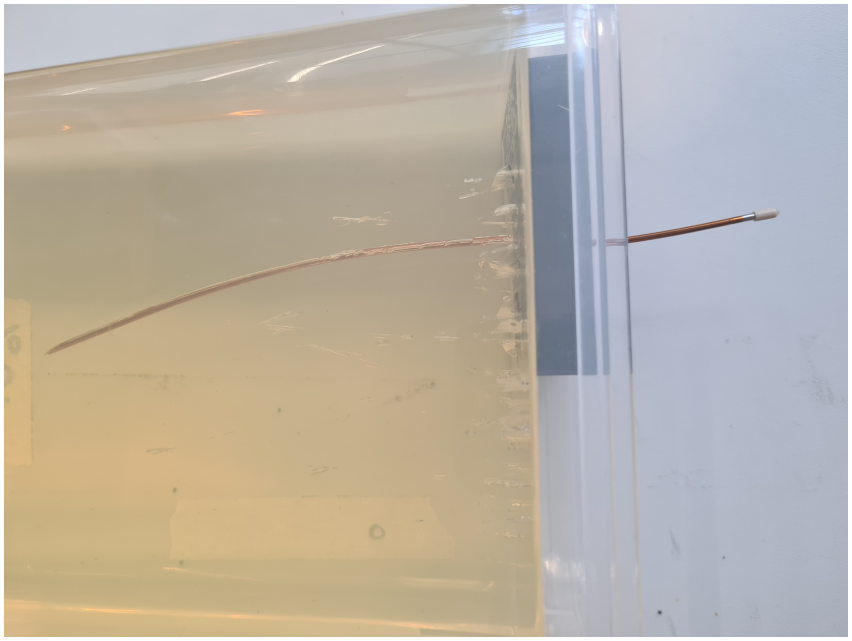

Figure J.5: Visualisation of the bending of the needle inside tissue stimulant.

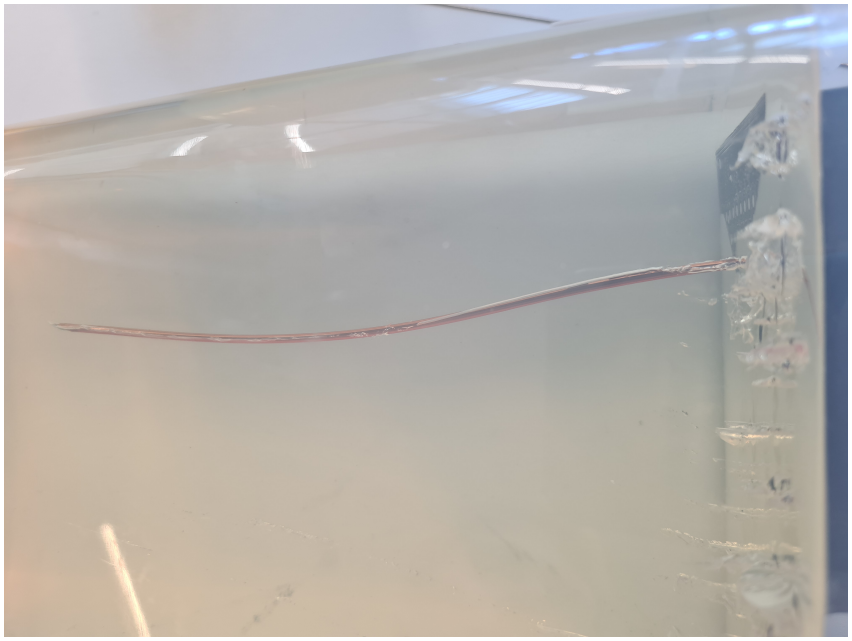

Figure J.6: Visualisation of the bending of the needle inside tissue stimulant.

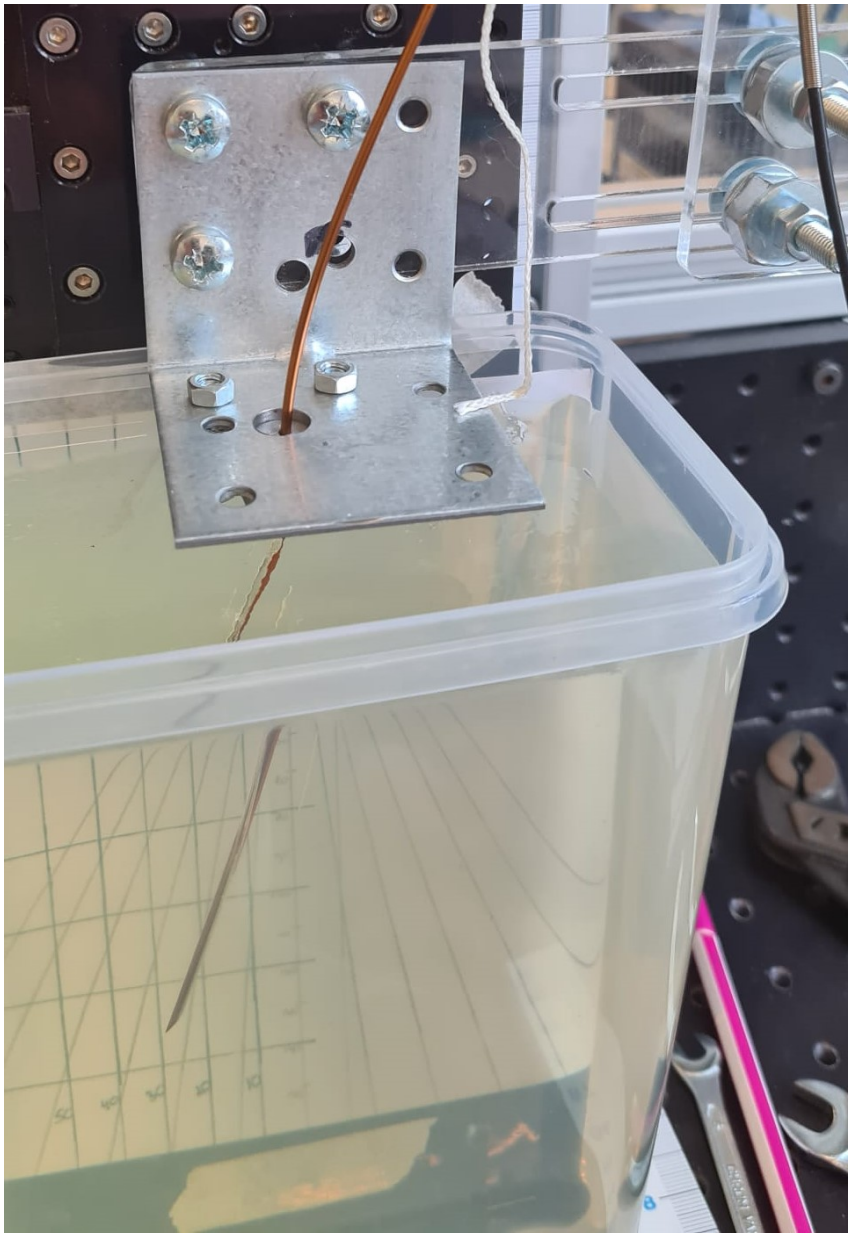

Figure J.7: Visualisation of the experiment set up for the experiment in tissue. Zoom in on the needle holder.

Bibliography

[1] Rebecca Siegel Mathieu Laversanne Isabelle Soerjomataram Ahmedin Jemal Freddie Bray Hyuna Sung, Jacques Ferlay. Global cancer statistics 2020: Globocan estimates of incidence and mortality worldwide for 36 cancers in 185 countries. *CA: a cancer journal for clinicians*, 71, 02 2021. doi: 10.3322/caac.21660.

[2] Sandra A Tincher, Robert Y Kim, Mark P Ezekiel, Tom Zinsli, John B Fiveash, David A Raben, Anton J Bueschen, and Donald A Urban. Effects of pelvic rotation and needle angle on pubic arch interference during transperineal prostate implants, 2000.

[3] S. Misra J.J. van den Dobbelsteen de Vries, J. Sikorski. Axially rigid steerable needle with compliant active tip control. *PLOS ONE*, page 18, 12 2020. doi: https://doi.org/10.1371/journal.pone.0261089.

[4] Fact sheet flexiguide needles. URL https://www.micknuclear.com/fileadmin/mick/user_uploads/PDF/Fact_sheet_FlexiGuide_Needles__Mick___Rev._D__USA.pdf.

[5] Ldr prostate brachytherapy brochure, dedicated solutions for real-time prostate seed implants. URL https://www.bebig.com/fileadmin/bebig_neu/user_uploads/Products/Seed_Brachytherapy/Brochure_Implants__Rev.07__English.pdf.

[6] Best medical international, inc. catalog. URL http://www.bestmedicalcanada.com/pdf/BMI_Catalog.pdf.

[7] Tarun Podder, Douglas Clark, Jason Sherman, Duane Fuller, Edward Messing, Deborah Rubens, John Strang, Ralph Brasacchio, Lydia Liao, Wan-Sing Ng, and Yanlin Yu. In vivo motion and force measurement of surgical needle intervention during prostate brachytherapy. *Medical Physics*, 33: 2915–2922, 07 2006. doi: 10.1118/1.2218061.

[8] Thomas Lehmann, Mahdi Tavakoli, Nawaid Usmani, and Ronald Sloboda. Force-sensor-based estimation of needle tip deflection in brachytherapy. *Journal of Sensors*, 2013, 01 2013. doi: 10.1155/2013/263153.

[9] Shi Jun Zhang, Hai Ning Qian, Yan Zhao, Kai Sun, Hui Qing Wang, Guo Qing Liang, Feng Hua Li, and Zheng Li. Relationship between age and prostate size. *Asian Journal of Andrology*, 15: 116–120, 1 2013. ISSN 1008682X. doi: 10.1038/aja.2012.127.

[10] M. Hehir B. King W.M. Garraway Collins, Raab. Reproducibility and observer variability of transrectal ultrasound measurements of prostatic volume. *Ultrasound in Medicine Biology*, 21: 1101–1105, 1995. doi: https://doi.org/10.1016/0301-5629(95)02001-2.

[11] M.M. Nobel. The design of a manually operated compliant mechanism steerable needle for high dose rate brachytherapy of the prostate. page 14, april 2020.

[12] Mohsen Khadem, Carlos Rossa, Nawaid Usmani, Ron S. Sloboda, and Mahdi Tavakoli. Robotic-assisted needle steering around anatomical obstacles using notched steerable needles. *IEEE Journal of Biomedical and Health Informatics*, 22:1917–1928, 11 2018. ISSN 21682194. doi: 10.1109/JBHI.2017.2780192.

[13] Erin Gibbons, Bruce Jacobs, Ryan Smith, Sushil Beriwal, Komanduri Krishna, and Ronald Benoit. Dosimetric outcomes in prostate brachytherapy: Is downsizing the prostate with androgen deprivation necessary? *Brachytherapy*, 8:304–8, 02 2009. doi: 10.1016/j.brachy.2008.11.009.

[14] Samir V. Sejpal, Vythialingam Sathiaseelan, Irene B. Helenowski, James M. Kozlowski, Michael F. Carter, Robert B. Nadler, Daniel P. Dalton, Kevin T. McVary, William W. Lin, John E. Garnett, and John A. Kalapurakal. Intra-operative pubic arch interference during prostate seed brachytherapy in patients with ct-based pubic arch interference of ≤1 cm. *Radiotherapy and Oncology*, 91:249–254, 5 2009. ISSN 01678140. doi: 10.1016/j.radonc.2009.02.006.

[15] Bellon J. Wallner K. Ellis W. Russell K. Cavanagh W. Blasko J. Use of pelvic ct scanning to evaluate pubic arch interference of transperineal prostate brachytherapy. *Int J Radiat Oncol Biol Phys*, 1999. doi: 10.1016/s0360-3016(98)00466-0.

[16] Ellis Russell K Cavanagh W Blasko J Bellon, Wallner. Use of pelvic ct scanning to evaluate pubic arch interference of transperineal prostate brachytherapy. *Int J Radiat Oncol Biol Phys*, 43(3): 579–581, 1999. doi: doi:10.1016/s0360-3016(98)00466-0.

[17] Junichi Fukada, Naoyuki Shigematsu, Jun Nakashima, Toshio Ohashi, Osamu Kawaguchi, and Mototsugu Oya. Predicting pubic arch interference in prostate brachytherapy on transrectal ultrasonography-computed tomography fusion images. *Journal of radiation research*, 53:753–759, 2012. ISSN 13499157. doi: 10.1093/jrr/rrs020.

[18] Yupeng Zheng, Jixiang Wu, Shan Chen, Yuexin Liu, and Guangyin Zhang. Predicting pubic arch interference in permanent prostate brachytherapy based on the specific parameters derived from nuclear magnetic resonance imaging. *Journal of Contemporary Brachytherapy*, 10:405–410, 10 2018. doi: 10.5114/jcb.2018.79247.

[19] Carolina Avila-Carrasco, Mirjana Ruppel, Rajendra Persad, Amit Bahl, and Sanja Dogramadzi. Analytical versus data-driven approach of modelling brachytherapy needle deflection. *IEEE Transactions on Medical Robotics and Bionics*, 2:519–528, 11 2020. doi: 10.1109/TMRB.2020.3032192.

[20] Tarun K. Podder, Adam P. Dicker, Parsaoran Hutapea, Kurosh Darvish, and Yan Yu. A novel curvilinear approach for prostate seed implantation. *Medical Physics*, 39:1887–1892, 2012. ISSN 00942405. doi: 10.1118/1.3694110.

[21] Konh Podder. Design and fabrication of a robust active needle using sma wires. page V001T08A021, 04 2017. doi: 10.1115/DMD2017-3470.

[22] Nick Berg, Jenny Dankelman, and John Dobbelsteen. Design of an actively controlled steerable needle with tendon actuation and fbg-based shape sensing. *Medical Engineering Physics*, 37, 04 2015. doi: 10.1016/j.medengphy.2015.03.016.

[23] Sepaldeep Dhaliwal, Taha Chettibi, Sarah Wilby, Wojciech Polak, Antony Palmer, Nick Reynaert, and Rochdi Merzouki. Review of clinical and technological consideration for mri-guided robotic prostate brachytherapy. *IEEE Transactions on Medical Robotics and Bionics*, PP, 07 2021. doi: 10.1109/TMRB.2021.3097127.

[24] Atsushi Yamada, Shigeyuki Naka, Norihisa Nitta, Shigehiro Morikawa, and Tohru Tani. A loop-shaped flexible mechanism for robotic needle steering. 3:648–655, 12 2017. doi: 10.1109/LRA.2017.2779273.

[25] E.M. boston-Mammah Engelen, A.E. de Nijs. Optimisation of an ldr brachytherapy steerable needle system. page 10.

[26] 302 stainless steel. URL https://www.matweb.com/search/datasheet_print.aspx?matguid=05efb28c10154f2796f4bf033363880a.

[27] R.C. Hibbeler. *Mechanics of Materials*, volume 9th edition.

[28] Vincent Rocher. Needle gauge table, 2019. URL https://darwin-microfluidics.com/blogs/tools/syringe-needle-gauge-table.

[29] Tissue properties, density database. URL https://itis.swiss/virtual-population/tissue-properties/database/density/.

[30] de Bever J Farrer Al, Odéen H. Characterization and evaluation of tissue-mimicking gelatin phantoms for use with mrgfus. *J Ther Ultrasound*, june 2015. doi: doi:10.1186/s40349-015-0030-y.